A PROBABILITY-BASED INSPECTION METHOD: PRINCIPLE AND IMPLEMENTATION

by

YIHUI ZHAO

A thesis presented in fulfilment of the requirements for the degree of
Doctor of Philosophy

Department of Design, Manufacture & Engineering Management
University of Strathclyde
Glasgow, Scotland, UK

2019

Declaration

This thesis is the result of the author's original research. It has been composed by the author and has not been previously submitted for examination which has led to the award of a degree.

Signed:

Date:

Abstract

Measurement and inspection technology are important parts of manufacturing industry today. They provide important feedbacks to modern control systems, detect failures and flaws either online or offline, and hence enhance boost the productivity and improve the quality of final products. The continued development and evolution of measurement principles and systems have produced increasingly precise and reliable results. Published literature and industry practice show that better measurement results usually require both a "ruler" of finer scales and a better method to make more stable readings; however, these are bottlenecks in developing new methods and improving existing systems.

In this thesis a probability-based method (PBM) for length measurement is proposed which produces measurement results more accurate than the physical scales on the "ruler". As a natural extension to the classic approach, this measurement model uses probability readings as indicators and evaluates the measurands. Around this method, a theory is established and proven for various levels of priori knowledge. Following this, real-world obstacles in implementation and practice usage of PBM are considered. For example, mis-alignments which not only cause trigonometric errors but also induce a discrete random behavior on the measurand, sources of sampling randomness consisting of synthetic parts and those from random errors, and impacts of laboratory gantry systems are fully investigated. A validation process is conducted using existing hardware with newly developed software. Multiple tests are conducted. The experiment results confirmed the validity of PBM and therefore shows that this method will make a positive contribution to the industrial inspection.

Acknowledgement

Firstly, I would like to express my sincere thanks to Prof. Yi Qin at University of Strathclyde, who as the supervisor provided me many help in the study, as the project leader offered me a working opportunity and supported my life in UK for all these years. I would also thank him for giving me the chance to gain experience in industry designs. I would thank University of Strathclyde, especially the department of Design, Manufacture and Engineering Management (DMEM) for all the facilities and academic resources. I would also thank all the technicians, academic and administrative staffs who provided help directly or indirectly.

I would also give thanks all the colleagues. Dr. Jie Zhao helped me settle down and later helped moving. Dr. Yankang Tian, Dr. Song Yang, Dr. Gerald Njiribeako Anyasodor, Dr. Zhenhai Xu and others in JW608 provided a lot of help in my work and life. The discussion with Dr. Wenbin Zhong and Dr. Fei Ding on electronics and programming was extremely fun and I learned a lot from them. Specially, the late Mr. Arthur Yip, who guided my early study and criticized my work will always be remembered.

Support from the EU research projects "Micro-Fast", "AUTOMAN", and "LoCoMaTech" are also acknowledged. All partners are appreciated. Specially, AFT Automation GmbH provided a lot of help and free water when I was working in Pforzheim.

Finally, I would like to thank my father Prof. Shiping Zhao, and mother Mrs. Yonghong Li. Thanks for their various advice in work and support for the life.

Contents

List of Figures

List of Tables

Notations and Conventions

Master Log File

Experiments, experiment data, and some of the engineering notes for the work conducted by the author for this thesis are tracked in a file in the markdown format. This is the *master log file*. The master log file is a ledger book that tracks data for integrity purposes, and it records necessary information for the development of software. It also records log files generated by the software used in the validation process, and in this sense the master log file is a log file for log files. For conciseness, the master log file and its recorded entries are not included in this thesis.

Conventions

Throughout the paper a word in the monospaced `Fira Code` font will be used to refer to items listed below. Grammatically, all such words should be treated as nouns, either having a meaning by itself, for example the `AbsDataSections` class, or referring to other entries, for example `F18102411` is a referring ID that points to an entry on the master log file.

- program codes or fragments of program code.
- program code related names — for example, `ExpFreeScan` is a class name that is used in the validation program and `DSCF.autoEdges` is a function call which detects the edges of gauge blocks in a given point cloud.
- names of software, commands and tools — for example, `gnuplot` is a tool for plotting graphs, `PhDSampline` is the name of the validation software.
- names of directly sampled or derived data — for example, "`SimpleDataSection 2018-10-24 16-25-17.3795 ExpValidation additional profiles.sdata`" is a file in the `sdata` format that is sampled in a validation experiment.
- IDs in the master log file — for example, `F18102441` is the ID of the file above. The pattern for such id is `F` followed by a 6-digit date and then a number.
- models of hardware — for example, `NLE-50-A` is the model number of linear stages used for x and y axes.
- steps and data in flowcharts — for example `S9` or `D11`.

Symbols

$\lfloor x \rfloor$	the largest integer that is smaller than or equal to x
$(\Omega, \mathcal{F}, P)$	probability space; see page 144
$\succ$	binary relation, generally used in this thesis for the meaning of being preferred to; variations like $\succeq, \prec, \preceq$ exist; mainly used in chapter 2, see page 7
$\mathfrak{b}$	laser beam; see page 52
$\mathcal{B}(X)$	generated Borel σ-algebra on a topological space X; see page 144
$\beta(x, y)$	the Beta function $\beta(x, y) = \int_0^1 t^{x-1}(1-t)^{y-1}\,\mathrm{d}t$
$d(A, B)$	discrepancy for comparison under a scale defined by some standard sequence; see equation (2.10) on page 22
δ	the length of the left part of a line segment that is covered by a loose scale; defined in chapter 3, see Fig. 3.3 on page 26
δ_m	residual of scaled after adjustment; see page 75
δ_p	randomness from placement; see page 64
δ_r	randomness from various sources of error; see equation (4.11) page 64
Δ	size of scale on a ruler, distance between two carved marks; see Fig. 3.2 on page 25; this symbol is also used to indicate differences, for example, Δx
$\overline{\Delta}, \underline{\Delta}$	$\lvert\overline{B}_i\overline{B}_{i+1}\rvert$, $\lvert\underline{B}_i\underline{B}_{i+1}\rvert$ respectively; see page 56
Δ_m, Δ_M	minimum and maximum distance between adjacent laser beams in the trapezoidal effective scanning area at different horizontal sections; see Fig. 4.1[b] and page 52
$\Delta_x, \Delta_y, \Delta_z$	minimum incremental motion along the x-axis, y-axis, and z-axis respectively; see page 74
e_s	sparse constant; see page 92
$E(\cdot)$	expectation of a random variable

$E_{AB}(\Delta)$	expectation of $m(AB)$; defined by equation (3.6) in chapter 3 on page 27
H_S	height of the trapezoidal effective scanning area of a laser profile scanner; see Fig. 4.1[b] and page 52
$K(\overrightarrow{n}, \overrightarrow{m})$	$\frac{(\overrightarrow{n}\times\overrightarrow{e_1})\cdot\overrightarrow{e_2}}{(\overrightarrow{n}\times\overrightarrow{e_1})\cdot(\overrightarrow{n}\times\overrightarrow{m})}$; see page 57
$\kappa(\alpha)$	$1 - \tan\theta_s \tan\alpha$; see page 58
$\mathfrak{l}$	length of line segment or width of the extrusion of the gauge object, as a random variable
$\bar{l}, \underline{l}$	upper bound and lower bound of $\mathfrak{l}$ respectively; see page 59
L_N	length of Type II interval; see page 61
l_n	nominal value of the length of line segment or width of the extrusion of the gauge object as measurand
l_t	true value of the length of line segment or width of the extrusion of the gauge object as measurand
$\overrightarrow{m}$	direction of the extrusion; if with subscription, it may refer to the direction of an edge of the extrusion; see page 52
m_m	minimum possible increments of Δ using a real-world gantry; see page 75
m_r	bound for δ_r; see page 64
μ	measure, an extended real-value function; see definition on page 144
μ_L	Lebesgue measure; see page 144
$\overrightarrow{n}$	normal of the top surface pointing upwards; see page 52
$\mathbb{N}$	natural numbers
$\mathcal{N}(\mu, \sigma^2)$	normal distribution of expectation μ and variance σ^2
N_S	number of laser beams, or number of points in a laser profile scanner; see page 52
$\mathfrak{n}(A, B)$	an integer defined by equation (2.9); see more on page 22
$\Omega(p_h, m_m)$	oscillation of p_h; see page 75

$p_h(x)$	the probability of high readings; defined by equation (3.12) on page 31
$p_h(x, l)$	same as $p_h(x)$; see remark 3.1 on page 32
P_δ	probability distribution function of random variable δ; $P_{\delta,\Delta}$ stresses on the fact that P_δ is also a function of Δ; see page 27
ϕ	measurement functions as representation, homomorphisms; mainly used in chapter 2; see definition on page 6, 13
Φ	function from $\mathbb{R}_+$ to $L^1(\mathbb{R}, \mu_L)$; defined in chapter 3; see page 27
$\mathbb{R}$	real numbers
R_M	result set, result function; has R_∞ as a variation; see page 39
$\mathcal{T}_\phi$	set of all permissible transformations of homomorphism ϕ; see definition on page 14
θ_m	included angle between $\overrightarrow{m}$ and $(1, 0, 0)^T$; see page 55
θ_n	included angle between $\overrightarrow{n}$ and $(0, 0, 1)^T$; see page 56
$\mathfrak{u}$	random variable with uniform distribution on $[0, 1]$
$\mathbb{Z}$	integers

1 Introduction

1.1 Background

Since the dawn of human civilization, metrology has been impacting society in many ways, from productive activities to cultural and political ideologies. After unifying China in 221 BC, the Qin Empire unified scales that were used by different kingdoms and this enforcement of standardization in metrology is an example of centralization of power in early human history [Lew07]. In modern industry world, production quality can be improved by involving metrology in various design methodologies and approaches; for example, in a PDCA (Plan-Do-Check-Act) cycle, metrology usually occurs in the check cycle [SPP10]. Nowadays it is no longer rare to see metrology subsystems in large and complicated systems; and it has been reported that machine tool metrology can improve the overall accuracy of the system [CL96]. More recently, people have begun to realize that metrology (sub)systems are actually adding value to every step of the production process; and therefore it is no long proper nowadays to consider metrology costs a waste [Kun+05][Sav+16]. Case studies in [Sav+16] reveal huge economic benefits by actively involving metrology technology into production lines. Metrology technologies are good investment targets themselves — every €1 investment in metrology causes €3 EU GDP growth [Kun+05].

The evolution of metrology standards, methods and tools never stopped. Narrowing down the discussion to length measurement, in ancient times, the units and measures were based on human bodies; for example, *foot* and *cubit*, as units of length found in many different cultures and regions, are believed to be derived from the size of foot and forearm respectively [Dil87]. Nowadays the metre is defined using the the speed of light which is a physical constant. From ropes to calipers, micrometers to interferometers, the development of measuring tools endows people with finer measurements and more reliable results. Currently, length/distance measurement can be conducted reliably at nano/sub-nano level [Har16]. Metrology methods have diversified as sensor and peripheral technology advanced. Optical triangulation, confocal microscope, SEM (scanning electron microscope), AFM (atomic force microscope) and SICM (scanning ion-conductance microscope) are splendid non-contact metrology technologies for various fields like rigid body profiling, material surface investigation and biological techniques. Although the achievement of metrology so far seems to be adequate, there are still problems to be solved.

Table 1.1: Specification of commercial and research devices: `2900-10/BL` is from Micro-Epsilon; `ZeGage Pro HR` is from Zygo; and AOTF WSI 2013 is from University of Huddersfield [Muh13]

Model	Method	Resolution	
		vertical	lateral
`LLT 2900-10/BL`	laser triangulation (blue light)	1μm	$7.3\mu\text{m} \sim 8.4\mu\text{m}$
`ZeGage Pro HR`	scanning white light interferometer	0.01nm	0.52μm ($50\times$ objective)
AOTF WSI 2013	wavelength scanning inteferometer	15nm	2.98μm ($5\times$ objective)

Table. 1.1 lists specifications of commercial and research devices. Although these devices are used for different purposes, for example, geometric dimensions and topography, and deliver satisfactory results; the discrepancy of resolution in different spatial directions quickly draws one's attention. Simple calculation shows that the lateral resolutions are 7 times to 52000 times rougher than the vertical resolution. Tremendous efforts have been conducted to improve resolutions, for example, `LLT 2900-10/BL` as the latest model in the product line of the compact laser triangulation sensors uses the blue laser instead of red so that the resolution is improved by the shorter wavelength, also more efficient algorithms have been developed which improved the vertical resolution of AOTF WSI 2013 from about 2μm to 15nm [Muh13]. Nevertheless the gap between the vertical and lateral resolution remains huge. In other fields, for example, materials and biology, SEM, AFM and SICM are capable of providing more uniform resolutions in all directions by using piezo stages; however, the measuring principle of these scanning probe microscopes, which requires direct manipulation of electron beam, probe, and pipette, greatly limits the speed of measurement [Gol+11][Kor+97]. The difficulties in shrinking the gaps between the vertical and lateral resolution are complex and many-sided. Physical barriers like diffraction limits in optical systems and the limits and finiteness of sensor technologies confine the lateral resolutions to relatively low levels [Hec16][Fra15]. The industry has been working hard trying to make improvements, for example, in the satellite imaging systems time delay and integration (TDI) sensors and staggered CCDs of half pixels have been developed and have greatly improved ground sample distance (GSD) [Jac05]. However, it is not optimistic to expect greater improvements by simply staggering more sensors.

1.2 Aim and Objectives

The overall aim of this research is to develop a measurement method which enables accurate measurement below the "scale" of the measurement systems. This new method will henceforth be referred to as PBM (probability-based method) in the rest of the thesis. Narrowing down the scope for concrete theories and validation work, the work will be focused on length/distance measurement. For the widest accessibility and ease of update of old production lines and devices, this method should be feasible by using existing sensors.

The detailed objectives are as follows:

(1) Determine an approach for digital measurement that is both theoretically robust and digitally implementable. Discuss different scenarios where variations of data sampling and processing are necessary. Investigate the relation of PBM to the traditional method.

(2) Demonstrate its feasibility by considering the problems that occur when PBM is applied to real world devices. Tricks in implementation and influence from various disturbance should be covered by the discussion. In conclusion, a theoretic foundation for real world implementation of PBM is expected to be developed.

(3) Justify the validity of PBM in laboratory environment and identify the weakness and limitations of the method by implementing PBM in the lab environment and developing software that is necessary for the validation process. Collect, analyze data and compare to the developed theoretic work.

1.3 Thesis Outline

An outline of the paper is presented in this section as an overview of this thesis.

Chapter 1 explains the general background of the work. Through a brief review of the historic and current state of metrology, the discussion is focused on the distance/ length measurement where the challenge is found. Brief motivation and objectives are presented, which aim at conducting a trial to solve a more general problem — to perform finer measurement using a rough ruler.

Besides a in-depth literature review, chapter 2 also contains relevant materials and knowledge that are used in this thesis. Following three aspects — an overview of measurement, the framework and change of philosophy of measurement, and the evolution of the method of length/distance measurement — the contents to review are selected and this sets the range of discussion. In this chapter, the review of general concepts, like measurand and error, will be from multiple views, including the very practical aspect of industry standards and the more academic aspect of representation. Different frameworks of measurement will be reviewed which reveal the evolution of the philosophy of measurement. The trend is from deterministic to probabilistic, from values to representations. As this thesis mainly deals with distance/length measurement, a brief review of the history of the definition of metre is included. Finally, various existing methods of distance/length measurement will be reviewed. At the same time, existing machines and devices will be briefly introduced as examples. Supplementary materials on probability theory are put in Appendix C.

PBM, the new method, and the core theory are introduced in chapter 3. Firstly, the challenges stated in chapter 1 are modelled as Problem 3.1, where one is asked to check whether the length of a line segment is within 150 ± 0.4mm using a ruler with an adjustable scale from 2mm to 4mm. The PBM approach and the theory behind it are gradually developed as various trials for solutions to the problem are conducted. The key ideal is that by loosing the restriction on alignment of a scale to an end of a line segment, probabilities on high/low readings can be obtained. It is shown then that p_h, the probability of a high reading can be used as an indicator because its continuity fails when and only when the true length of the line segment is a multiple of the scale of the ruler. Probability tools can then be used to solve the problem. Detailed procedures in solutions for various scenarios with different levels of prior knowledge are discussed with examples. Finally, the relation of the method to the classic approach is shown by a theorem and the position of PBM is finalised.

Chapter 4 extends the theoretic discussions of PBM conducted in chapter 3, covering real-world cases where new challenges arise. This chapter also aims at paving the way for the real-world validation of the new method; and the discussions are selected to be relevant to the problems that the later validation is likely to be confronted with. Three topics will be discussed, the mis-alignment of a tool and the gauge that is usually found on real-world devices, the source of randomness and its impact to PBM, and the

realistic multi-axis systems, or the gantry, where discreteness instead of continuity occurs. The discussion on these topics emphasizes the aspects that are closely linked to PBM, while traditional treatments like error analysis are also included in this chapter.

Chapter 3 and 4 contain most of the theoretic works. To make the discussion vivid and easy to follow, many examples are included in these chapters. Other important but not so closely relevant examples are put in Appendix A.

Chapter 5 presents in detail the validation work for PBM, the new method proposed in this thesis. Firstly it explains the design of the laboratory set up and software, then gives flow charts for the validation experiments. Following one real-world validation experiment, every step of data preparation, sampling, and processing is explained and visual illustrations are given wherever possible. Reasons for specific designs and treatments are explained. Finally, results of more than 200 tests of validation experiments in 8 different sets of parameters are presented; and this proves the validity and feasibility of PBM.

Chapter 6 summarizes the thesis and discusses other possibilities as well as the potentials of PBM. After a short section of concluding comments and remarks, other possible implementations of this method are discussed. Finally, based on the theoretic works and validation data, thoughts on future work are included in the hope of setting up good starting points for future researchers.

2 Literature Review

In this chapter, a brief review of the basics of general metrology will be conducted, including topics on distance/length measurement, common methods, equipment, and standards. Accompanied with this review, historic facts and the evolution of measurement frameworks will be investigated, aiming at providing a wide base for discussion and correctly positioning the work of this thesis. The contents in this chapter will also serve as supplementary material in order to make the thesis self-explanatory. A brief introduction of probability theory is included at the end of this thesis as Appendix C.

As interpreted by the Webster's dictionary [GS71] and the Chambers dictionary [Sch94], *metrology* may refer to a system of weights and measures, or the science of measurement. Depending on the situation, the meaning of measurement as well as other relative concepts, like error and uncertainty, vary accordingly. In a production environment where the dimension of each part needs to be found before assembly, measurements are conducted; and in such cases, the word is used in a more practical way referring to a sequence of operations to identify certain quantities. Industrial standards [DIN95][BIP+09], metrology handbooks and guidance [Sug07][CSS11] support these scenes and provide direct, clear, pragmatic and operable definitions and instructions on measurement. For example [DIN95] and [BIP+09] describe measurement as an experimental process where certain operations are performed to determine or obtain value of quantity. In [CSS11] the definition of measurement gets more procedural starting with the definition of quantities (measurands), then the specification and realization followed by the measurement method and model, and finally the measurement results via calculation. In such contexts, measurements are usually conducted for a "true value". This definition of measurement has been proven to be working well in the real world and has been supporting industry for a long time.

In the scenes above, a "true value" is obtained or assigned by measurement processes. The fact that many quantities can be assigned "regardless of the choice of unit, ratios of numerical assignments and are uniquely determined by the procedure" (quoted from [KSL71]), has been noticed by many researchers at the end of 19^{th} century. Since [Hel87] and [Höl01], the representation model of measurement theory has been under intensive development for about a hundred years and summarized in Krantz's work [KSL71]. Under this model, measurements are regarded as assignment functions ϕ which keeps the inequality and equality relations. For example, if rod A is longer than

rod B, denoted by $A \succeq B$, a measurement should give $\phi(A) \geq \phi(B)$. This representation view of measurement has been found useful in finding out more subjective measurands, like the human sensations (loudness of sound, chapter 4 of [SH38]). More complex measurements then become possible where in-exactness is allowed within the process [Luc56][Ada65]. The representation model opened the door to a new world by introducing more sophisticated relations/systems (i.e. the $\succeq$ relation) and well-designed numerical functions into measurement processes. More recently, works like [Fal76][Fal80] and later [MR95][Ros06][Ros14] made systematic efforts to integrate the powerful tool of probability into the already-established deterministic representation framework. Compared to practical measurement, representations lean towards the theoretic side; yet, they provide guidance for more people from various fields like psychology and economics.

The view of measurement above follows Mari's work [Mar05] where the words "realist view" and the "representation view" were used not only to distinguish for different scenes but also to indicate the change of philosophy. Michell proposed similar ideas in both [Mic04] and [Mic05]. As this thesis intends to keep the discussion in a close connection to real-world operations and experiments, philosophical considerations of measurements beyond the work [Mar05] will be avoided. Before going into details of measurement, it is better to clarify here that according to the context, the word *measure* in this thesis might be referring to functions that satisfy the mathematical definition of being a measure ([Hal14][ISO3534-1]).

In the rest of this chapter, a brief review of measurement will be given, followed by a introduction to common methods of distance/length measurement. Finally there will be a subsection for the basics of probability theory, including the contents that are used by this thesis.

2.1 A Brief Review of Measurement

Beginning with the realist view, the fact that when discussion on measurement is conducted, most materials like books [CSS11][Lir02] and articles [Mar05][Sad11] all make reference to two documents provided by the International Bureau of Weights and Measures (BIPM), "Evaluation of measurement data - Guide to the expression of uncertainty in measurement" [BIP+08], known also as the GUM, and "The 2007 International Vocabulary of Metrology (VIM)" [BIP+09] proves the importance and leading position of both GUM and VIM. This thesis is no exception in that all the discussions will be

mainly following both [BIP+08]and [BIP+09]; moreover, to make the review more concrete, examples will be provided alongside for the purpose of clarification of certain concepts. In addition, other documents and standards, like [DIN95][How+08], will also be referred to as supplements. Following the realist view, the representation view of measurement will be briefly reviewed. As an example of representation, a concise introduction to the probabilistic framework is included at the end of this section.

2.1.1 The Realist View

It all begins with the concept of *measurand*, which is defined as the quantity to be measured. For example, the resistance of a given resistor or the length of a given rod are measurands. Without specific objects, people also use measurand to refer to more general concepts like mass or density. This general usage is separately noted in [BIP +09]as *kind of quantity*, where, heat and kinetic energy, wavelength and circumference, are considered to be of the same kind. *Quantities*, or properties of a phenomenon, body, or substance are restricted to be scalar (NOTE 5 of [BIP+09]) as they have to be expressed as a combination of numerical magnitude and a reference. It covers most of the empirical cases, for example, vector quantities can be seen as a combination of the scalar components. This view is typically restricted to the realist framework, examples in [KSL71][SK06] as well as those found in [Mar05] showing a much wider range of measurands and these will be reviewed later in this section.

To avoid vagueness and to stay close to the empirical reality, it is better to continue with a concrete example. Like Lira did in [Lir02], the review shall continue with the assumption that one is asked to be measuring the length of a given cylindrical metal rod. Thus, length of the cylindrical metal rod is the measurand following what is discussed above.

True value is commonly defined to be the value or quantity consistent with the definition of a quantity; and in [DIN95], it is stressed that this value should be obtained by a perfect measurement. The definition of the length a cylindrical rod can be described as the distance between the two end section surfaces. Unlike the ideal case, real-world cylindrical metal rods can neither have parallel end sections nor ideal planar surfaces. Within a certain tolerance, it might be acceptable for people to claim the length of the rod to be 10.1mm; however, it is never possible to claim the true value to be 10.1000000000001mm due to the failure of the definition at sub-atomic level. The unknowable essence of a true value is widely accepted and clearly documented in [BIP

+09][DIN95]and [BIP+08]. In section D.1.1 of [BIP+08]this essence of true value is linked to the the fundamental failure of giving a precise definition of the measurand with finite information.

Despite of the endless pursuit of the philosophic nature of true value, it is easy for anyone to use a vernier caliper to find the length of the rod to be 10.1mm as an acceptable, reliable result. This is mainly attributed to the fact that the main and vernier scales on the caliper are agreed to be of 1.0mm and 0.9mm (usually more precise) as *conventional true values*. A conventional true value is usually defined as quantity value attributed by agreement or convention, and it is stressed that the error or the uncertainty should be small. In particular, [DIN95] explicitly requires that the process through which a conventional true value is obtained should be at least ten times more precise than the admissible error. As criticized in [Mar05], the conventional true value has been used conveniently to fill the gap between the more theoretically true value and the more empirical real world requirement on measurement.

How the conventional true values of the main and vernier scales are made widely admissible is also rigorously defined by industrial standards and will be briefly reviewed here. Following [BIP06], where a metre is defined as the length of path traveled by light in vacuum during a time interval of $1/299792458$ of a second, substantial reproduction (*measurement standard* or *etalon*) are conducted by state metrology labs, organizations and corporations at various scales [BIP+09]. During this process, *calibrations* are conducted to find out the discrepancies; and then adjustments are made for compensation. A fully documented chain of calibration is carefully maintained, establishing the *metrological traceability* of each intermediate and end reproduction [BIP+09][Lir02]. Under such a framework, it is justifiable to make the claim that the conventional true values of the scales on a given vernier caliper are 1.0mm and 0.9mm.

A *measurement model* of general form is described by an equation $h(Y, X_1, \ldots, X_n) = 0$, where Y is the output and X_i the inputs. Locally a measurement model may be expressed by a *measurement function* of the form $Y = f(X_1, \ldots, X_n)$ [BIP+09][Rud76]. Henceforth these two forms of measurement model will be used without distinction. For example, to measure the volume of our cylindrical rod, the one of the measurement models can be $V = \pi r^2 l$, where r is the radius of the cylindrical rod and l the length of the rod. As pointed out in [BIP+09], a measurement function can also be as complicated as a symbolized algorithm, which cannot be simply expressed in an analytic way. The main contribution of this thesis is that a new probability based measurement model is proposed and validated.

Error is commonly found in various fields to be defined as the difference between the assigned or computed value and the true value [MM05][DB08][Fei91][Fra15] or vice versa [Kal60][DB08]. Because of the fact that the true value of a measurand is unknowable, [BIP+09] gives the definition of error as the difference between a measured quantity value and a reference quantity value. While practically, the expectation or mean has been chosen to be playing the role of the conventional true value or the reference quantity value and the residual the role of error ([Fei91] and §E.5.1, §E.5.2 of [BIP+08]); the conventional true value can also be specified if it is obtained by some more precise measurement [Lir02][BIP+09]. For example, to estimate the error when measuring the length of a cylindrical rod, it is possible to measure 10 times using a caliper and use the statistical mean as the conventional true value and then find the residuals; also it is possible to measure the length of the rod using a micrometer and use the result as the conventional true value and compare results from a caliper to find out the error.

Further more, error can be split into two parts, namely the *systematic error* and *random error*. Following [BIP+09], systematic error is defined as the component of measurement error that is predictable in replicated measurements. Systematic error is not necessarily constant under this definition, and also it is clearly stated in [BIP+09] that the cause can either be known or unknown. Contrary to the systematic error, random error is the unpredictable component of measurement error [BIP+09]. [DIN95] and books like [Lir02][Fei91] treat systematic error and random error in a more practical way. The systematic error is regarded as the difference between the expectation (or mean) of replicates of measurement and the (conventional) true value, while the random error is defined as the difference between the measured value and the expectation (or mean). These are special cases of the definition in [BIP+09], and the systematic error becomes a constant value. In Annex A of [DIN95], which is incompatible with [BIP+09], systematic error is deliberately split into the known part and unknown part.

Uncertainty, another concept describing measurement inexactness commonly accepted today [UW03][CSS11], roughly speaking, describes the magnitude of error [Fra15]. In [BIP+09] and [BIP+08], uncertainty is defined as a non-negative parameter describing the dispersion of measurement results which reflects the lack of exact knowledge of the measurand. As criticized in [CSS11], the philosophy behind [BIP+08] and [ISO98-1] is that the measurement quantities should be regarded as random variables and hence uncertainty is indispensable for descriptions of degree of belief of measurement results. For example, after measuring the length of a given rod 1000 times, it

is found that the results is of normal distribution around 10.1mm. Then 10.1mm, the expectation can be reported as the estimate and, for example 0.08mm, the standard deviation can be reported as the standard uncertainty with this estimate (4.9 [ISO98-1]). The point needs to be noted that with all the imperfection caused by many sources (§3.3 of [BIP+08]), the measurement result is of the normal distribution $\mathcal{N}(10.1, 0.08^2)$, and the 1000 statistical data is a verification of this fact. The evolution and gradual admission of the concept of uncertainty from the error was not easy. Early trials in 1970s like [CBW73] proposed the ideas of random uncertainty and systematic uncertainty in parallel with the definitions of random error and systematic error; but this was later deemed as a failure [CB80]. Even nowadays the close connection between error analysis and uncertainty evaluation can still be seen in equations (10), (E.3), (E.8) of [BIP +08].

In chapter 7 of [ISO98-1], three different methods of computation of uncertainty are proposed, the GUM uncertainty framework where the estimation is made under the law of propagation of uncertainty, the analytic methods where the distribution of the output quantity Y is computed through a given measurement function f, and the Monte Carlo method where the distribution of the output quantity Y is approximated by experiments or simulations with random input samples through a known measurement model. [BIP +08] categorizes the manner of evaluation of uncertainty into two types, Type A which is based on observation of replicates of measurement results and Type B which is not Type A.

2.1.2 The Representation View

At the same era when the BIPM was found and the Metre Convention was signed; different opinions on measurement began to sprout — the representations. H. v. Helmholtz, O. Hölder and B. Russell are the three pioneers for the representational framework of measurement [Mic93]. Their work [Hel87][Höl01][Rus09] reflected the early struggles in understanding of "magnitudes" in measurements; while in the realist framework of measurement, even today, the meaning of the word "magnitude" is considered to be primitive without definition (Terminology rules [BIP+09]). To make the review concise and easy to understand, the example of measuring the length of cylindrical rods will be used throughout the rest of this section.

Helmholtz's approach in [Hel87] is epistemological. He believes that "when different perceptions force themselves upon us, we are entitled to infer from this a difference

in the real conditions under which they were formed" ([Hel87]), and this essentially means that through human sensations different qualities can be reflected. Russell in his work [Rus09] included discussion on basic properties of magnitude and quantity, his philosophical approach granted him a co-founder position in the representation framework of measurement [Mic93].

Unlike Helmholtz and Russell, Hölder in his work [Höl01][ME96] built a mathematical model and made the contribution by introducing an ordering relation $\succ, \sim, \prec$ on a commutative semigroup and by implementing a numerical measurement $\phi(a) = [a : b]N_b$ where $[a : b]$ is defined in §10 of [Höl01] as a ratio and N_b an arbitrarily chosen positive number for a fixed magnitude b. To explain Hölder with an example, let S be the set of the totality of the length of the perfect cylindrical rods. Then define $A \succ B$ if rod A is longer than rod B; and $A \sim B$ if rod A and B are of exactly same length. Addition or concatenation on S is defined in a way that $A + B$ represents the length of a rod that is of the same length when rod A and B are perfectly concatenated. Thus

$$\mathfrak{H} = \langle S, \succ, \sim, + \rangle \tag{2.1}$$

satisfied all the 7 axioms of [Höl01]. Then $[A : B]$ the ratio of length of rod A to rod B can be uniquely defined as a real number for every $A, B \in S$. Now it is possible to fix a given rod B and assign its length to be a fixed number $N_B > 0$, and thus the length function $\phi(A) = [A : B]N_B$ can be defined. This measurement function guarantees that $A \succ A'$ if and only if $\phi(A) > \phi(A')$. Moreover, ϕ is also a semigroup homomorphism, i.e. $\phi(A + A') = \phi(A) + \phi(A')$.

Before the 1950s other trials were conducted. Following Hölder, Nagel in [NH31] proposed a 12-axiom formalization on the empirical quantity and was important in this period for the efforts in mathematical formalization. Meanwhile, individually S. S. Stevens approached the representation model through his research on auditory sensation. In [Ste36] and [SVN37], he realized not only such measurements are needed to be reflecting relations of being greater or smaller, but also scales for the concrete sensational magnitude. For example, $N/2$ should represent half of the loudness of N (p. 407 [Ste36]). This is not simple. Representation theorist N. R. Campbell, believed measurements, like Mohs' hardness or density, without intrinsic additivity or concatenation are "not satisfactory" [Cam57][Cam40]; and his idea can be translated as a negative statement on the existence of certain scales. Stevens in [Ste46] bypassed this point by proposing scales that keep statistical invariants, for example, the "interval scale" keeps

the mean and standard deviation. Although this statistical approach was still primitive, Stevens' work successfully loosened the firm bond of the concatenation operation $+$ (which can also be represented by a relation) on the rods and the relation $\succ$ of being longer. Thus, instead of being less satisfactory as claimed by Campbell, lacking additivity in hardness measurement is merely because there is no canonical definition of the additive relation on $\langle M, \succ \rangle$ where M is the set of all materials and $\succ$ represents the relation of being harder than.

Into the 1950s the development of representation models of measurement accelerated. Patrick C. Suppes, a student of Nagel in 1951 pointed out two limitations of Hölder's theory [Sup51]. Suppes believes that Hölder imposed too strong restrictions on the relations and treated identity too simply which in return suppressed the prosperity of different measurement types. Later in [SW55], an axiomatization of difference structure with 2 relations was proposed and the existence of representation (measurement function) was proven. In [SS58], Suppes and Winet generalized the concept of representation of measurement to be homomorphisms between structures of finite relations and this is the early model of modern representation theory of measurement. In [SZ62], Suppes and Zinnes addressed two fundamental problems of measurement, i.e. the existence of representation, and uniqueness of representation. Nine years after [SZ62], the first volume of *Foundations of Measurement* [KSL71] was published and it summarizes the 80-year efforts of developing representational measurement theory. Now the thesis will mainly follow [KSL71][SZ62] and [SS58] to give a concise review of measurement as representations.

A *relational structure* $\mathfrak{A} = \langle A, R_1, \ldots, R_n \rangle$, consists of a non-empty set A, and relations R_i on $\prod_{j=1}^{n_i} A$. For example, Hölder's $\mathfrak{H}$ in equation (2.1) is a relational structure where the concatenation "$+$" can be regarded a ternary relation on $S \times S \times S$ that $\{(a, b, c) | \text{the length of rod } c \text{ equals to the length of concatenation of rod } a \text{ and rod } b\}$. Assume that R_i is an m_i-ary relation, and let $s = \langle m_1, \ldots, m_n \rangle$; then $\mathfrak{A}$ is of *type* s. Given another relational structure $\mathfrak{B} = \langle B, S_1, \ldots, S_n \rangle$ that is of the same type as $\mathfrak{A}$, then a mapping $\phi : A \to B$ is a *homomorphism* (or *scale*) if ϕ keeps all the relations, i.e.

$$R_i(a_1, \ldots, a_{m_i}) \Longleftrightarrow S_i(\phi(a_1), \ldots, \phi(a_{m_i})) \quad \forall i = 1, \ldots, n, \forall (a_1, \ldots, a_{m_i}) \in R_i$$

A relational structure is *numerical* if the underlying set is $\mathbb{R}$, the real number, otherwise *empirical*. Thus measurement as a process of assignment of numbers to quantities [BIP+09][Car66][MR95] can be regarded as construction of homomorphisms from an empirical relational structure to a numerical relational structure [KSL71]. Now let $\mathfrak{A}$

be an empirical relational structure and $\mathfrak{B}$ be a numerical relational structure and ϕ, ϕ' be homomorphisms from $\mathfrak{A}$ to $\mathfrak{B}$. A mapping T is a *permissible transformation* of ϕ if the diagram

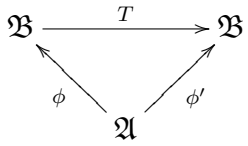

is commutative. Let $\mathcal{T}_\phi$ denote the set of all permissible transformations of ϕ, and this $\mathcal{T}_\phi$ describes the type of scale of ϕ. For example, if all $T \in \mathcal{T}_\phi$ are of the form that $T(x) = \alpha_T x$ for some $\alpha_T > 0$, then ϕ is of *ratio scale*. If all $T \in \mathcal{T}_\phi$ are of the form $T(x) = \alpha_T x + \beta_T$ where $\alpha_T > 0$, then ϕ is of *interval scale*. Finally if all $T \in \mathcal{T}_\phi$ are monotonically increasing, ϕ is of *ordinal scale*. This classification of scales contains the scale types that Stevens proposed in [Ste46]. For example, any $\phi_{N_B}(A) = [A : B]N_B$ from Hölder's $\mathfrak{H}$ to $\langle \mathbb{R}, >, =, + \rangle$ is a ratio scale, because by Theorem 4 of §2.2 of [KSL71] it is true that for every homomorphism $\phi' : \mathfrak{H} \to \langle \mathbb{R}, >, =, + \rangle$, there exists $\alpha > 0$ such that $\phi' = \alpha\phi_{N_B} = \phi_{(\alpha N_B)}$. If one drops the concatenation operation in $\mathfrak{H}$, then homomorphisms like $\phi_e(A) = \exp(\phi_{N_B}(A) + 1)$ exist, and one finds $T(x) = \exp(x + 1) \in \mathcal{T}_{\phi_{N_B}}$. This means that ϕ_{N_B} cannot be ratio scales, but only ordinal (Theorem 2, §2.1 of [KSL71]). Without diving deeply into the topic, the two fundamental problems of measurement [SZ62] can be briefly stated as to prove the existence of representation (homomorphism) and to find out the set of all permissible transformations (uniqueness).

There are many interesting examples under the representation framework of measurement. Luce's semiorder relation proposed in [Luc56], where quantities, instead of being considered as exactly equal to each other, are allowed to be "indifference" to each other, is nowadays known as representations with thresholds. In Falmagne's [Fal76][Fal80], and later Rossi's [Ros14] a relation is proposed in a probabilistic framework and sometimes this is referred to as representation of random variables (§16.8 of [SK06]). The idea is that after repeated observations on two given objects x, y, the probability $P(x, y)$ of preference or indifference of x to y can be obtained. Then a representation ϕ should somehow keep this empirical observation, that is, $P(x, y) \geq \frac{1}{2}$ if and only if $\phi(x) \geq \phi(y)$. It is also possible to view this in a way that this repeated observation induces a relation on the set that $x \succeq y$ if and only if $P(x, y) \geq \frac{1}{2}$ [Fal80], or in a way that $x \succeq y$, instead of merely being a relation, is an event to which a probability can be assigned or observed [Ros14]. Different stochastic transitivity assumption can be imposed so that the relation induced by $P(x, y)$ become transitive, for example, the

weak stochastic transitivity asserts that $P(x,y) \geq \frac{1}{2}, P(y,z) \geq \frac{1}{2}$ implies $P(x,z) \geq \frac{1}{2}$. With proper axiomatization, various structures and representations become possible, see [Deb58] and [Fal80] for examples.

Finally, a concise introduction to the measurement process under the probability framework is included here. Rossi in [Ros03] and later with Cox in [Cox+08] proposed the idea that when a measurement system is modelled as a function $y = f(x)$ where x is the (scalar) quantity of the measurand and y the observation then a general measurement process should consist of observation and restitution. For example, a measurement system for the length of the rod takes the (length of) rod as input and the numeric reading as output. Then observation is a process where the output $y = f(x)$ is obtained and the restitution is the process to solve the original quantity $\widehat{x} = f^{-1}(y)$. Generally speaking, $\widehat{x} \neq x$ and f^{-1} may fail to exist. When quantities are considered as random variables, the observation $y = f(x)$ can be extended to the conditional probabilistic formation $P(y|x)$. When $P(y|x)$ is of Dirac distribution, it degenerates to the deterministic case. The restitution can then be formulated as $P(x|y)$ and is linked with $P(y|x)$ by Bayesian's theorem. From this point of view, the measurement model proposed in this thesis uses the tool of statistics and shares some common ideas of this framework.

2.2 Distance/Length Measurement

A review for some existing and widely used methods for distance/length measurement will be conducted in this section. Starting with the definition of the metre, which once was based on the international prototype of platinum-iridium, is now defined as the length of the path traveled by light in vacuum during a time interval of $1/299792458$ second [BIP06]. Compared to the historic definition using a prototype, the modern definition is a physical constant which is irrelevant to exterior conditions like temperature. As a result, reproduction processes are made universal and impartial everywhere in the world. Without diving too deep into the technological details and variations of each method, brief reviews will be given for interferometers and laser triangulations. Finally, a short subsection about standard sequences will be included which draws the attention back to theoretic considerations and tries to tie to the realist origin where a result of distance/length measurement is written as a combination of magnitude and chosen unit. The review and analysis conducted in this section clarify the position of this thesis.

2.2.1 Interferometry

Light is an effective tool in length measurement for various scales, for example, optical radars for distances larger than 10km, intensity modulated beams for distances from about 100m to about 50km, and interferometric techniques for distances up to 50m in the free air [Son72]. Interferometric methods are usually known for their high precision in micro-/nano-manufacturing. It is also possible to use them for measurement of large objects, for example, [BH69] uses Moiré patterns to analyze the deformation of large turbine blades. The common knowledge about optics used in this section mainly follows [Hec16]; for more detailed facts about interference, one can refer to additional materials like [Har16] and [Yos09]. The meaning of most of the symbols used here for interferometry will be restricted to this subsection, and may be of different meaning outwith according to the context.

Express the electric field of light of wavelength λ in vacuum by

$$E(z,t) = A_0 \exp\left(2\pi\sqrt{-1}(ft - \frac{z}{\lambda})\right)$$

where A_0 denotes the amplitude of the electric field, z the physical path length,and f the oscillation frequency. Then up to a constant, the irradiance I is computed as $I = EE^* = A_0^2$, where E^* is defined as the conjugate of E. Consider the superposition of two light beams

$$E_i(z,t) = A_i \exp\left(2\pi\sqrt{-1}(ft - \frac{z_i}{\lambda})\right)$$

at one point in space, the irradiance is

$$I = (E_1 + E_2)(E_1 + E_2)^* = I_1 + I_2 + 2\sqrt{I_1 I_2}\cos\left(\frac{2\pi}{\lambda}(z_1 - z_2)\right). \tag{2.2}$$

Shown by equation (2.2), the irradiance is periodic to the difference of length of the path traveled by the light beams. This is the principal ideal behind the phase-shifting interferometer (PSI). Fig. 2.1 shows a typical Michelson type interferometer device, where $2L$ equals to the difference of length of path. Thus equation (2.2) can be rewritten as

$$I(\lambda, L) = I_A(\lambda) + I_B(\lambda)\cos\frac{4\pi L}{\lambda} \tag{2.3}$$

where $I_A = I_1 + I_2$ and $I_B = 2\sqrt{I_1 I_2}$. Thus the change of irradiance reflects a change in phase $\varphi = \frac{4\pi L}{\lambda}$ and ultimately encodes the change of L. The irradiance of each pixel of a camera is described by equation (2.3), and all pixels together form various

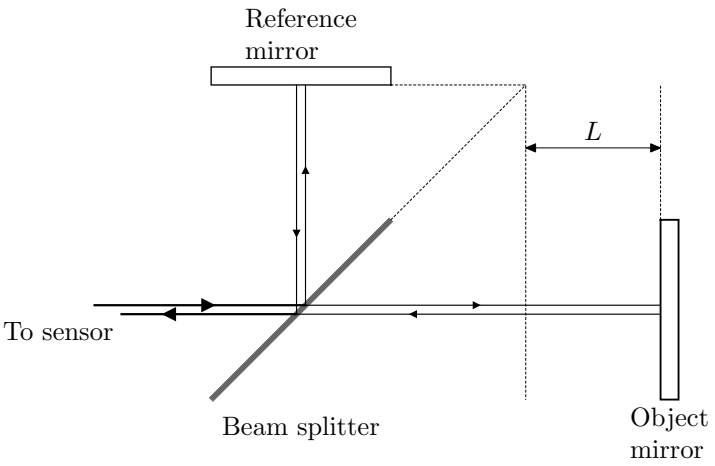

Figure 2.1: Michelson type interference (from [Har16])

interference fringes. The period of equation (2.3) is $\frac{\lambda}{2}$, which means that any gradual change within $\frac{\lambda}{4}$ can be detected without ambiguity and sudden changes larger than $\frac{\lambda}{4}$ causes ambiguity in determining the phase (fringe order) [Wya02][Har16]. It is possible to enlarge the unambiguity range by using two different wavelengths. The theoretic irradiance of two light beams of wavelengths λ_1, λ_2, polarized perpendicular to each other, is

$$\begin{aligned} I_{\lambda_1,\lambda_2} =& I(\lambda_1, L) + I(\lambda_2, L) \\ =& I_A(\lambda_1) + I_A(\lambda_2) \\ &+ \sqrt{(I_B(\lambda_1) + I_B(\lambda_2)\cos\Delta)^2 + (I_B(\lambda_2)\sin\Delta)^2}\cos\left(\frac{4\pi L}{\lambda_1} + \psi\right) \end{aligned} \tag{2.4}$$

where $\Delta = (\frac{4\pi}{\lambda_2} - \frac{4\pi}{\lambda_1})L$, and ψ is chosen in a way such that

$$\tan\psi = \frac{I_B(\lambda_2)\sin\Delta}{I_B(\lambda_1) + I_B(\lambda_2)\cos\Delta}.$$

If $I_B(\lambda_2) = I_B(\lambda_1) = I_B$, then equation (2.4) has a simpler form

$$I_{\lambda_1,\lambda_2} = I_A(\lambda_1) + I_A(\lambda_2) + 2I_B\cos\left(2\pi L(\frac{1}{\lambda_1} - \frac{1}{\lambda_2})\right)\cos\left(2\pi L(\frac{1}{\lambda_1} + \frac{1}{\lambda_2})\right) \tag{2.5}$$

Thus the modulation represented by equations (2.4) and (2.5) permits any sudden changes smaller than $\frac{1}{4}\frac{\lambda_1\lambda_2}{|\lambda_1-\lambda_2|}$ in both directions of depth [Wya02][Mei+09]. Systematic study on synthetic lights using two wavelengths is seen in works like [Mat86], and research on encoding using three lights can be found in [MS05]. For long range measurements up to several metres, implementation is by moving the objective lens and recording the total numbers of valley-peak alternation of one or several pixels on the camera. Then the estimation of displacement with a resolution of $\frac{\lambda}{2}$ becomes possible, and this

kind of displacement measuring interferometer (DMI) is found appropriate for many low-precision applications [Har16].

White light interferometry is one of the interesting variations that overcomes the fringe order problem. Wyant in [Wya02] reported three different white light interferometers; and in the following a brief introduction to the vertical scanning white light interferometer (SWLI) will be included. Although Mirau and Linnik objective lenses are widely used for medium-high magnification cases [Har16], it is possible to make explanation of the principle of SWLI using a Michelson type interference device [LS90]. When using timely incoherent white light, I_A and I_B in equation (2.3) are distributed in a wide range, and the overall irradiance is computed as

$$I(L) = \int \rho(\lambda) I(\lambda, L)\,\mathrm{d}\lambda \tag{2.6}$$

where $\rho(\lambda)$ is the probability density function and L is the optical path difference. Suppose that ρ is finite and distributed in a finite interval $[\lambda_a, \lambda_b]$, that is, ρ is bounded and compactly supported. Assume that I_B is continuous on $[\lambda_a, \lambda_b]$. This is reasonable because sensors have finite dynamic range and people usually possess an interest in some certain range, for example visible lights. Thus $I(L)$ is symmetric to the line $L = 0$. Let $\overline{I_A} = \int_{\lambda_a}^{\lambda_b} \rho(\lambda) I_A(\lambda)\,\mathrm{d}\lambda$ be the expectation and $B_n(\rho I_B)(\lambda)$ be the n^{th}-order Bernstein approximation of $\rho(\lambda) I_B(\lambda)$ on the interval $[\lambda_a, \lambda_b]$. Then it holds true that

$$\begin{aligned}
\lim_{L\to\infty} (I(L) - \overline{I_A}) &= \lim_{L\to\infty} \int_{\lambda_a}^{\lambda_b} \rho(\lambda) I_B(\lambda) \cos\frac{4\pi L}{\lambda}\,\mathrm{d}\lambda \\
&= \lim_{L\to\infty} \lim_{n\to\infty} \int_{\lambda_a}^{\lambda_b} B_n(\rho I_B)(\lambda) \cos\frac{4\pi L}{\lambda}\,\mathrm{d}\lambda \\
&= \lim_{n\to\infty} \lim_{L\to\infty} \int_{\lambda_a}^{\lambda_b} B_n(\rho I_B)(\lambda) \cos\frac{4\pi L}{\lambda}\,\mathrm{d}\lambda \\
&= 0.
\end{aligned}$$

This means that the variation of irradiance disappears as the the optical path difference goes larger and the white light interference is obvious only when the optical path difference is small. This enveloping signal has been observed by many scholars and is the foundation of SWLI (Fig. 2.2). Deck and Groot in [DG94] proposed an implementation of SWLI with a dedicated design for high-speed data process, and recently Gao in [GTJ13] used a diffracting grating with GPGPU for real-time realization. Detailed analysis of precision and error of commercial SWLI devices are conducted by Gao et al. in [Gao+08].

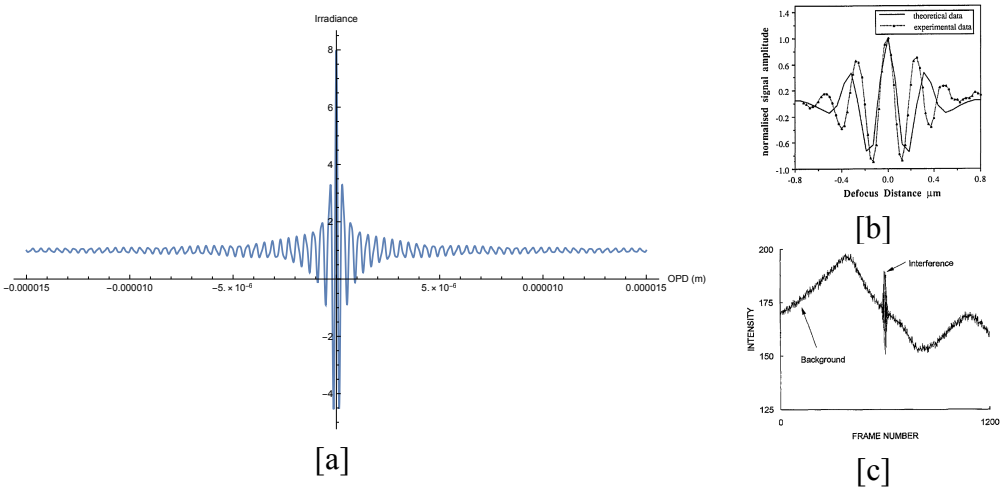

Figure 2.2: White light interference intensity: **[a]** computation using equation (2.6) with uniform distribution of light in $[380\text{nm}, 800\text{nm}]$ and $I_A = 1, I_B = 7$ a.u.; **[b]** theoretic computation and experiment result by Kino and Chim in [KC90]; **[c]** intensity captured in a 100μm vertical scan with background signal by Deck and Groot in [DG94]

By equation (2.3), it is true that the light irradiance changes if λ changes and this is the foundation of wavelength scanning interferometry (WSI). From (2.3), the change of phase corresponding to a wavelength change can be expressed

$$\Delta\varphi = 4\pi L\left(\frac{1}{\lambda} - \frac{1}{\lambda + \Delta\lambda}\right)$$

and this implies

$$\frac{\mathrm{d}\varphi}{\mathrm{d}\lambda} = \frac{4\pi L}{\lambda^2}$$

Early works like [KIN86], modulated the wavelength by adjusting the injection current. Later Kuwamura and Yamaguchi in [KY97] implemented a real-time WSI by computing the number of 180° phase changes and scans were made in a range of 25nm wavelengths. Wang et al in [Jia+10] used an acousto-optic tunable filter (AOTF) to select specific wavelength and the scanning wavelength range was from about 530nm to 680nm. Recently in [Muh13], the use of CUDA for acceleration of data processing is seen and is proven to be about 20 times faster than processing by Matlab.

2.2.2 Laser Triangulation

The basic principle of laser triangulation is that by setting laser beams, camera and the object being measured in dedicatedly designed positions, then the position of the

captured laser spot on the object surface encodes the position of the laser spot on the object surface in the real world and it is possible to retrieve the real-world coordinate from the sensor coordinate via computation. In the following, a brief introduction to the principle will be included, and the symbols used here for triangulation will be restricted to this subsection.

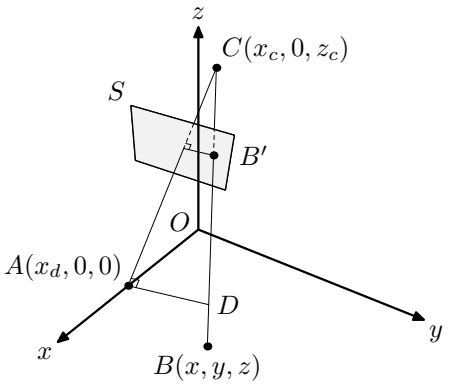

Figure 2.3: Laser triangulation model

Fig. 2.3 shows the basic setup of a typical laser triangulation device. Let O-xyz be the real-world coordinate system and O'-$x'y'$ be the coordinate system of the camera. For simplicity, the camera is assumed to be of pin-hole type. Let S denote the plane of the image sensor of the camera. The camera is set in a way that C, the pin hole of the camera, is at $(x_c, 0, z_c)$, and that the x'-axis is parallel but opposite to the y-axis. Let point A of coordinate $(x_d, 0, 0)$ be the intersection of CO' and the x-axis. Let B of coordinate (x, y, z) be the laser spot on the object surface, and assume B' of coordinate (x', y') be point captured by the camera. Let D be a point on line BC such that $AD \perp AC$, then the coordinate of B' can be computed as follows. Firstly compute $\overrightarrow{OD}$ by

$$\begin{aligned}\overrightarrow{OD} =& \overrightarrow{OC} + \overrightarrow{CD} = (x_c, 0, z_c) + \frac{\left|\overrightarrow{CA}\right|}{\left|\overrightarrow{CB}\right|} \frac{\overrightarrow{CB}}{\cos \angle BCA} \\ =& (x_c, 0, z_c) + \frac{(x_d - x_c)^2 + z_c^2}{(x - x_c)(x_d - x_c) - z_c(z - z_c)} (x - x_c, y, z - z_c) \\ =& (x_1, y_1, z_1)\end{aligned}$$

where placeholders x_1, y_1, z_1 are functions of x, y, z. Let d be distance of point C to

plane S, then by the fact that $\triangle CO'B'$ is similar to $\triangle CAD$, it holds that

$$\begin{aligned} -\frac{x'}{y_1} &= \frac{d}{\sqrt{(x_d - x_c)^2 + z_c^2}} \\ \frac{y'}{\frac{z_c}{\sqrt{(x_c - x_d)^2 + z_c^2}}(x_1 - x_d) + \frac{-x_c + x_d}{\sqrt{(x_c - x_d)^2 + z_c^2}} z_1} &= \frac{d}{\sqrt{(x_d - x_c)^2 + z_c^2}} \end{aligned} \tag{2.7}$$

Although equations (2.7) look complicated, after simplification both x' and y', as functions of x, y, z, are of the form

$$\frac{k_1 x + k_2 y + k_3 z + k_4}{k_5 x + k_6 y + k_7 z + k_8} \tag{2.8}$$

If the laser beam is vertical to the xOy plane, then x, y are known and one can use x', y' to retrieve z, the height information. If the laser beam is arbitrary, then equations (2.7) together with the line equation representing the laser beam give adequate information to solve x, y, z, the coordinate of the laser spot.

A laser triangulation system usually requires calibration and adjustment before use [Tru+98][Wan+02][San+11]. Nowadays, compact units of laser triangulation sensor are sold by many companies, and this design enables much easier installation for industrial usage. Variations of the laser triangulation are also abundant. Davis and Chen in [DC01] used mirrors and achieved a stereo sampling. To cover the shadowed area, the use of a multi-camera system is seen in [Tru+98]. Zhang et al. in [ZCS02] used structured light and provided a quick way to retrieve data in a large area. Meanwhile, Hartley in a series of works ([Har93][Har95][HS97b]) conducted serious discussions on the mathematics behind the triangulation method, especially for the retrieval of real-world coordinates from rational polynomial cameras.

The validation of PBM proposed in this thesis is conducted using a commercial laser triangulation sensor attached to a 3-axes gantry system, which is developed in the University of Strathclyde for the EU Micro-Fast project.

2.2.3 Standard Sequences

Length is a typical *extensive measure*, which means that it naturally possesses a concatenation operation on the quantity (chapter 3 of [KSL71]). Length measurement methods, from simple ones like a ruler to the complicated ones like triangulation, at some step utilize "discrete scales" in various forms from carved marks to pixels or other electric signals. This kind of scale is known as standard sequences in the representation view

of measurement; and in the following a brief introduction will be given using the example of rods. Suppose there are perfect copies of a chosen rod A, and recursively one can define $1A = A$ and $nA = (n-1)A + A, n \geq 2$ where $+$ is the operation of concatenation. Then the sequence of $A, 2A, 3A, \cdots$ is called a *standard sequence* on A [KSL71]. This construction is commonly seen in works of many representation theorists [Hel87][Höl01][Sup51]; and usually the construction of standard sequence is the first step of proving the existing of an extensive representation[Höl01][Sup51][Fal02]. Now for another given rod B, there exists $n \in \mathbb{N}$ such that $(n+1)A \succ B \succeq nA$. The special case $n = 0$ represents the fact that B is shorter than A. The existence and uniqueness of such n, also known as the Archimedean axiom, either comes from pragmatic experience, or guaranteed by certain axioms in representation theories. For example, Definition 2 in §2.2.1 of [KSL71] explicitly includes the Archimedean property as an axiom; while instead of explicit definition, the Archimedean property can be deduced from Hölder's axiomatization in [Höl01]. Henceforth the discussion assumes the Archimedean property; and for any given measure ϕ it implies that

$$(n+1)\phi(A) > \phi(B) \geq n\phi(A). \tag{2.9}$$

When $\phi(A) = 1\text{mm}$, equation (2.9) essentially reflects the daily scene of length measurement using a metre steel ruler. Let $\mathfrak{n}(A, B) \in \mathbb{N}$ denote the integer such that equation (2.9) holds true. Sometimes a standard sequence is also known as a scale [Fal02].

In a scale defined by certain standard sequence, the discrepancy is defined as

$$d(A, B) = \phi(B) - \mathfrak{n}(A, B)\phi(A), \tag{2.10}$$

and it holds true that $0 \leq d(A, B) < \phi(A)$. To minimize discrepancies, Falmagne in [Fal02] proposed two general methods. If there are perfect copies of B, then instead of measuring directly B, one could measure mB. Thus $d(A, mB) < \phi(A)$ and it implies that $d(A, B) < \frac{1}{m}\phi(A)$. Ideally, the discrepancy can be suppressed arbitrarily small by choosing sufficiently large m. The other approach assumes that the unit can be refined, that is, instead of using A, one could use $A_n = \frac{A}{n}$ which essentially means a rod whose length is $\frac{1}{n}$ of that of A. Thus $d(A_n, B) < \phi(A_n) = \frac{1}{n}\phi(A)$. These two approaches are widely adopted nowadays. For example, when measuring spatial wavelengths, people measure the distance covering several periods; and a vernier caliper is a tool using finer units. The limitations and constraints of these methods are obvious. It is not possible to find perfect copies of the measurand B, and the refinement on the unit A stops quickly

because of the physical restriction. In addition, as pointed out by Falmagne in [Fal02], an error in measurement usually makes the reading indeterministic. For example, when $\phi(A)$ is very small, it becomes common that one finds 17 times that $\mathfrak{n}(A, B) = 990$ and 3 times $\mathfrak{n}(A, B) = 989$ after 20 observations.

2.3 Knowledge Gaps and the Root of the Challenge

Suppes in [SK06] pointed out that instead of a number, $\mathfrak{n}(A, B)$ should be treated as a random variable. But he criticizes this random variable representation as having "so little variability that they do not perturb the calculations seriously". Similar critics are found in Falmagne's work (p282 [Fal80]) as he believed that some benefits can be derived from $P(a, b)$, the probability of preference or indifference, in the sense of finer grading of objects to be measured, but "the puzzle is not very deep and disappears when one realizes that the added precision is derived essentially from averaging results over trials". Suppes further pointed out (p361 [SK06]) that refinement of measurement should be involving both a finer sequence and also the discovery of a method that produces the random variable $\mathfrak{n}(A, B)$ in a way that the coefficients of variation are markedly reduced. And by these reasons Suppes believes that purely averaging (converges in probability) is not unduly optimistic and hence such measurement needs careful examination empirically.

Focusing on the length/distance measurement, this thesis creates a stir in Falmagne's comments and tries to make developments bypassing Suppes' thought. The new probabilistic approach proposed in this thesis provides improvement to precision by manipulating the random variable $\mathfrak{n}(A, B)$ without the need of finer standard sequences (scales). The method itself does not average the reading. Indeed Theorem 3.1 states that without certain priori knowledge the mean always contains unknown systematic error and Example 3.6 demonstrates this phenomenon. The PBM approach treats p_h, p_l, the probabilities of high/low reading as signals, which are defined in chapter 3; and with the tool of probability and statistics the precision of length measurement can be greatly improved.

3 Probability-Based Method and Core Theory

In this chapter, the core theory and the PBM approach are presented addressing a very specific problem (Problem 3.1). To quickly reveal the essence of the theory and the probability-based method of measurement, realistic considerations are simplified and assumptions are put to provide an ideal base where unnecessary distractions are eliminated. Discussions for real-world obstacles that are commonly found in laboratory and productive environments are postponed until chapter 4 after the establishment of the method and the core theory. Henceforth the classic and deterministic measurement framework will be adopted; because it dominates the practical and production scenarios of measurements and inspections. Some of the thoughts and rationale conducted by the author is included in this thesis as Appendix D.

The problem this thesis tries to solve is stated as follows. Given a line segment AB that is claimed to be of length l_n with tolerance $\pm T$, find whether this claim is true or not. The available tool is a ruler, longer than AB and with continuously adjustable scales that the finest possible scale is still larger than T. All operations for measurement are restricted to a simple dimension, the direction of the line segment AB. A concrete version of the problem is stated below:

Problem 3.1. A line segment AB is claimed to be of length 150mm with tolerance ± 0.4mm. Given a ruler of total length 200mm with scale marks adjustable in the range $[2, 4]$mm, find out whether the claim is true. □

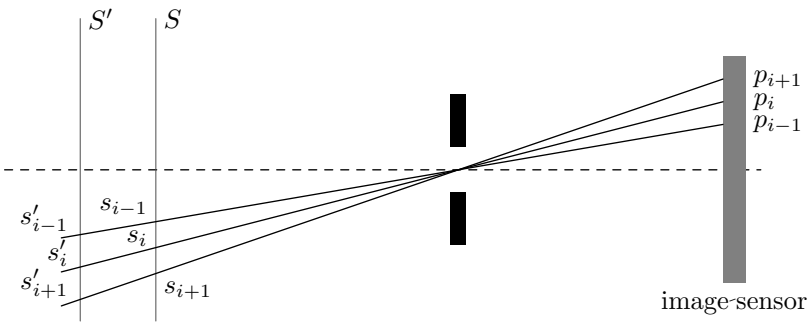

Figure 3.1: Pinhole camera

At first glance, a ruler with "adjustable scales" might sound other-worldly; indeed, many sensors and devices fulfill this assumption. Fig. 3.1 illustrates a pinhole camera that is commonly found in modern vision systems. Adjacent pixels p_i, p_{i+1} on the image sensor represent different real-world distance when the reference plane changes,

for example, $\left|s'_i s'_{i+1}\right| > |s_i s_{i+1}|$ as shown by Fig. 3.1. If pixels are regarded as carved marks on the ruler, then the scale is adjustable once the distance between the reference plane and the image sensor can be manipulated.

3.1 The Classic Approach

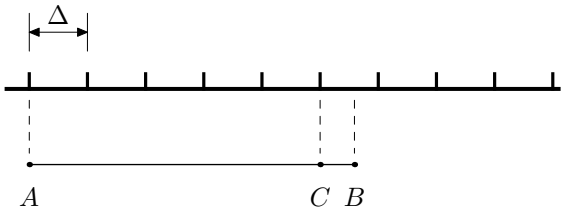

Figure 3.2: Measurement with ruler, the classic approach

The classic approach is briefly introduced in this section. Fig. 3.2 illustrates the scenario where one end of the line segment (measurand) is aligned to a carved mark on the ruler. Let the size of the scale of the ruler be Δ. Then by observation, it is easy to see that AB is covered by 6 scales and fully covers 5 scales. Let AC be the part of the line segment which fully covers scales. $|AC|$, the length of AC, is read 5Δ. For the part of CB, the rounding process is usually subject to the judge of the inspector, that is, if it is observed to be covering more than half of a scale, then $|CB|$ is read Δ otherwise 0Δ. Depending on the rounding, the reading of $|AB|$ can be either 6Δ or 5Δ.

If the rounding process is always perfectly conducted, it can be deduced from the measurement procedure that the error is within the range $(-\frac{\Delta}{2}, \frac{\Delta}{2}]$. To eliminate the human intervention, a slight modification of the procedure can be made by directly assigning the length of AB to be $|AC| + \frac{\Delta}{2}$. Mathematically it means that the measurement m_c, as a real-valued function, is defined as

$$m_c(AB) = |AC| + \frac{\Delta}{2} = \lfloor \frac{|AB|}{\Delta} \rfloor \Delta + \frac{\Delta}{2}, \tag{3.1}$$

where $\lfloor x \rfloor$ denotes the largest integer smaller than or equal to x. Then the error is by definition within the range $(-\frac{\Delta}{2}, \frac{\Delta}{2}]$ and the whole procedure is more deterministic than the rounding process. One fact is that the result of measurement m_c will always be with a fraction $\frac{\Delta}{2}$. Using the symbols from section 2.2.3 for standard sequences, $\lfloor |AB| / \Delta \rfloor$ is an explicit expression of $\mathfrak{n}(\Delta, |AB|)$.

Looking back into Problem 3.1, the above discussion shows that the range of error will be within $(-1, 1]$ mm using the finest scale. While the tolerance range is ± 0.4mm, it is not possible to solve the problem in the classic way.

3.2 An Alternative Approach

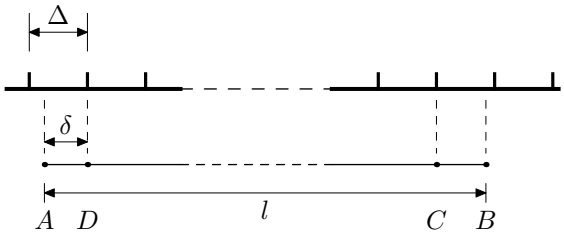

Figure 3.3: Measurement under random alignments

Now consider another approach to Problem 3.1. Fig. 3.3 illustrates a scenario where no end of line segment is aligned to any of the carved marks on the ruler. Let δ denote the length of AD which represents the left ending of the line segment that is not fully covered by a scale. The theory can be developed with no difference if δ is defined to be $|CB|$. Scales that are fully covered by the line segment will be called *full*. For example, scales between CD on Fig. 3.3 are full. Scales that are only partially covered by the line segment will be called *loose*, for example, the ones on Fig. 3.3 covering AD and CB. This non-aligned scenario is commonly seen in various application, especially when fixture of specimen is hardly possible.

By definition $\delta \in [0, \Delta)$, and the length of CD is

$$|CD| = \lfloor \frac{l-\delta}{\Delta} \rfloor \Delta. \tag{3.2}$$

If $|CD|$ is assigned to be the result of measurement of $|AB|$, then the error is

$$l - \lfloor \frac{l-\delta}{\Delta} \rfloor \Delta, \tag{3.3}$$

which is within the range $[0, 2\Delta)$. To balance the interval, a modified version of the measurement assignment function is adopted as follows

$$m(AB) = \lfloor \frac{l-\delta}{\Delta} \rfloor \Delta + \Delta. \tag{3.4}$$

Thus the error

$$e(AB) = |AB| - m(AB) = l - (\lfloor \frac{l-\delta}{\Delta} \rfloor \Delta + \Delta) \tag{3.5}$$

lies within $[-\Delta, \Delta)$.

Now the discussion advances with the presumption that δ is actually a random variable valuing on the interval $[0, \Delta)$. That is, δ is a measurable function from some probability space $(\Omega, \mathcal{F}, \mu)$ to $(\mathbb{R}, \mathcal{B}(\mathbb{R}), \mu_L)$, where $\mathcal{B}(\mathbb{R})$ denotes the Borel σ-algebra on $\mathbb{R}$

and μ_L the Lebesgue measure. At this point no specific restriction is put on $(\Omega, \mathcal{F}, \mu)$. Let P_δ be the probability distribution function of δ, that is, $P_\delta = \mu\delta^{-1}$ a measure on $(\mathbb{R}, \mathcal{B}(\mathbb{R}))$.[1] For the source of randomness of δ, refer to section 4.3 in chapter 4.

Because $\lfloor\cdot\rfloor : \mathbb{R} \to \mathbb{R}$ is measurable, it implies that both $m(AB)$ and $e(AB)$ are random variables. By changing the variables the expectations are

$$E(m(AB)) = \int_{[0,\Delta)} \left(\lfloor \frac{l-\delta}{\Delta} \rfloor \Delta + \Delta \right) \mathrm{d}P_\delta \tag{3.6}$$

$$E(e(AB)) = \int_{[0,\Delta)} \left(l - \lfloor \frac{l-\delta}{\Delta} \rfloor \Delta - \Delta \right) \mathrm{d}P_\delta \tag{3.7}$$

$$= l - E(m(AB)) \tag{3.8}$$

Now both $E(m(AB))$ and $E(e(AB))$ are functions of Δ; and re-write $E(m(AB))$ as $E_{AB}(\Delta)$. As a remark, P_δ is also a function of Δ, and let it be denoted by $P_{\delta,\Delta}$ whenever clarification is needed. The most important property of this function is that:

Theorem 3.1. *Let $E_{AB}(x)$ be defined as above, if*

(a) $P_{\delta,x}$ is absolutely continuous with respect to μ_L, the Lebesgue measure,

(b) the mapping $\Phi : \mathbb{R}_+ \to L^1(\mathbb{R}, \mu_L)$ by $\Phi : P_{\delta,x} \mapsto h_x$ is continuous, where h_x is the Radon-Nikodym derivative $\frac{\mathrm{d}P_{\delta,x}}{\mathrm{d}\mu_L}$;

then

(I) $E_{AB}(x)$ is continuous in $(0, \frac{l}{2})$,

(II) $E_{AB} = l$ at each $x = \frac{l}{N}$ where $N \in \mathbb{Z}, N \geq 2$.

Before proving the theorem, some remarks will be put on the conditions in Theorem 3.1. The first condition that $P_{\delta,x}$ is absolutely continuous with respect to μ_L excludes the cases where P_δ is discrete. For example, consider P_1 whose cumulative distribution function (CDF) is

$$F_1(x) = \begin{cases} 0 & x < \frac{\Delta}{2}, \\ 1 & x \geq \frac{\Delta}{2}. \end{cases}$$

It represents the case that δ is of Dirac distribution. In the real world, it means that this δ "loses" randomness and every time the line segment AB has A aligned at the middle of two carved marks.

[1] The theory works for both Borel σ-algebra and the Lebesgue σ-algebra. In the following, the boundary is blurred unless distinction must be made.

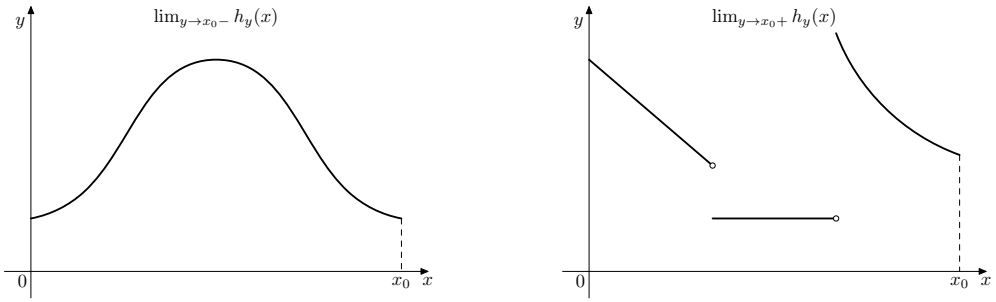

Figure 3.4: Abrupt change of distribution

The second condition on continuity of Φ expresses the fact that the deformation of $P_{\delta,x}$ over x must be gradual. Cases of abrupt changes as shown in Fig. 3.4 are excluded by this condition. The thought behind this assumption is that the randomness of δ should be consistent in a given system and environment. For example, by saying that δ is uniform, one expresses the expectation that this property of being uniform is true however the scale is adjusted, or explicitly

$$h_y(x) = \begin{cases} \frac{1}{y} & x \in [0, y), \\ 0 & \text{elsewhere.} \end{cases}$$

for all $y > 0$. In this case, the continuity of $y \mapsto h_y$ is obvious. More complicated cases, like the truncated Gaussian distribution or the Beta distribution (with proper parameters), condition (b) is automatically satisfied; and this condition is not too strong.

Proof of Theorem 3.1. Firstly we show that $E_{AB}(x)$ is continuous in $(\frac{l}{N}, \frac{l}{N+1}), \forall N \in \mathbb{Z}, N \geq 2$. Because $E_{AB}(x) = \int_{[0,x)} \lfloor \frac{l-\delta}{x} \rfloor x \, \mathrm{d}P_\delta + x$, it is enough to show that

$$f(x) = \int_{[0,x)} \lfloor \frac{l-\delta}{x} \rfloor x \, \mathrm{d}P_{\delta,x}$$

is continuous. For any $x_0 \in (\frac{l}{N+1}, \frac{l}{N})$, we have

$$\begin{aligned} \lim_{\Delta x\to 0} f(x_0+\Delta x) &= \lim_{\Delta x\to 0} \int_{[0,x_0+\Delta x)} \lfloor \frac{l-\delta}{x_0+\Delta x} \rfloor (x_0+\Delta x) \, \mathrm{d}P_{\delta,x_0+\Delta x} \\ &= \lim_{\Delta x\to 0} \int_{[0,x_0)} \lfloor \frac{l-\delta}{x_0+\Delta x} \rfloor x_0 \, \mathrm{d}P_{\delta,x_0+\Delta x} \\ &\quad + \lim_{\Delta x\to 0} \int_{[0,x_0)} \lfloor \frac{l-\delta}{x_0+\Delta x} \rfloor \Delta x \, \mathrm{d}P_{\delta,x_0+\Delta x} \\ &\quad + \lim_{\Delta x\to 0} \int_{[x_0,x_0+\Delta x)} \lfloor \frac{l-\delta}{x_0+\Delta x} \rfloor (x_0+\Delta x) \, \mathrm{d}P_{\delta,x_0+\Delta x}. \end{aligned}$$

$\lfloor \frac{l-\delta}{x_0+\Delta x} \rfloor (x_0+\Delta x)$ is bounded. By the fact that P_δ is absolutely continuous with respect to μ_L and the fact that Φ is continuous, we have

$$\lim_{\Delta x \to 0} \int_{[x_0, x_0+\Delta x)} \lfloor \frac{l-\delta}{x_0+\Delta x} \rfloor (x_0+\Delta x) \, \mathrm{d}P_{\delta, x_0+\Delta x} = 0$$

$$\lim_{\Delta x \to 0} \int_{[0, x_0)} \lfloor \frac{l-\delta}{x_0+\Delta x} \rfloor \Delta x \, \mathrm{d}P_{\delta, x_0+\Delta x} = 0$$

and

$$\lim_{\Delta x \to 0} f(x_0+\Delta x) = \lim_{\Delta x \to 0} \int_{[0, x_0)} \lfloor \frac{l-\delta}{x_0+\Delta} \rfloor x_0 \, \mathrm{d}P_{\delta, x_0+\Delta x}$$

For any $x \in (\frac{l}{N+1}, \frac{l}{N})$, it holds true that

$$\frac{l-\delta}{x} \leq \frac{l}{x} < \frac{l}{\frac{l}{N+1}} = N+1$$

$$\frac{l-\delta}{x} > \frac{l-\delta}{\frac{l}{N}} > \frac{l-\frac{l}{N}}{\frac{l}{N}} = N-1.$$

Therefore the only possible values for $\lfloor \frac{l-\delta}{x} \rfloor$ are $N-1$ and N. Let $\psi(x) = l - Nx$, then

$$\lfloor \frac{l-\delta}{x} \rfloor = \begin{cases} N & \delta \in [0, \psi(x)) \\ N-1 & \delta \in [\psi(x), x). \end{cases} \tag{3.9}$$

Because $x_0 \in (\frac{l}{N+1}, \frac{l}{N})$, there exists $\alpha > 0$ such that for all $|\Delta x| < \alpha$, $x_0 + \Delta \in (\frac{l}{N+1}, \frac{l}{N})$ holds true.

$$\begin{aligned}
&\lim_{\Delta x \to 0} (f(x_0+\Delta x) - f(x_0)) \qquad (3.10)\\
=& \lim_{\Delta x \to 0} \left(\int_{[0, x_0)} \lfloor \frac{l-\delta}{x_0+\Delta x} \rfloor x_0 h_{x_0+\Delta x} \, \mathrm{d}\mu_L - \int_{[0, x_0)} \lfloor \frac{l-\delta}{x_0} \rfloor x_0 h_{x_0} \, \mathrm{d}\mu_L \right) \\
=& \lim_{\Delta x \to 0} \left(\int_{[0, \psi(x_0+\Delta x))} \lfloor \frac{l-\delta}{x_0+\Delta x} \rfloor x_0 h_{x_0+\Delta x} \, \mathrm{d}\mu_L + \int_{[\psi(x_0+\Delta x), x_0+\Delta x)} \lfloor \frac{l-\delta}{x_0+\Delta x} \rfloor x_0 h_{x_0+\Delta x} \, \mathrm{d}\mu_L \right. \\
&\left. - \int_{[0, \psi(x_0))} \lfloor \frac{l-\delta}{x_0} \rfloor x_0 h_{x_0} \, \mathrm{d}\mu_L - \int_{[\psi(x_0), x_0)} \lfloor \frac{l-\delta}{x_0} \rfloor x_0 h_{x_0} \, \mathrm{d}\mu_L \right) \\
=& \lim_{\Delta x \to 0} \left(\int_{[0, \psi(x_0+\Delta x))} N x_0 h_{x_0+\Delta x} \, \mathrm{d}\mu_L + \int_{[\psi(x_0+\Delta x), x_0+\Delta x)} (N-1) x_0 h_{x_0+\Delta x} \, \mathrm{d}\mu_L \right. \\
&\left. - \int_{[0, \psi(x_0))} N x_0 h_{x_0} \, \mathrm{d}\mu_L - \int_{[\psi(x_0), x_0)} (N-1) x_0 h_{x_0} \, \mathrm{d}\mu_L \right) \\
=& N x_0 \lim_{\Delta x \to 0} \left(\int_{[0, \psi(x_0+\Delta x))} h_{x_0+\Delta x} \, \mathrm{d}\mu_L - \int_{[0, \psi(x_0))} h_{x_0} \, \mathrm{d}\mu_L \right) \\
&+ (N-1) x_0 \lim_{\Delta x \to 0} \left(\int_{[\psi(x_0+\Delta x), x_0+\Delta x)} h_{x_0+\Delta x} \, \mathrm{d}\mu_L - \int_{[\psi(x_0), x_0)} h_{x_0} \, \mathrm{d}\mu_L \right) \qquad (3.11)
\end{aligned}$$

Now by continuity of Φ, and the absolute continuity assumption

$$\begin{aligned}
&\lim_{\Delta x\to 0}\left(\int_{[0,\psi(x_0+\Delta x))} h_{x_0+\Delta x}\,\mathrm{d}\mu_L - \int_{[0,\psi(x_0))} h_{x_0}\,\mathrm{d}\mu_L\right)\\
=&\lim_{\Delta x\to 0}\left(\int_{[0,\psi(x_0+\Delta x))} (h_{x_0+\Delta x}-h_{x_0})\,\mathrm{d}\mu_L - \int_{[\psi(x_0+\Delta x),\psi(x_0))} h_{x_0}\,\mathrm{d}\mu_L\right)\\
=&0,
\end{aligned}$$

and similar argument holds for the second entry in (3.11). Hence (3.10) is actually 0. Thus proves the continuity of $E_{AB}(x)$ in $(\frac{l}{N+1},\frac{l}{N})$.

Then we prove the continuity of $E_{AB}(x)$ at $\frac{l}{N}$ by showing that

$$\begin{aligned}
&\lim_{\Delta x\to 0+} E_{AB}(\frac{l}{N}+\Delta x)\\
&\lim_{\Delta x\to 0-} E_{AB}(\frac{l}{N}+\Delta x)\\
&\qquad\qquad E_{AB}(\frac{l}{N})
\end{aligned}$$

are equal. Now

$$\begin{aligned}
E_{AB}(\frac{l}{N}) =&\frac{l}{N}+\int_{[0,\frac{l}{N})} \lfloor\frac{l-\delta}{\frac{l}{N}}\rfloor\frac{l}{N}\,\mathrm{d}P_\delta\\
=&\frac{l}{N}+\int_{(0,\frac{l}{N})}(N-1)\frac{l}{N}\,\mathrm{d}P_\delta+\int_{\{0\}} N\frac{l}{N}\,\mathrm{d}P_\delta\\
=&\frac{l}{N}+(N-1)\frac{l}{N}=l
\end{aligned}$$

and

$$\begin{aligned}
\lim_{\Delta x\to 0+} E_{AB}(\frac{l}{N}+\Delta x) =&\frac{l}{N}+\lim_{\Delta x\to 0+}\int_{[0,\frac{l}{N}+\Delta x)} \lfloor\frac{l-\delta}{\frac{l}{N}+\Delta x}\rfloor(\frac{l}{N}+\Delta x)\,\mathrm{d}P_\delta\\
=&\frac{l}{N}+\lim_{\Delta x\to 0+}\int_{[0,l-\lfloor\frac{l}{\frac{l}{N}+\Delta x}\rfloor(\frac{l}{N}+\Delta x))}(N-1)(\frac{l}{N}+\Delta x)\,\mathrm{d}P_\delta\\
&+\lim_{\Delta x\to 0+}\int_{[l-\lfloor\frac{l}{\frac{l}{N}+\Delta x}\rfloor(\frac{l}{N}+\Delta x),\frac{l}{N}+\Delta x)}(N-2)(\frac{l}{N}+\Delta x)\,\mathrm{d}P_\delta\\
=&\frac{l}{N}+(N-1)\frac{l}{N}+0=l
\end{aligned}$$

Similarly $\lim_{\Delta x\to 0-} E_{AB}(\frac{l}{N}+\Delta x)=l$, and thus completes the proof. □

By the proof, it is clear that if the scale of the ruler is dedicatedly set to be very close to $\frac{l}{N}$, then the reading $m(AB)$ is of finite possibilities. In case that $\Delta\in(\frac{l}{N}-\varepsilon,\frac{l}{N}]$,

$m(AB)$ will either be $(N-1)\Delta$ or $N\Delta$, while $\Delta \in (\frac{l}{N}, \frac{l}{N}+\varepsilon)$, $m(AB)$ will either be $(N-2)\Delta$ or $(N-1)\Delta$. Actually, for any Δ, there will be two possible readings of $m(AB)$; namely $\lfloor l/\Delta \rfloor \Delta$ and $(\lfloor l/\Delta \rfloor - 1)\Delta$. When this is observed after a series of sampling, the result readings can be identified as "high" or "low". Let

$$p_h(\Delta) = \int_{[0, l-\lfloor \frac{l}{\Delta} \rfloor \Delta)} \mathrm{d}P_{\delta,\Delta} \qquad p_l(\Delta) = \int_{[l-\lfloor \frac{l}{\Delta} \rfloor \Delta, \Delta)} \mathrm{d}P_{\delta,\Delta}, \tag{3.12}$$

and these represent the probability of high and low reading respectively. Immediately, one shows the following proposition:

Proposition 3.1. *p_h and p_l are continuous in $(\frac{l}{N+1}, \frac{l}{N})$ for all $N \in \mathbb{Z}, N \geq 2$ and are discontinuous at $\frac{l}{N}$.*

Proof. Because $p_h + p_l = 1$, it is enough to prove the statement for p_h. For $x_0 \in (\frac{l}{N+1}, \frac{l}{N})$ and sufficiently small Δx,

$$\begin{aligned}
\lim_{\Delta x \to 0+} (p_h(x_0+\Delta x) - p_h(x_0)) = &\lim_{\Delta x \to 0+} \left(\int_{[0, l-\lfloor \frac{l}{x_0+\Delta x} \rfloor (x_0+\Delta x))} \mathrm{d}P_{\delta, x_0+\Delta x} \right. \\
&\left. - \int_{[0, l-\lfloor \frac{l}{x_0} \rfloor x_0)} \mathrm{d}P_{\delta, x_0} \right) \\
= &\lim_{\Delta x \to 0+} \int_{[0, l-\lfloor \frac{l}{x_0+\Delta x} \rfloor (x_0+\Delta x))} h_{x_0+\Delta x} - h_{x_0} \, \mathrm{d}\mu_L \\
&- \lim_{\Delta x \to 0+} \int_{[l-\lfloor \frac{l}{x_0+\Delta x} \rfloor (x_0+\Delta x), l-\lfloor \frac{l}{x_0} \rfloor x_0)} \mathrm{d}P_{\delta, x_0} \\
= &0
\end{aligned}$$

Similarly it can be shown that $\lim_{\Delta x \to 0-} (p_h(x_0+\Delta x) - p_h(x_0)) = 0$. Now we show

the discontinuity of $p_h(x)$ at $x = \frac{l}{N}$.

$$\begin{aligned}
\lim_{\Delta x\to 0+} p_h(\frac{l}{N}+\Delta x) &= \lim_{\Delta x\to 0+}\int_{[0,l-\lfloor\frac{l}{\frac{l}{N}+\Delta x}\rfloor(\frac{l}{N}+\Delta x))} \mathrm{d}P_{\delta,\frac{l}{N}+\Delta x}\\
&= \lim_{\Delta x\to 0+}\int_{[0,l-(N-1)(\frac{l}{N}+\Delta x))} \mathrm{d}P_{\delta,\frac{l}{N}+\Delta x}\\
&= \lim_{\Delta x\to 0+}\int_{[0,\frac{l}{N}+(N-1)\Delta x)} \mathrm{d}P_{\delta,\frac{l}{N}+\Delta x}\\
&=1\\
\lim_{\Delta x\to 0-} p_h(\frac{l}{N}+\Delta x) &= \lim_{\Delta x\to 0-}\int_{[0,l-\lfloor\frac{l}{\frac{l}{N}+\Delta x}\rfloor(\frac{l}{N}+\Delta x))} \mathrm{d}P_{\delta,\frac{l}{N}+\Delta x}\\
&= \lim_{\Delta x\to 0-}\int_{[0,l-N(\frac{l}{N}+\Delta x))} \mathrm{d}P_{\delta,\frac{l}{N}+\Delta x}\\
&= \lim_{\Delta x\to 0-}\int_{[0,N\Delta x)} \mathrm{d}P_{\delta,\frac{l}{N}+\Delta x}\\
&=0
\end{aligned}$$

Moreover it is easy to see that $p_h(\frac{l}{N}) = 0$. □

Remark 3.1. Sometimes the symbol $p_h(x)$ will be written as $p_h(x,l)$ stressing on the fact that the length of AB is a variable in the definition of the probability of high readings. $p_h(x,l)$ as a function of l is of less interest, because neither the (conventional) true value l_t nor the nominal value l_n of a given measurand changes significantly while x can be manipulated.

Similar to Proposition 3.1, continuity and discontinuity exist for $p_h(x,l)$ as a function of l with fixed x.

Proposition 3.2. *Fixing an $x > 0$, then $p_h(x,l)$ is continuous on every $(Nx,(N+1)x)$ and discontinuous at every Nx where $N \in \mathbb{N}$ and $(N+1)x < l$.*

Proof. Assume l and $l+\Delta$ in $(Nx,(N+1)x)$ for small $\Delta > 0$, then

$$\begin{aligned}
\lim_{\Delta\to 0+} p_h(x,l+\Delta) - p_h(x,l) &= \lim_{\Delta\to 0+}\int_{[0,l+\Delta-Nx)} \mathrm{d}P_{\delta,x} - \int_{[0,l-Nx)} \mathrm{d}P_{\delta,x}\\
&= \lim_{\Delta\to 0+}\int_{[l+\Delta-Nx,l-Nx)} \mathrm{d}P_{\delta,x} = 0. \qquad (3.13)
\end{aligned}$$

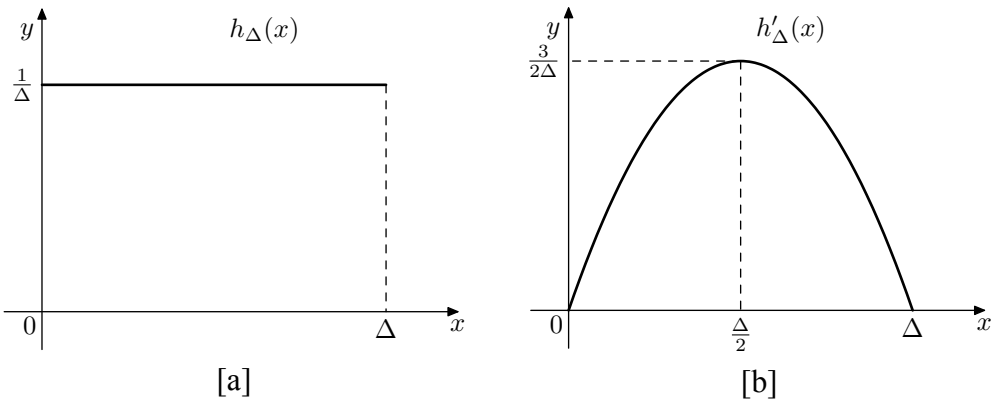

Figure 3.5: δ with different distributions: **[a]** uniform family; **[b]** $(2,2)$-Beta distribution

Similarly it can be shown that $\lim_{\Delta\to 0-} p_h(x, l-\Delta) = p_h(x,l)$, and thus completes the proof of continuity. For discontinuity

$$\lim_{l\to Nx+} p_h(x,l) = \lim_{\Delta\to 0+} p_h(x, Nx+\Delta) = \int_{[0,\Delta)} \mathrm{d}P_{\delta,x} = 0$$
$$\lim_{l\to Nx-} p_h(x,l) = \lim_{\Delta\to 0+} p_h(x, Nx-\Delta) = \int_{[0,x-\Delta)} \mathrm{d}P_{\delta,x} = 1$$

and furthermore it can be computed that $p_h(x, Nx) = 0$. □

Now it is time to investigate Problem 3.1 with a little bit more details.

Example 3.1. In addition to assumptions in Problem 3.1, consider two distributions P_δ, P'_δ such that

$$h_\Delta(x) = \begin{cases} \frac{1}{\Delta} & x\in[0,\Delta), \\ 0 & \text{elsewhere} \end{cases} \qquad h'_\Delta(x) = \begin{cases} \frac{6x}{\Delta^2}(1-\frac{x}{\Delta}) & x\in[0,\Delta), \\ 0 & \text{elsewhere} \end{cases}$$

This means that P_δ represents the uniform family and P'_δ represents the $(2,2)$-Beta distribution family as shown by Fig. 3.5. Simple computation shows that for any $x \in (\frac{l}{N+1}, \frac{l}{N})$,

$$\begin{aligned} E_{AB}(x) =& \int_{[0,x)} \left(\lfloor \frac{l-\delta}{x} \rfloor x + x \right) \mathrm{d}P_\delta \\ =& x + \int_{[0,l-Nx)} N\,\mathrm{d}\delta + \int_{[l-Nx,x)} (N-1)\,\mathrm{d}\delta = l \end{aligned}$$

and

$$\begin{aligned}
E'_{AB}(x) &= \int_{[0,x)} \left(\lfloor \frac{l-\delta}{x} \rfloor x + x \right) \mathrm{d}P_\delta \\
&= \int_{[0,l-Nx)} (Nx+x)\frac{6\delta}{x^2}(1-\frac{\delta}{x})\,\mathrm{d}\delta \\
&\quad + \int_{[l-Nx,x)} ((N-1)x+x)\frac{6\delta}{x^2}(1-\frac{\delta}{x})\,\mathrm{d}\delta \\
&= (2N^3+3N^2+N)x - 6lN(N+1) + (6Nl^2+3l^2)\frac{1}{x} - \frac{2l^3}{x^2}
\end{aligned}$$

Fig 3.6[a] and [b] depict $E_{AB}(x)$ and $E'_{AB}(x)$ respectively. One observes that the uniform distribution gives the very trivial result that the expectation is simply the length of the line segment. However, contradictory to intuition, if the distribution of δ is not uniform, the expectation does not equal to l except for several discrete points. It can be shown that besides the uniform distribution, there are other non uniform distributions which make $E_{AB}(x) = l$. Example A.1 in Appendix A. contains a non-trivial example where δ is non-uniform but yet gives constant E_{AB}.

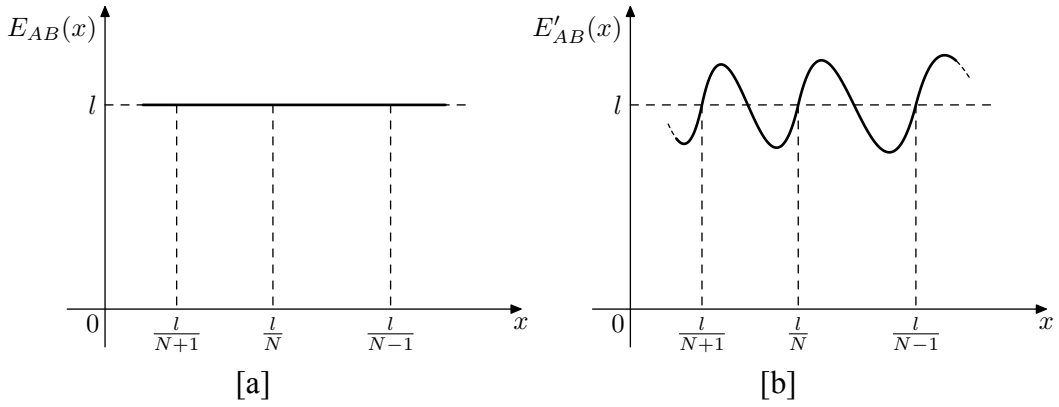

Figure 3.6: Expectations of different δ distribution

Similarly p_h (or equivalently p_l) can be computed, and the results are

$$p_h(x) = \frac{l}{x} - \lfloor \frac{l}{x} \rfloor \tag{3.14}$$

$$p'_h(x) = \frac{(l - \lfloor \frac{l}{x} \rfloor x)^2(-2l + (3 + 2\lfloor \frac{l}{x} \rfloor)x)}{x^3}. \tag{3.15}$$

The graphs of p_h and p'_h are depicted in Fig. 3.7. □

Now it is ready to develop the new method (PBM) for Problem 3.1.

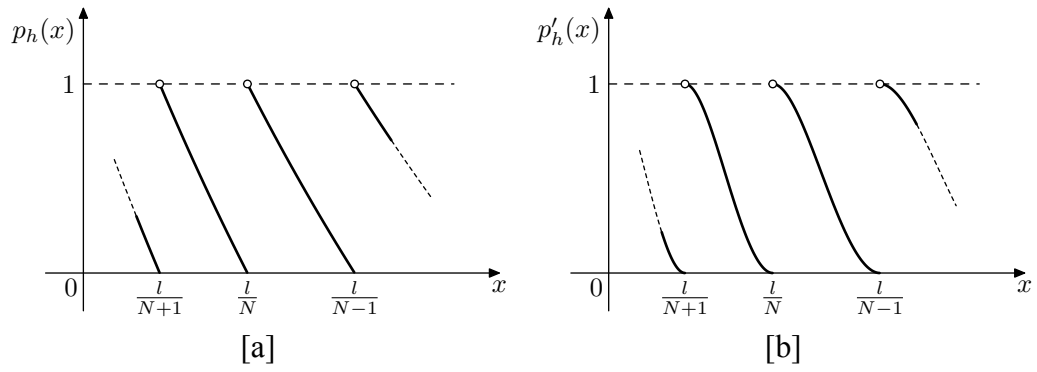

Figure 3.7: p_h under different distribution, continuity and discontinuity are invariant

3.3 The Probability-Based Method

Based on the observations so far, the PBM method will be developed in this section to solve Problem 3.1. From Example 3.1, it is clear that simply taking the average of many measurement results does not necessarily give the true value for δ of general distributions. Instead, PBM utilizes the discontinuity of p_h (or p_l). One adjusts the scale to be near $\frac{l}{N_0}$ for some chosen $N_0 \geq 2$, sample multiple times and find p_h from the samples. The answer to Problem 3.1 can then be found in this p_h.

Although examples illustrated in Fig. 3.7 show that p_h are decreasing within each $(\frac{l}{N+1}, \frac{l}{N})$, conditions of Theorem 3.1 do not generally guarantee the monotonicity of p_h in each $(\frac{l}{N+1}, \frac{l}{N})$. Priori knowledge, including but not limited to monotonicity of p_h, can greatly simplify the measuring process and provide additional estimation for the result. The following proposition states two sufficient conditions for the monotonicity of p_h:

Proposition 3.3. *$p_h(x)$ is non-ascending on every $(\frac{l}{N+1}, \frac{l}{N})$, if either of the following condition are satisfied:*

(a) for every $y > x$, $h_y \leq h_x$ almost everywhere on $[0, x]$

(b) P_δ is a family obtained by scaling, i.e. satisfying

$$h_x(\delta) = \frac{y}{x} h_y(\frac{y}{x}\delta).$$

p_h is strictly decreasing, if further $P_{\delta,x}(I) > 0$ for any open interval I.

Proof. (a): Suppose $x \in (\frac{l}{N+1}, \frac{l}{N})$, and for any $\Delta x > 0$ such that $x + \Delta x \in (\frac{l}{N+1}, \frac{l}{N})$, it holds

$$\begin{aligned} p_h(x+\Delta x) - p_h(x) =& \int_{[0,l-N(x+\Delta x))} \mathrm{d}P_{\delta,x+\Delta x} - \int_{[0,l-Nx)} \mathrm{d}P_{\delta,x} \\ =& \int_{[0,l-N(x+\Delta x))} (h_{x+\Delta x} - h_x)\,\mathrm{d}\mu_L - \int_{[l-N(x+\Delta x),l-Nx)} \mathrm{d}P_{\delta,x} \\ \leq& 0 \end{aligned}$$

(b): Suppose $x \in (\frac{l}{N+1}, \frac{l}{N})$, fix a $y \in (\frac{l}{N+1}, \frac{l}{N})$, then

$$\begin{aligned} p_h(x) =& \int_{[0,l-Nx)} \mathrm{d}P_{\delta,x} \\ =& \int_0^{l-Nx} h_x(\delta)\,\mathrm{d}\mu_L(\delta) \\ =& \int_0^{l-Nx} \frac{y}{x} h_y(\frac{y}{x}\delta)\,\mathrm{d}\mu_L(\delta) \\ =& \int_0^{(l-Nx)\frac{y}{x}} h_y(\delta)\,\mathrm{d}\mu_L(\delta) \\ =& P_{\delta,y}([0,(l-Nx)\frac{y}{x})) = P_{\delta,y}([0,\frac{ly}{x} - Ny)), \end{aligned}$$

and

$$p_h(x+\Delta x) - p_h(x) = -P_{\delta,y}([\frac{ly}{x+\Delta} - Ny, \frac{ly}{x} - Ny)) \leq 0$$

It is obvious that $p_h(x)$ is non-ascending.

The statement of p_h being strictly decreasing is obvious, because if the condition is satisfied both $\int_{[l-N(x+\Delta x),l-Nx)} \mathrm{d}P_{\delta,x}$ and $P_{\delta,y}([\frac{ly}{x+\Delta x} - Ny, \frac{ly}{x} - Ny))$ are positive. □

Some brief comments on the conditions of Proposition 3.3 will be put here. Condition (a) covers the cases where the family of finitely supported derivative h_x "condenses" on the common part of the support sets, for example, the uniform distribution family $h_x(y) = \frac{1}{x}$ satisfies this condition. Another non-trivial example satisfying condition (a) is

$$h_x(y) = \begin{cases} \frac{1}{2(x-x^2)} & y \in [0, x-x^2), \\ \frac{1}{2x^2} & y \in [x-x^2, x), \\ 0 & \text{elsewhere} \end{cases} \qquad \text{for} \qquad x \in (0, \frac{1}{2}).$$

Condition (b) covers the cases where the family h_x is similar to each other via simple linear transformations. Again the uniform distribution satisfies this condition, and so does the normalized (n, m)-Beta distribution family

$$h_x(y) = \begin{cases} \frac{1}{y\beta(n,m)} \left(\frac{y}{x}\right)^n \left(1 - \frac{y}{x}\right)^{m-1} & y \in [0, x), \\ 0 & \text{elsewhere.} \end{cases}$$

The next example shows that the monotonicity can be non-strict.

Example 3.2. Consider the distribution $P_{\delta,x}$ with h_x defined as

$$h_x(y) = \begin{cases} \frac{3}{x} & y \in [\frac{x}{3}, \frac{2x}{3}), \\ 0 & \text{elsewhere.} \end{cases}$$

Through simple computation, one finds

$$p_h(x) = \begin{cases} 1 & x \in (\frac{l}{\lfloor \frac{l}{x} \rfloor + 1}, \frac{l}{\lfloor \frac{l}{x} \rfloor + \frac{2}{3}}), \\ \frac{3l}{x} - 3\lfloor \frac{l}{x} \rfloor - 1 & x \in (\frac{l}{\lfloor \frac{l}{x} \rfloor + \frac{2}{3}}, \frac{l}{\lfloor \frac{l}{x} \rfloor + \frac{1}{3}}], \\ 0 & x \in (\frac{l}{\lfloor \frac{l}{x} \rfloor + \frac{1}{3}}, \frac{l}{\lfloor \frac{l}{x} \rfloor}]. \end{cases}$$

Its graph (Fig. 3.8) clearly shows that around each point $x = \frac{l}{N}$, there are regions in which p_h is constant. □

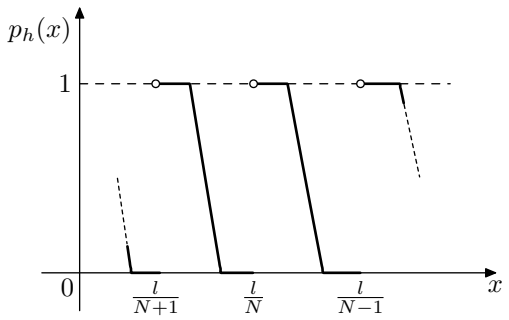

Figure 3.8: Graph of p_h, not strictly decreasing in every $(\frac{l}{N+1}, \frac{l}{N})$

Although the monotonicity of $p_h(x)$ on every $(\frac{l}{N+1}, \frac{l}{N})$ is not universal, the monotonicity of $p_h(x, l)$ as a function of l on every $(Nx, (N+1)x)$ with a fixed x is unconditional. Equation (3.13) clearly shows that $p_h(x, l)$ is non-decreasing as a function of l.

Three tiers of condition will be proposed reflecting different levels of priori knowledge on p_h which encodes the information of the measurand. For each condition, variations of PBM exist in the sampling procedures and the post process of data; and these should be considered from the beginning of the development of the probability-based method.

(L1) $p_h(x)$ is analytically known and computable. Or a satisfactory, analytically known approximation/estimation of $p_h(x)$ can be found and used as a pragmatic alternative.

(L2) $p_h(x)$ is monotone on every $(\frac{l}{N+1}, \frac{l}{N})$. Or pragmatically, the monotonicity assumption on $p_h(x)$ or its satisfactory approximation/estimation on every $(\frac{l}{N+1}, \frac{l}{N})$ is reasonable.

(L3) The knowledge of $p_h(x)$ is no more than the continuities in Proposition 3.1.

Intuitively, the restriction of each condition becomes looser as the tier index goes higher; however, it is worthwhile pointing out that the L1 condition does not necessarily imply monotonicity of p_h, and the L2 condition does not imply the L3 condition. Example A.2 in Appendix A. analytically constructs a $p_h(x)$ whose monotonicity fails in some $(\frac{l}{N+1}, \frac{l}{N})$. Indeed, the behavior of $p_h(x)$ on $(\frac{l}{N+1}, \frac{l}{N})$ can be very wild. Example A.2 also shows that the shape of $p_h(x)$ on each $(\frac{l}{N+1}, \frac{l}{N})$ can be significantly different regardless of the gradual change of h_x. Therefore, it is more practical to propose the tier of conditions as:

(P1) $p_h(x)$ is analytically known and computable. Or a satisfactory, analytically known approximation/estimation of $p_h(x)$ can be found and used as a pragmatic alternative. And the P2 condition is satisfied.

(P2) $p_h(x)$ is monotone on every $(\frac{l}{N+1}, \frac{l}{N})$. Or pragmatically, the monotonicity assumption on $p_h(x)$ or its satisfactory approximation/estimation on every $(\frac{l}{N+1}, \frac{l}{N})$ is reasonable. And the P3 condition is satisfied.

(P3) The knowledge of $p_h(x)$ is no more than the continuities in Proposition 3.1.

In addition, another condition will be proposed, which independently asserts that the monotonicity of $p_h(x, l)$ in x and l are strict wherever continuity is true. It shall be called the S condition. From equation (3.13), one sufficient condition for $p_h(x, l)$ as a function of l to be strictly monotone is that P_δ is positive on any open interval or equivalently $h_x(y) \not\equiv 0$ on any open interval. Henceforth the S condition will be used accompanying either the P1 or P2 condition for more in-depth discussions. In the rest of this section, the PBM method, as an answer to Problem 3.1 under different tiers of condition, will be presented. Before the end of this section, some symbols and definitions will be introduced and general arguments conducted.

Let l_t, l_n denote the true value and nominal value of the length of the line segment AB respectively and T denote the tolerance range. For example, in Problem 3.1, $l_n = 150$mm and $T = 0.4$mm. Choose and fix an N_0, and adjust the scale of the ruler to be $\Delta_0 = \frac{l_n}{N_0}$. Measure M times without alignment of ends of line segment to the carved marks, and record the results as

$$R_M = \{(n, c_n) | n \in \mathbb{Z}, c_n \in \mathbb{N}\} \tag{3.16}$$

where (n, c_n) is a paired entry recording c_n the number of experiments in which n full scales exist. Immediately from the definition, it holds that

$$\sum_{n \in \mathbb{Z}} c_n = M, \tag{3.17}$$

and that R_M is a finite set. Without ambiguity, the symbol R_M will also be used as a function by $R_M(n) = c_n$, and 0 elsewhere. This R_M will be called a *result set* or *result function*. Theoretically, for an infinite number of measurements, R_∞ contains at least one (n, c_n) such that $c_n = \infty$. In this case, instead of using c_n that counts the number of experiment, R_∞ will be defined as

$$R_\infty = \{(n, p_n) | n \in \mathbb{Z}, p_n \geq 0\}$$

where p_n is the probability of the event of a measurement result consisting of n full scales. Hence the discussion will be presuming that the law of large numbers ([Ete81]) holds so that each p_n exists. Define

$$f_n = \frac{R_M(n)}{M},$$

then it holds that $f_n \to p_n$ as $M \to \infty$ and $\sum_{n \in \mathbb{Z}} p_n = 1$. Ideally, R_∞ should be either supported on two points or one point. If the scale is adjusted to be l_t/N_0 exactly, then the support of R_∞ will be $\{N_0 - 1\}$. Henceforth it will always be assumed that by conducting the measurement using a large M, each f_n well approximates p_n. In the following, without ambiguity, the unit of millimeter is omitted.

3.3.1 P3 Condition

The discussion begins with the loosest condition of P3, defined on page 38. In this case the only theoretical solution is to find out the discontinuity of $p_h(x)$ by adjusting x, the scale of the ruler. Suppose that by searching around $x = \Delta_0$, $p_h(x)$ is found to be discontinuous at Δ_1 with R_∞ (or R_M with a sufficiently large M) supported solely

at $\{n\}$, then $l_t = (n+1)\Delta_1$. However this is practically impossible. Example A.3 in Appendix A. shows that within one $(\frac{l}{N+1}, \frac{l}{N})$, $p_h(x)$ can oscillate between 0 and 1 arbitrarily many times. Detecting discontinuity of $p_h(x)$ of this kind essentially means detecting discontinuity of very high-frequency signals, which is not possible without more analytic information.

3.3.2 P2 Condition

Monotonicity of $p_h(x)$ guaranteed by the P2 condition (defined on page 38) makes the search for discontinuity practically possible. This begins with some general discussion. Because the process of measurement in the real world is always finite; henceforth discussion focuses on those R_M with a finite M. Even in this case, a result set R_M might be supported on a single point $\{n\}$ or two points $\{n-1, n\}$.

If R_M is supported on $\{n-1, n\}$, then it implies that $n\Delta_0 \leq l_t < (n+1)\Delta_0$. Therefore, if either $n\Delta_0 > l_n + T$ or $(n+1)\Delta_0 \leq l_n - T$, the answer to Problem 3.1 is immediately negative. If R_M is supported solely on $\{n\}$, then this could either be the case that $R_M(n-1) = 0$ or $R_M(n+1) = 0$. Now for a given R_M supported on $\{n-1, n\}$, define

$$f_h = f_n = \frac{R_M(n)}{M} \tag{3.18}$$

as the *frequency of high reading*. By the law of large numbers, with $M \to \infty$ it can be expected that $f_h \to p_h$ almost surely [Ete81]. If R_M is supported on a single point, it might reflect either the case $f_h \approx 1$ or the case $f_h \approx 0$.

The search for discontinuity can be performed in the following way. Choose $[\Delta_0 - t_0, \Delta_0 + t_0]$, an interval around Δ_0 for search of discontinuity, and choose a sequence for refinement

$$\Delta_0 - t_0 = x_0 < x_1 < \cdots < x_{n-1} < x_n = \Delta_0 + t_0.$$

Then at each x_i, find out $f_h^{(i)}$ and the discontinuity is between a rising edge. That is, if $f_h^{(i)} < f_h^{(i+1)}$, then there exists x_* such that $x_i \leq x_* < x_{i+1}$ and $p_h(x)$ is discontinuous at x_*. The P2 condition guarantees that for any $j \neq i$ it holds true that $f_h^{(j)} \geq f_h^{(j+1)}$; and Proposition 3.1 guarantees that this jump from $f_h^{(i)}$ to $f_h^{(i+1)}$ is significant enough

Table 3.1: Searching between 2.98 and 3.02, $M = 1000$

x_i	2.980	2.984	2.988
R_M	$\{(49, 583), (50, 417)\}$	$\{(49, 622), (50, 378)\}$	$\{(49, 700), (50, 300)\}$
x_i	2.992	2.996	3.000
R_M	$\{(49, 782), (50, 218)\}$	$\{(49, 822), (50, 178)\}$	$\{(49, 905), (50, 95)\}$
x_i	3.004	3.008	3.012
R_M	$\{(49, 986), (50, 14)\}$	$\{(48, 21), (49, 979)\}$	$\{(48, 100), (49, 900)\}$
x_i	3.016	3.020	
R_M	$\{(48, 180), (49, 820)\}$	$\{(48, 214), (49, 786)\}$	

Table 3.2: Searching between 2.98 and 3.0008, $M = 1000$, showing only the frequency

x_i	2.9800	2.9816	2.9832	2.9848	2.9864	2.9880	2.9896
f_h	0.188	0.119	0.115	0.092	0.061	0.020	0.000
x_i	2.9912	2.9928	2.9944	2.9960	2.9976	2.9992	3.0008
f_h	0.997	0.959	0.902	0.903	0.884	0.852	0.816

for detection. For a refinement fine enough, $f_h^{(i)}$ should be near 0 and $f_h^{(i+1)}$ near 1, and the result sets should be of the form

$$R_{M_i} = \{(n, R_{M_i}(n)), (n+1, R_{M_i}(n+1))\}$$
$$R_{M_{i+1}} = \{(n-1, R_{M_{i+1}}(n-1)), (n, R_{M_{i+1}}(n))\}$$

and that

$$R_{M_i}(n) \ll R_{M_i}(n+1) \qquad\qquad R_{M_{i+1}}(n-1) \ll R_{M_{i+1}}(n).$$

In this case, the range of the true value is determined by

$$(n+1)x_i \leq l_t < (n+1)x_{i+1}, \tag{3.19}$$

and answer to Problem 3.1 can thus be drawn. The following example with simulated data illustrates this process in detail:

Example 3.3. To determine whether the length of a given line segment is within $(150 - 0.4, 150 + 0.4)$ one searched around $\Delta_0 = \frac{150}{50} = 3$, and recorded the results as shown in Table 3.1. Thus by estimation (3.19), the range of the true value should be within $(150.2, 150.4)$ and hence the answer to the problem is positive.

Table 3.2 shows another search result for a different line segment. This time, the true value is estimated to be within $(149.48, 149.56)$, outside of the tolerance range.

Indeed, data in Table 3.1 and 3.2 are simulated results for δ of the distribution

$$h_x(y) = \begin{cases} \frac{2}{x}\sin^2\left(\frac{10\pi y}{x}\right) & y \in [0, x), \\ 0 & \text{elsewhere}, \end{cases} \tag{3.20}$$

with l_t set to 150.3, 149.5 respectively. □

Before moving to the next section, it would be better to make some brief comments here. Although there might be some space for optimization of the searching process; the process is generally laborious and slow by the restriction of the non-strict monotonicity of p_h. One might have noticed that in Table 3.2, $f_h(2.9944) = 0.902 < 0.903 = f_h(2.9960)$, which seems to be violating the monotonicity of the P2 condition. This is because the frequency is merely an approximation to the probability and statistical error occurs. Indeed, under the distribution defined by equation (3.20), the computation yields

$$p_h(2.9944) \approx 0.910 \qquad\qquad p_h(2.996) \approx 0.900.$$

Nevertheless, the rising edge that truly represents the discontinuity of p_h is always sufficiently significant and hence the search process is statistically robust.

3.3.3 P2+S Condition

It seems that the S condition implies the P2 condition, however, it is worth pointing out that the S condition does not assume the continuity of $p_h(x)$. What has been established in the subsection of P2 condition remains valid; and one expects to profit a little bit more from the strict monotonicity of $p_h(x)$. If f_h in a given R_M is very close 1; then it implies that the true value l_t is close to but smaller than l_n. Similarly, if f_h is very close to 0, then l_t is close to but larger than l_n. In particular, if R_M is supported on a single point, then regardless of f_h being close to 0 or 1, it can be deduced that l_t, the true value, is very close to l_n. Because of cases like Example 3.2, the claims above fail in general without the S condition. Fixing a Δ_0 for search of discontinuity of p_h around it, let $R_M^{(1)}$ and $R_M^{(2)}$ be result sets for two line segments. If $f_h^{(1)} < f_h^{(2)}$ and both of them are close to 1, then $l_t^{(1)} < l_t^{(2)} < l_n$. Similarly if $f_h^{(1)} < f_h^{(2)}$ and both are close to 0, then $l_n < l_t^{(1)} < l_t^{(2)}$. Such qualitative analysis provides quick estimation and helpful feedback in practical applications.

3.3.4 P1 Condition

The discussion and method established for the P2 scenarios remain valid for the P1 situations (defined on page 38). Searching for discontinuity of p_h is very slow, because it needs many result sets of p_h at different points. When the P1 condition is satisfied, only one result set is needed and hence the process of solving Problem3.1 is drastically accelerated. The discussion begins with the case where R_M is supported on two points $\{n-1, n\}$.

If $n\Delta_0 > l_n + T$ or $(n+1)\Delta_0 \leq l_n - T$, then the true length l_t is outside of the tolerance range.

If $n\Delta_0 = l_n$, then it implies that the true value l_t is larger than the nominal length. Statistical tests can be conducted for hypotheses H_0 that $n\Delta_0 = l_n \leq l_t \leq l_n + T$, and H_1 that $l_n + T < l_t < (n+1)\Delta_0$. A likelihood ratio test (LR test) can be performed for the number of high readings $R_M(n) = k$. If an equal chance of H_0, H_1 are assumed, $\Lambda_H(k)$, the likelihood ratio can be written as

$$\Lambda_H(k) = \frac{P(R_M(n) = k|H_0)}{P(R_M(n) = k|H_1)} = \frac{\int_{l_n}^{l_n+T} \frac{1}{T}\binom{M}{k} p_h^k(\Delta_0, x) p_l^{M-k}(\Delta_0, x)\,\mathrm{d}x}{\int_{l_n+T}^{l_n+\Delta_0} \frac{1}{\Delta_0 - T}\binom{M}{k} p_h^k(\Delta_0, x) p_l^{M-k}(\Delta_0, x)\,\mathrm{d}x}.$$

Then choose a threshold c_h and the result is accepted for the null hypothesis H_0 if $\Lambda_H(k) \geq c_h$.

If $n\Delta_0 = l_n - \Delta_0$, then it implies that the true value l_t is smaller than the nominal length l_n. Similar to the previous case, let H_0 be the hypothesis that $l_n - T \leq l_t \leq l_n = (n+1)\Delta_0$ and H_1 be the hypothesis that $l_n - \Delta_0 < l_t < l_n - T$. With a properly chosen threshold c_l for acceptance of H_0, conduct the LR test on the number of *low readings* using

$$\Lambda_L(k) = \frac{P(R_M(n) = k|H_0)}{P(R_M(n) = k|H_1)} = \frac{\int_{l_n-T}^{l_n} \frac{1}{T}\binom{M}{k} p_h^k(\Delta_0, x) p_l^{M-k}(\Delta_0, x)\,\mathrm{d}x}{\int_{l_n-\Delta_0}^{l_n-T} \frac{1}{\Delta_0 - T}\binom{M}{k} p_h^k(\Delta_0, x) p_l^{M-k}(\Delta_0, x)\,\mathrm{d}x}.$$

That is, if $\Lambda_L(k) \geq c_l$, then the true value is within the tolerance range. The following example with simulated data illustrates this process in detail:

Example 3.4. Suppose the P1 condition holds. To determine whether the length of four different line segments is within $(150 - 0.4, 150 + 0.4)$, one conducted random sampling and the result sets are summarized in Table 3.3. The data shows that the true

Table 3.3: Result sets for four line segments

index	distribution of δ	Δ_0	result set
1	uniform	$l_n/50 = 3$	$R^{(1)}_{1000} = \{(49, 842), (50, 158)\}$
2	uniform	$l_n/50 = 3$	$R^{(2)}_{1000} = \{(49, 923), (50, 77)\}$
3	(2,2)-Beta	$l_n/50 = 3$	$R^{(3)}_{1000} = \{(48, 73), (49, 927)\}$
4	(2,2)-Beta	$l_n/50 = 3$	$R^{(4)}_{1000} = \{(48, 18), (49, 982)\}$

value of the line segment is larger than the nominal for first two cases and is smaller than the nominal for the last two. Using (3.14) and (3.15), direct computation shows

$$\Lambda^{(1)}_H(158) \approx 0.0740 \qquad \Lambda^{(2)}_H(77) \approx 5.22 \times 10^8$$
$$\Lambda^{(3)}_L(927) \approx 0.0024 \qquad \Lambda^{(4)}_L(982) \approx 3.99 \times 10^7$$

Setting $c_h = c_l = 10$, then the line segments used for $R^{(1)}$ and $R^{(3)}$ are rejected while the ones used for $R^{(2)}$ and $R^{(4)}$ are accepted for being within the range 150 ± 0.4. Indeed the simulated results $R^{(i)}$ are generated by setting l_t, the true length, to $150.48, 150.23, 149.52$ and 149.77 respectively. □

Now the discussion handles the case where R_M is solely supported on $\{n\}$. The result is interpreted as that either the low reading or the high reading dominates in chance. That is, either $R_M = \{(n, M), (n + 1, 0)\}$ or $R_M = \{(n - 1, 0), (n, M)\}$ occurs. Under the assumption that it is of equal chance that the true value is larger than or equal to the nominal and that the true value is smaller than the nominal; a similar LR test can be conducted with the likelihood ratio defined as

$$\begin{aligned}
\Lambda_S(M) &= \frac{P(R_M|H_0)}{P(R_M|H_1)} \\
&= \frac{\frac{1}{2}\int_{l_n}^{l_n+T} \frac{1}{T} p_l^M(\Delta_0, x)\,\mathrm{d}x + \frac{1}{2}\int_{l_n-T}^{l_n} \frac{1}{T} p_h^M(\Delta_0, x)\,\mathrm{d}x}{\frac{1}{2}\int_{l_n+T}^{l_n+\Delta_0} \frac{1}{\Delta_0 - T} p_l^M(\Delta_0, x)\,\mathrm{d}x + \frac{1}{2}\int_{l_n-T\Delta_0}^{l_n-T} \frac{1}{\Delta_0 - T} p_h^M(\Delta_0, x)\,\mathrm{d}x} \\
&= \frac{\int_{l_n}^{l_n+T} \frac{1}{T} p_l^M(\Delta_0, x)\,\mathrm{d}x + \int_{l_n-T}^{l_n} \frac{1}{T} p_h^M(\Delta_0, x)\,\mathrm{d}x}{\int_{l_n+T}^{l_n+\Delta_0} \frac{1}{\Delta_0 - T} p_l^M(\Delta_0, x)\,\mathrm{d}x + \int_{l_n-T\Delta_0}^{l_n-T} \frac{1}{\Delta_0 - T} p_h^M(\Delta_0, x)\,\mathrm{d}x},
\end{aligned}$$

where H_0 is the hypothesis that $l_n - T \le l_t \le l_n + T$ and H_1 the hypothesis that $l_t \notin [l_n - T, l_n + T]$. Choose a proper threshold c_m for acceptance of H_0; and then H_0 can be claimed if $\Lambda_S(M) \ge c_m$.

Example 3.5. For Problem 3.1, find out the likelihood ratios of the measurement readings $R_M = \{(49, M)\}$ where $M = 10, 50, 100, 200, 400$. Δ_0 is set to $\frac{l_n}{50} = 3$ and the computation includes both the uniform distribution and $(2, 2)$-Beta distribution of

Table 3.4: Likelihood ratio of single supported experiment

M	10	50	100	200	400
uniform Λ_S	24.87	9.59×10^3	1.23×10^7	2.02×10^{13}	5.42×10^{25}
$(2,2)$-Beta Λ_S	13.48	237.80	3.89×10^3	7.70×10^5	2.26×10^{10}

δ. With the help of (3.14) and (3.15), the computed data are summarized in Table 3.4. The result shows that as M goes larger, the likelihood ratio grows rapidly, which agrees with the intuition that single point supported result sets reflect the fact that l_t is very close to l_n. □

Before moving to the next subsection, it would better to remark on several facts. Firstly, the method established here for the P1 cases is immediately applicable to the L1 cases. That is, cases like Example A.2 can be handled. Compared to the procedure for P2 cases, multiple trials on different choices of Δ around Δ_0 are not needed and hence the overall process is much faster. Additionally, it is possible to prepare $\Lambda_H(k), \Lambda_L(k), \Lambda_S(k)$ as look-up tables. For online measurements, one only needs to check for specific results and this greatly reduces the complexity of computation and system design. It is also worth mentioning that the thesis only used the LR test as a tool, and claims no "optimum" of any kind. Further improvement on statistics is not the key concern here and is left to experts. Finally, if the nominal length l_n and tolerance range T are fixed, the need of "adjustable scale" on the ruler is no longer required. The measurement can be conducted using a specific ruler with the scales equal to $\Delta_0 = l_n/N_0$ and the whole process remains valid.

3.3.5 P1+S Condition

If the S condition holds in addition to the P1 condition, it is possible to make faster estimation of the measurand without using the tool of statistical tests. Compute

$$p_1 = p_h(\Delta_0, l_n + T) \qquad\qquad p_2 = p_h(\Delta_0, l_n - T)$$

and then compare f_h from R_M to p_1, p_2 in the following way. If f_h is close to 1 and $f_h > p_2$, then it is true that $l_t \in [l_n - T, l_n]$. If f_h is close to 0 and $f_h < p_1$, then it is true $l_t \in [l_n, l_n + T]$. If R_M is solely supported on a single point, it indicates either $f_h \approx 1$ or $f_h \approx 0$, and both imply that the true value l_t is very close to l_n.

Example 3.6. It is known that δ is of $(3,4)$-Beta distribution and $\Delta_0 = 3$, examine the following results for tolerance range $(150-0.4, 150+0.4)$:

$$R^{(1)}_{1000} = \{(49,938),(50,62)\} \qquad R^{(2)}_{1000} = \{(49,972),(50,28)\}$$
$$R^{(3)}_{1000} = \{(48,0),(49,1000)\} \qquad R^{(4)}_{1000} = \{(49,11),(50,989)\}.$$

The $(3,4)$-Beta distribution implies that $p_h(x,l)$ is strictly monotone in both x and l and hence the P1+S condition holds. By simple computation

$$p_1 \approx 0.03465 \qquad\qquad p_2 \approx 0.99621.$$

$f^{(1)}_h = 0.062 > p_1, f^{(4)}_h = 0.989 < p_2$ and hence sample 1 and 4 are outside of the tolerance range $(150-0.4, 150+0.4)$. $f^{(2)}_h = 0.028 < p_1, f^{(3)}_h = 1. > p_2$ and these samples are within the tolerance range. Indeed the simulated result sets are obtained by setting l_t to $150.5, 150.38, 149.87, 149.49$ respectively. □

As a remark, the average of $R^{(1)}_{1000}$ in Example 3.6 is 150.186 and this shows that one cannot simply rely on the average of random samples as asserted by Theorem 3.1.

3.4 Relation to the Classic Method

This section establishes the connection between PBM and the classic method. It will be shown that PBM proposed in this chapter is a natural extension to the classic method. The next theorem formulates the relation mathematically:

Theorem 3.2. *Let $C_n(x), D_n(x)$ be real functions such that $0 < C_n(x) < D_n(x) < x$ and that $\lim_{n\to\infty} C_n(x) = 0$ and $\lim_{n\to\infty} D_n(x) = x$. Let $\delta^{(n)}$ be a series of random variables such that $h^{(n)}_x(y)$ satisfy*

$$\lim_{n\to\infty} \int_{(0,C_n(x))} h^{(n)}_x(y)\, \mathrm{d}\mu_L(y) = \lim_{n\to\infty} \int_{(D_n(x),x)} h^{(n)}_x(y)\, \mathrm{d}\mu_L(y) = \frac{1}{2}. \tag{3.21}$$

Then for any $x \in (\frac{l}{N+1}, \frac{l}{N})$

$$\lim_{n\to\infty} E^{(n)}_{AB}(x) = Nx + \frac{x}{2} \tag{3.22}$$
$$\lim_{n\to\infty} p^{(n)}_h(x) = \frac{1}{2} \tag{3.23}$$

Proof. Let $\psi(x)$ be defined as by equation (3.9). Then for sufficiently large n, it is true that $C_n(x) < \psi(x) < D_n(x)$ because $C_n(x) \to 0$ and $D_n(x) \to 0$. Thus

$$\begin{aligned}
\lim_{n\to\infty} E_{AB}^{(n)}(x) &= \lim_{n\to\infty} \int_{[0,x)} \left(\lfloor \frac{l-\delta}{x} \rfloor x + x \right) \mathrm{d}P_{\delta^{(n)},x} \\
&= \lim_{n\to\infty} \int_{[0,C_n(x))} \lfloor \frac{l-\delta}{x} \rfloor x \, \mathrm{d}P_{\delta^{(n)},x} + \lim_{n\to\infty} \int_{[C_n(x),D_n(x))} \lfloor \frac{l-\delta}{x} \rfloor x \, \mathrm{d}P_{\delta^{(n)},x} \\
&\quad + \lim_{n\to\infty} \int_{[D_n(x),x)} \lfloor \frac{l-\delta}{x} \rfloor x \, \mathrm{d}P_{\delta^{(n)},x} + x \\
&= \lim_{n\to\infty} \int_{[0,C_n(x))} Nx h_x^{(n)}(\delta) \, \mathrm{d}\mu_L(\delta) + \lim_{n\to\infty} \int_{[C_n(x),D_n(x))} \lfloor \frac{l-\delta}{x} \rfloor x h_x^{(n)}(\delta) \, \mathrm{d}\mu_L(\delta) \\
&\quad + \lim_{n\to\infty} \int_{[D_n(x),x)} (N-1) x h_x^{(n)}(\delta) \, \mathrm{d}\mu_L(\delta) + x \\
&= \frac{N}{2}x + \frac{N-1}{2}x + 0 + x = Nx + \frac{x}{2}
\end{aligned}$$

Similarly

$$\begin{aligned}
\lim_{n\to\infty} p_h^{(n)}(x) &= \lim_{n\to\infty} \int_{[0,l-Nx)} \mathrm{d}P_{\delta^{(n)},x} \\
&= \lim_{n\to\infty} \int_{[0,C_n(x))} h_x^{(n)}(\delta) \, \mathrm{d}\mu_L(\delta) + \lim_{n\to\infty} \int_{[C_n(x),l-Nx)} h_x^{(n)}(\delta) \, \mathrm{d}\mu_L(\delta) \\
&= \frac{1}{2}
\end{aligned}$$

□

In the following, some comments will be made for Theorem 3.2. Fig 3.9 visually illustrates the geometric meaning of the symbols used in the theorem. The effort of aligning one end of the line segment to one of the carved marks on the ruler is described by $\delta^{(n)}$. The conditions that $C_n(x) \to 0$ and $D_n(x) \to x$ say that as n becomes larger, the purple regions come narrower; and equation (3.21) says that the probability of δ falling into these two purple regions dominates and is of equal chance. Thus the larger n is, the better the alignment is. Distributions, including but not limited to, truncated normal distributions, (truncated) Beta distributions and uniform distributions all satisfy the assumption of the theorem; therefore the theorem covers most of the common usages. The graph in Fig. 3.9 is actually generated using the truncated normal distributions.

The first conclusion of the theorem is on $E_{AB}^{(n)}$ and links the new method (3.6) with the classic method (3.1). It says that if the measurand is well aligned at a carved mark

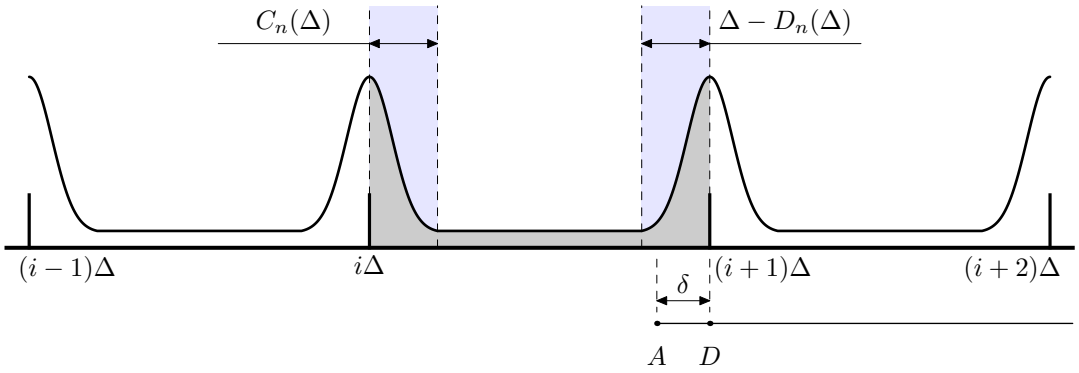

Figure 3.9: Alignment in the view as probability distribution.

on the ruler, then the expectation of PBM becomes identical to the classic method. Fig. 3.10 visually shows the second conclusion of the theorem on $p_h^{(n)}$, using

$$h_x^{(n)}(y) = \begin{cases} \left(1 - \frac{1}{n}\frac{n-2}{n}x\right)\frac{n}{2x} & y \in [0, \frac{x}{n}), \\ \frac{1}{n} & y \in [\frac{x}{n}, \frac{n-1}{n}x), \\ \left(1 - \frac{1}{n}\frac{n-2}{n}x\right)\frac{n}{2x} & y \in (\frac{n-1}{n}x, x), \\ 0 & \text{elsewhere.} \end{cases}$$

where $n \geq 3$. It shows that as n becomes larger, $p_h^{(n)}(x) \to \frac{1}{2}$ for every x in the middle of $\frac{l}{N+1}, \frac{l}{N}$. A larger region on which $p_h \approx \frac{1}{2}$ implies that the region of the sensitive reading becomes smaller and the region for rounding becomes larger.

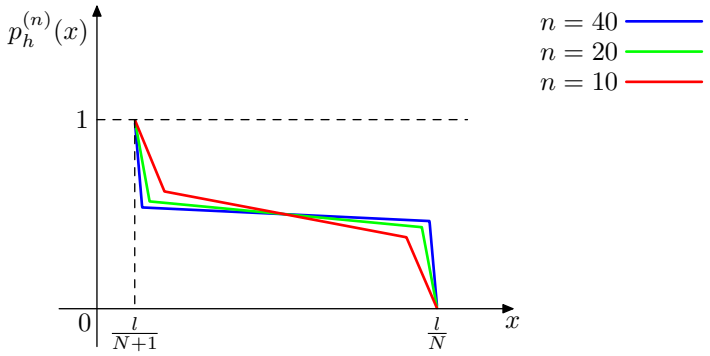

Figure 3.10: Illustration of trends of p_h as n becomes larger

3.5 Summary

This chapter proposes Problem 3.1 as the main challenge for this thesis. Then by loosing the restriction of alignment of the measurand to carved marks on the ruler, the measurement results consist of high and low readings and this forms the base of PBM. p_h the probability of a high reading is then calculated and many propositions are shown.

Tiers of conditions reflecting different levels of priori knowledge are proposed and theoretical solutions to Problem 3.1 are provided for each of these conditions. Finally, the connection of PBM with the traditional approach is summarized in Theorem 3.2, which shows that the new approach is a natural extension to the classic method.

4 Theory for Implementation

The main purpose of this chapter is to gradually add realistic considerations into the theory established in the previous chapter for ideal situations, and to carefully analyze the possible impacts from these real world disturbances. At the beginning, the model of a measurement system consisting of sensors, tools and the gauge object will be built with levels of detail which support both the theoretic analysis later in this chapter and the validation in the next chapter. With the modelling of the hardware, the ideal measuring process which has been discussed in chapter 3 will be made more concrete. Thus, the content of this chapter serves as a bridge between the theory and practical application.

Following the modelling, three topics will be discussed in this chapter. The misalignment of a measurand in a measurement system usually causes trigonometric error, and PBM is of no exception. Through detailed analysis, it shows that a certain misalignment causes a discrete random behavior on l_t. Besides alignment, there will be a section on the source of randomness. The discussion shows that there are many factors, including the measurement process, that contribute to the randomness of δ. It justifies the appropriateness of the usage of synthetic pseudo-randomness and robustness of PBM in the sense of being resistant to random disturbance. Because controllers in the real-world for multi-axis systems (gantries) only make discrete displacements, a section will be used to discuss the impact from this discrete behavior.

Henceforth, the *gauge object*, the *gauge* or simply *the object* will be used to refer to the workpiece that carries the measurand as a feature. The word *gantry* will be used to refer to a multi-axes system that carries sensors. The word *profiler* or *scanner* will be used to refer to the compact laser triangulation profiler in the modelled measurement system.

4.1 Modelling

In this section, the modelling of the measurement system and the gauge object will be established. As stated in chapter 3, the PBM method requires a sensor itself or with the help of other devices in a measurement system to be of adjustable scales. Illustrated by the pin-hole camera model (Fig. 3.1), the modelled measurement system will be using a laser triangulation profiler, which provides adjustable scales with the help of a gantry.

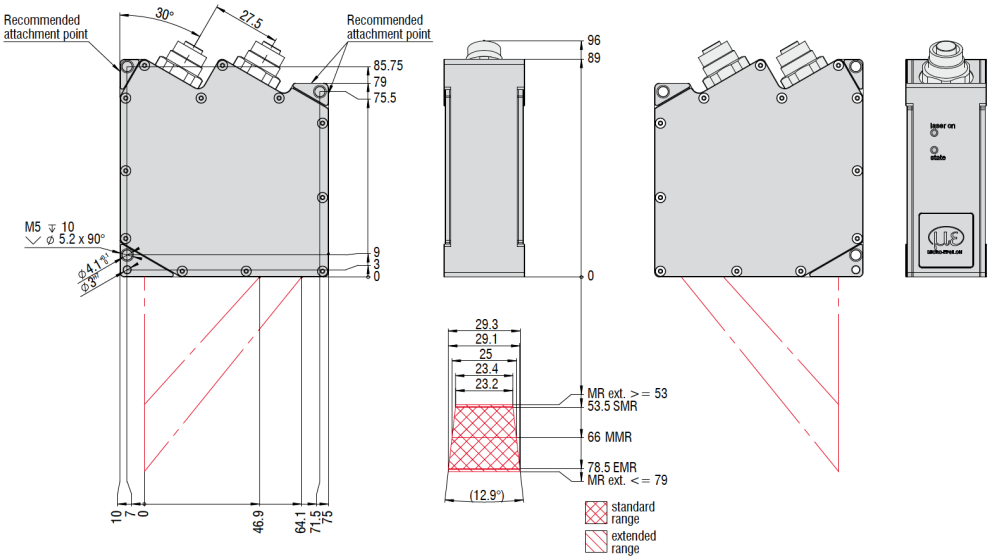

[a]

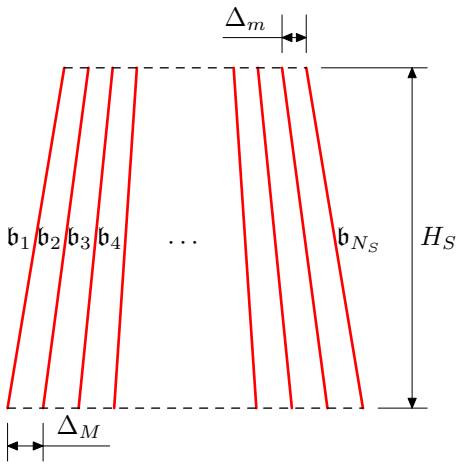

[b]

Figure 4.1: Laser triangulation profiler and its scanning range: **[a]** from Micro-Epsilon catalog [Mic18], schema for `LLT26xx/29xx-25`; **[b]** trapezoidal effective scanning area.

Fig. 4.1[a] shows the drawing of a typical compact laser triangulation profiler. The effective scanning area is usually trapezoidal and let N_S be the number of points in a sampled profile. It is equivalent to modelling the profiler as having N_S laser beams spanned equally in the trapezoidal scanning area. Let $\mathfrak{b}_i$ denote the i^{th} laser beam, and Δ_M, Δ_m denote the distance between adjacent laser beams at different horizontal sections as depicted in Fig. 4.1[b]. Let H_S be the height of the trapezoidal effective scanning area. Taking the Micro-Epsilon scanner `LLT29xx-25` for example, it can be found from the product catalog [Mic18] that

$$N_S = 1280 \qquad \Delta_m \approx 18.3\mu\text{m} \qquad \Delta_M \approx 22.8\mu\text{m} \qquad H_S = 25\text{mm}$$

using the standard scanning range and default scanning field. It will be assumed that the trapezoidal effective scanning area is perfectly symmetric and the laser beams span the area uniformly.

Then the modelling of the measurand and the gauge object is going to be built here. The gauge object used for the analysis in this chapter and the validation in the next chapter is a metal block with an extrusion of parallel walls; and the ideal shape is shown by Fig. 4.2. The measurand is the width of the extrusion. Let $\overrightarrow{n}$ denote the normal direction of the top surface of the extrusion pointing outwards the block. Let $\overrightarrow{m}$ denote the direction of the extrusion as shown in Fig. 4.2. Real-world extrusions cannot have absolutely parallel edges, thus $\overrightarrow{m}_1, \overrightarrow{m}_2$ will be used for directions of each edge according to the context. Similarly, for non-ideal cases, $\overrightarrow{n}$ will be referring to the normal direction of the plane which approximates the top surface of the extrusion. Let H_E be the height of the extrusion.

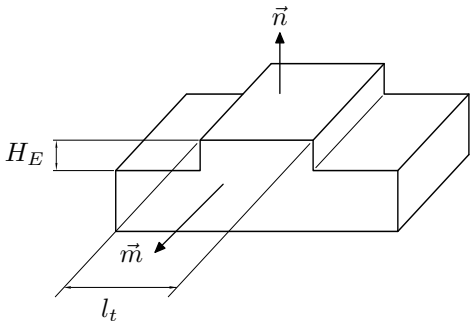

Figure 4.2: Measuring width of the extrusion.

The laser profiler will be attached to a 3-axis gantry system and the whole system will be positioned as illustrated by Fig. 4.3. For now, assume that the gantry system is ideal and provides movement in three directions that are pairwise orthogonal. In

real-world cases, it should be understood as that the gantry system is well-designed and assembled so that the systematic error is sufficiently insignificant. Later in section 4.4, there will be detailed discussion for the error caused by multi-axis systems. The movement directions of the gantry system are used as

$$\overrightarrow{e_1} = (1,0,0)^T \qquad \overrightarrow{e_2} = (0,1,0)^T \qquad \overrightarrow{e_3} = (0,0,1)^T$$

for the x, y and z direction respectively. The orientation of the scanner is fixed in a way that the plane containing the trapezoidal effective scanning area is parallel to the zOy-plane and the symmetric axis of the trapezoid is parallel to the z-axis. Ideally, the gauge object is placed in a way that $\overrightarrow{n}$ is parallel to $\overrightarrow{e_3}$ and $\overrightarrow{m}$ is parallel to $\overrightarrow{e_1}$. However, in the real world it is impossible to make such perfect alignment. The mis-aligned cases will be discussed in section 4.2 later. The origin of the coordinate system is of less importance and could be chosen in a way that benefits the analysis and discussion.

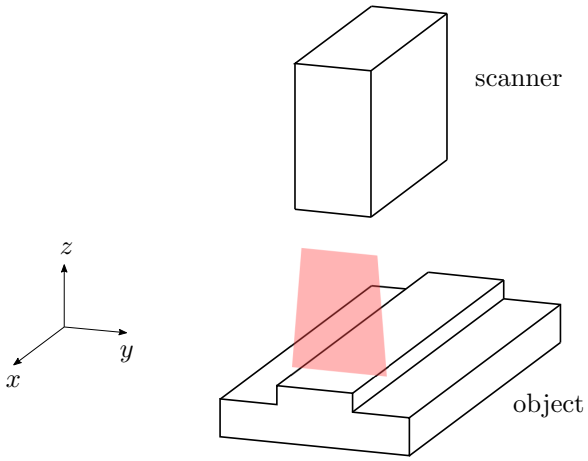

Figure 4.3: Positions

Under this setting, it can be claimed that the system provides an adjustable scale as required in chapter 3. Fig. 4.4[a] illustrates typically how a profile is sampled by the scanner. Valid readings with different height information are provided by beam $\mathfrak{b}_h$ and $\mathfrak{b}_l$. Beam $\mathfrak{b}_v$ fails to provide a valid feedback, because the laser spot falls somewhere outside of the effective scanning range. Such failure also occurs if the a laser spot is hidden from the field of view (FoV) of the camera or is wildly reflected. Modern commercial scanners are able to identify such failures and feedback properly. Using Fan's simple method ([Fan97]), one can identify the valid points on the top surface of the extrusion as they will have a larger z coordinate. For example in Fig. 4.4[a], by the fact that $z_h > z_l$, it can be told that beam $\mathfrak{b}_h$ has its spot on the top surface of the extrusion. Fig. 4.4[b] and [c] show the cases where the scanner is profiling at different

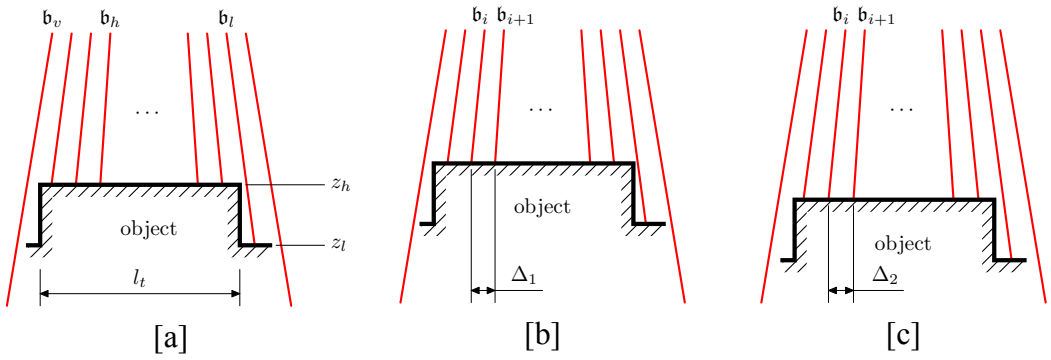

Figure 4.4: Laser on the surface of the object: **[a]** shows lasers with different reading; **[b]** and **[c]** show scale change after scanner position is changed by the gantry.

heights with corresponding lateral scales $\Delta_1 < \Delta_2$. For ideal gantries, which provide continuous positioning, it is possible for the scale to take any value between Δ_m and Δ_M and this fails for the real devices. Discussions of the real-world gantries, where only discrete values of Δ are achievable will be conducted later in section 4.4.

Before moving to the detailed discussions, it is better to put some brief comments here on the sources of randomness. Compared to the traditional method, PBM does not require the alignment of measurands to carved marks and treats the left-most part of the measurand covered by a loose scale as a random variable. Although, there were no words on how the randomness occurs in the previous chapter, it is important to identify the sources of randomness in the real world, which might be systematic and intrinsic, like noises of signal or mechanical vibrations, or synthetic, generated by specific algorithms like pseudo-random numbers. As stated earlier, the contents in this chapter including the modelling pave the way for validation; therefore as an indispensable part, the source of randomness is entangled deeply with the sampling process. With detailed discussions postponed until section 4.3, the "major" part of the randomness is specified to be from the pseudo-randomness generated in the following way. As illustrated by Fig. 4.5, a pseudo-random displacement generated by the gantry system along the y-axis will induce a change in δ; and this will be the main source of randomness of δ. Fig. 4.5[b] shows that the induced δ is generally different to Δy.

With the basic modellings of the sensor, gantry system and randomness established, it is time to develop detailed discussion of the topics listed at the beginning of this chapter.

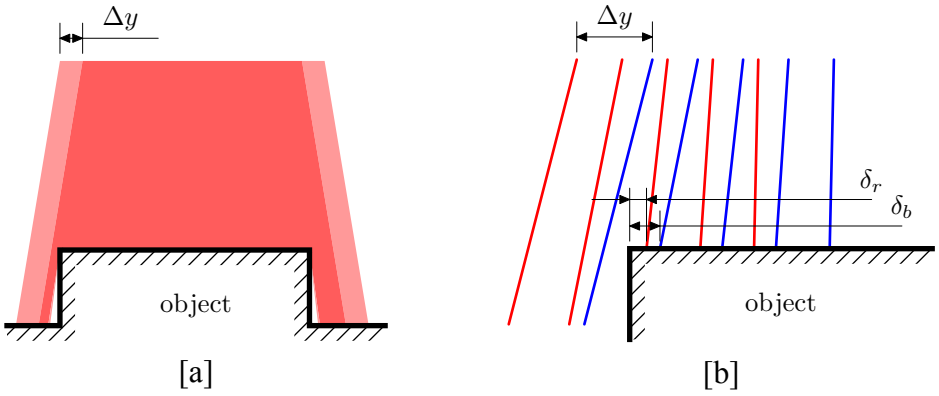

Figure 4.5: Generation of pseudo-randomness by randomly shifting Δy

4.2 Alignment

In this section, discussions will be conducted for the case where perfect alignment of the gauge object fails. Ideally it is expected that $\overrightarrow{n}$ is parallel to $\overrightarrow{e_3}$ and $\overrightarrow{m}$ is parallel to $\overrightarrow{e_1}$ as modelled in the previous section; and the imperfect alignments in this section mainly refers to the failure of these parallelisms. Fig. 4.6 shows the case where $\overrightarrow{m}$ fails to be parallel to $\overrightarrow{e_1}$ (while assuming $\overrightarrow{n}$ being parallel to $\overrightarrow{e_3}$). As a result, trigonometric error occurs. Let θ_m be the included angle between $\overrightarrow{m}$ and $\overrightarrow{e_1}$, then

$$\theta_m = \arccos \frac{\overrightarrow{m} \cdot \overrightarrow{e_1}}{\|\overrightarrow{m}\|}.$$

Because $l'_t = l_t / \cos\theta_m \geq l_t$, the measurement process will be equivalently examining a measurand that is larger than or equal to the origin. Practically, $\overrightarrow{m}$ can be found. For example, in the validation procedure of this thesis, $\overrightarrow{m}$ is obtained via a scan along the x-axis followed by edge detection using least square fitting. Henceforth it will be assumed that both $\overrightarrow{m}$ and θ_m are known. One possible way to deal with this case is to work with the new tolerance range $[l'_n - T', l'_n + T']$ where $l'_n = l_n / \cos\theta_m$ and $T' = T / \cos\theta_m$. Obviously it is true that $l_t \in [l_n - T, l_t + T]$ if and only if $l'_t \in [l'_n - T', l'_n + T']$.

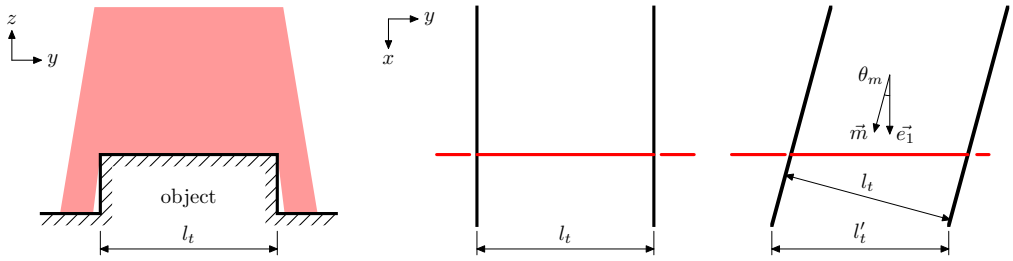

Figure 4.6: Trigonometric error when the extrusion is not along the x-axis

Now consider the case where only $\overrightarrow{n}$ is mis-aligned against $\overrightarrow{e_3}$. Let θ_n be the included angle between $\overrightarrow{n}$ and $\overrightarrow{e_3}$, and Fig. 4.7[a] provides a section view of this case. Similar to the previous case, it is assumed that both $\overrightarrow{n}$ and θ_n are known; and the trigonometric error occurs. Besides, there are more details to be checked. Fig. 4.7[b] illustrates the details of a section being sampled by the scanner. Let B_i be the laser spot of beam $\mathfrak{b}_i$ found on the top surface of the extrusion. The simple fact that

$$|B_{i-1}B_i| \neq |B_iB_{i+1}| \tag{4.1}$$

shows the need of more dedicated work, because the new method has only considered rulers of equal scales so far. Draw auxiliary lines parallel to $\overrightarrow{e_2}$ passing through ends of the top extrusion, and let $\overline{B}_i$ denote the intersection of the upper auxiliary line with $\mathfrak{b}_i$ and $\underline{B}_i$ denote the intersection of the lower auxiliary line with the extension of $\mathfrak{b}_i$. Then the equality $\left|\underline{B}_{i-1}\underline{B}_i\right| = \left|\underline{B}_i\underline{B}_{i+1}\right|$ and $\left|\overline{B}_{i-1}\overline{B}_i\right| = \left|\overline{B}_i\overline{B}_{i+1}\right|$ hold and these will be used to make a detailed estimation. Denote $\left|\overline{B}_i\overline{B}_{i+1}\right|$ and $\left|\underline{B}_i\underline{B}_{i+1}\right|$ by $\overline{\Delta}$ and $\underline{\Delta}$ respectively, then $\Delta_m \leq \overline{\Delta} \leq \underline{\Delta} \leq \Delta_M$. Denote the included angle of the top surface and $\overrightarrow{e_2}$ by θ_s as illustrated in Fig. 4.7[b]. Generally $\theta_s \neq \theta_n$. Because the trapezoidal effective scanning area is symmetric, henceforth the argument will be developed assuming $0 \leq \theta_s \ll 1$.

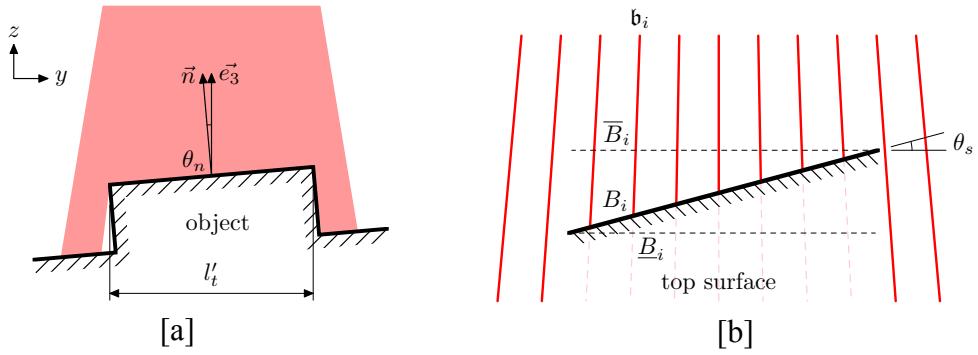

Figure 4.7: Non-horizontal alignment of the top surface

For general cases where both mis-alignments occur, that is, $\theta_m \neq 0$ and $\theta_n \neq 0$, one should find out $\overline{\Delta}$, $\underline{\Delta}$, and l'_t to make a correct estimation. The definition of $\overline{\Delta}$, $\underline{\Delta}$, and l'_t are sectional, and Fig. 4.7 can be used for reference in this case. Let

$$\overrightarrow{n} = (n_x, n_y, n_z)^T \qquad\qquad \overrightarrow{m} = (m_x, m_y, m_z)^T$$

be unit vectors. Then it holds true that

$$\cos\theta_s = \frac{(\overrightarrow{n} \times \overrightarrow{e_1}) \cdot \overrightarrow{e_2}}{\|\overrightarrow{n} \times \overrightarrow{e_1}\|} = \frac{n_z}{\sqrt{n_z^2 + n_y^2}}$$

and

$$l'_t = \frac{\|\overrightarrow{n} \times \overrightarrow{e_1}\| \cdot \|\overrightarrow{n} \times \overrightarrow{m}\|}{(\overrightarrow{n} \times \overrightarrow{e_1}) \cdot (\overrightarrow{n} \times \overrightarrow{m})} l_t \cos\theta_s = \frac{(\overrightarrow{n} \times \overrightarrow{e_1}) \cdot \overrightarrow{e_2}}{(\overrightarrow{n} \times \overrightarrow{e_1}) \cdot (\overrightarrow{n} \times \overrightarrow{m})} l_t.$$

Let

$$K(\overrightarrow{n}, \overrightarrow{m}) = \frac{(\overrightarrow{n} \times \overrightarrow{e_1}) \cdot \overrightarrow{e_2}}{(\overrightarrow{n} \times \overrightarrow{e_1}) \cdot (\overrightarrow{n} \times \overrightarrow{m})}$$

be the coefficient and will be abbreviated as K when there is no ambiguity. Then $l_t \in [l_n - T, l_n + T]$ if and only if $l'_t \in [Kl_n - KT, Kl_n + KT]$. Let $\Delta_0 = \frac{\overline{\Delta}+\underline{\Delta}}{2}$. and it is worth pointing out that $\overline{\Delta}$ and $\underline{\Delta}$ vary as the position of the gauge object in the effective scanning area changes. Nevertheless, it is reasonable to assume that Δ_0 is known. This is because the height coordinate of every B_i on the top extrusion can be retrieved from the scanner and the arithmetic mean will be very close to the height of the middle of the profile. Then Δ_0 can be solved using the geometric information of the trapezoidal effective scanning area. Hence

$$\overline{\Delta} = \Delta_0 - \frac{(\Delta_M - \Delta_m) l'_t \sin\theta_s}{2H_S} \tag{4.2}$$

$$\underline{\Delta} = \Delta_0 + \frac{(\Delta_M - \Delta_m) l'_t \sin\theta_s}{2H_S} \tag{4.3}$$

are also known. As shown in Fig. 4.8, let E_1, E_2 denote the ends of the top extrusion, let O_S denote the intersection of $\mathfrak{b}_i$ and $\mathfrak{b}_{i+1}$. Let F_2, F_1 be points on $O_S E_1$ and $O_S E_2$ respectively such that F_1E_1 and F_2E_2 are parallel to the y-axis. The subscription will always be put in the way that such that $|F_2E_2| \leq |F_1E_1|$.

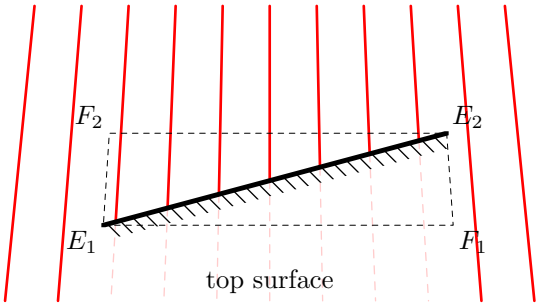

Figure 4.8: Equivalent edges

Now the trapezoid $E_1F_1E_2F_2$ provides equivalent measurands for PBM in the sense that if a line segment is placed with ends exactly at E_2 and F_2, the number of full scales will be the same as that read from the E_1E_2. It implies that the frequencies of high and low readings will be exactly the same when the real extrusion is replaced by the virtual line segment. Although the analysis in this section will be using E_2F_2, the shorter

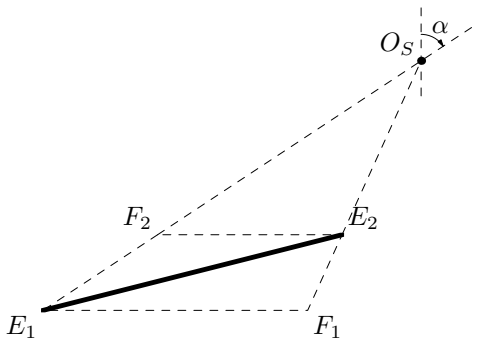

Figure 4.9: Geometry of the equivalent trapezium area

horizontal edge of the trapezium; equivalent work can be produced in parallel using E_1F_1. The discussion continues with the computation of the length of E_2F_2.

Let α be the directed angle as shown in Fig. 4.9. Then immediately $\alpha \in [-\alpha_0, \alpha_0]$, where

$$\alpha_0 = \arctan \frac{(N_S - 1)(\Delta_M - \Delta_m)}{2H_S}$$

is determined by the shape of the effective scanning area of the laser scanner. Direct computation shows that

$$|F_2E_2| = (1 - \tan\theta_s \tan\alpha) l'_t \tag{4.4}$$

Let $\kappa(\overrightarrow{n}, \overrightarrow{m}, \alpha) = (1 - \tan\theta_s \tan\alpha)$ and abbreviate it as $\kappa(\alpha)$ or κ when there is no ambiguity. Then

$$|F_2E_2| = \kappa(\alpha) l'_t = \kappa K l_t. \tag{4.5}$$

The following example shows concretely how these are computed in detail:

Example 4.1. Let the width of the extrusion on a given gauge object be $l_t = 2.7mm$. A scan using Micro-Epsilon `LLT2900-25` shows that

$$\overrightarrow{n} \approx (0.0000141, -0.0000736, 1.0)$$
$$\overrightarrow{m} \approx (0.999929, -0.0119105, 0).$$

The information of the effective scanning area of `LLT2900-25` can be found on page 52; and according to the data it can be computed that $\alpha_0 \approx 6.5°$, $\theta_s \approx 0.0000736$, $K \approx 1.00007$, and $|\kappa(\alpha) - 1| \leq 10^{-5}$. When the samplings are obtained with random shifts alongside the y-axis such that α ranges in $[-\alpha_0, \alpha_0]$, the equivalent measurand $|F_2E_2|$ ranges between 2.70017mm and 2.70021mm. If random shifts are controlled in a narrower range so that α ranges on a proper subset of $[-\alpha_0, \alpha_0]$, then $\kappa(\alpha)$ will be closer to 1 and the range of $|F_2E_2|$ shrinks. □

As shown by Example 4.1, it seems that the analysis ends here if the tolerance range is relatively large, like ± 0.01mm; however, the fact that $|F_2E_2|$ changes as the sensor is shifted alongside the y axis indicates that the theory proposed in chapter 3 must be examined in detail. The theory and analysis in chapter 3 is established by analyzing $p_h(\Delta, l)$ where l is a constant. Besides mis-alignments, there are many external factors that cause the measurand to change, for example, vibrations of table change the section of the extrusion one measures and a temperature drop shrinks the width of the extrusion. Although the thesis will provide some discussion in this chapter and later in chapter 6, extended discussion should be conducted in future work for its complexity.

Figure 4.10: Same δ different $|F_2E_2|$

It is natural to extend the theory of PBM by analyzing $p_h(\Delta, l)$ with the assumption that l is also a random variable. By common sense and pragmatic experience, it is reasonable to assume that l is bounded in a finite range$[\underline{l}, \bar{l}]$. Then instead of merely analyzing the random variable δ, it is natural to analyze the random vector (δ, l). Fig. 4.10 illustrates the case where equal δ is obtained after shifting Δy along the y-axis. After the shift α changes, and hence $|F_2E_2|$ differs. Because $N_S < \infty$, for a given δ there are finitely many possible values of $|F_2E_2|$. Let $P_{\delta,l}$ be the probability distribution of the random vector (δ, l), then by the arguments above, $P_{\delta,l}$ is not absolutely continuous to μ_L, the Lebesgue measure for $\mathbb{R}^2$.[2] Moreover the discussion also shows that $P_{\delta,l}$ is of mixed type — continuous with respect to δ but discrete to l.

It will be assumed that $\bar{l} - \underline{l} < \Delta$, and this should be understood as saying that the magnitude of the variance of the measurand is insignificant compared to the scale. $\mathfrak{l}$ will be used when one wants to stress that l is treated as a random variable. The following example shows how the result set is impacted by a random vector (δ, l):

Example 4.2. Let $\mathfrak{l}_t \in [150 - 0.001, 150 + 0.002]$ be of uniform distribution, and δ is also known to be of uniform distribution. Let $\Delta_0 = 3$. If $\mathfrak{l}_t$ and δ are independent, then

[2] When there is no ambiguity of dimension, we shall always use μ_L for the Lebesgue measure.

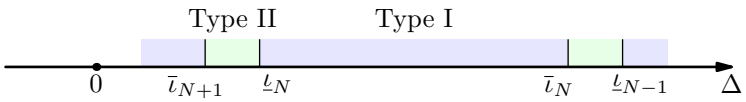

Figure 4.11: Different interval ranges of Δ

the result set (in probability) is

$$R_\infty(n) = \begin{cases} 0.000002 & n = 50, \\ 0.9999975 & n = 49, \\ 0.0000005 & n = 48, \\ 0 & n \in \mathbb{Z} \setminus \{48, 49, 50\}. \end{cases}$$

□

As shown by Example 4.2, one significant difference to the situations in chapter 3 is that result sets R_M can be supported on more than two points. Indeed the support of R_M is always a subset of

$$\left\{ \lfloor \frac{\mathfrak{l} - \delta}{\Delta} \rfloor \middle| \mathfrak{l} \in [\underline{l}, \bar{l}], \delta \in [0, \Delta) \right\} = \left\{ \lfloor \frac{\mathfrak{l}}{\Delta} \rfloor \middle| \mathfrak{l} \in [\underline{l}, \bar{l}] \right\} \cup \left\{ \lfloor \frac{\mathfrak{l}}{\Delta} \rfloor - 1 \middle| \mathfrak{l} \in [\underline{l}, \bar{l}] \right\}, \quad (4.6)$$

and the conditions of Example 4.2 yield that the result set R_M there can be at most supported on three points. This indicates that the theory based on high and low readings needs modification and improvements. Let

$$\underline{\iota}_N = \frac{\bar{l}}{N+1} \qquad\qquad \bar{\iota}_N = \frac{\underline{l}}{N},$$

then for N not too large, Δ is always from one of the two types of intervals as illustrated by Fig. 4.11. If $\underline{\iota}_N < \Delta \leq \bar{\iota}_N$, then the support of R_M can be at most two points. If $\bar{\iota}_{N+1} < \Delta \leq \underline{\iota}_N$, then R_M might be supported on three points as in Example 4.2. These intervals will be called Type I and Type II respectively for convenience.

For Δ from Type I intervals, there are only two possible non-zero points of R_M, the concept of high and low readings remain valid. Then the discussion advances with the investigation of $p_h(\Delta, \mathfrak{l})$ with Δ from intervals of Type I. As $P_{\delta,l}$ is of mixed type, it can be written as

$$p_h(\Delta, \mathfrak{l}) = \sum_{j \in J} \omega_j p_h(\Delta, l_j) \quad (4.7)$$

where J is finite and the weights $\omega_j \geq 0, \sum_{j \in J} \omega_j = 1$. Each l_j is in $[\underline{l}, \bar{l}]$ and let $\bar{j}$, $\underline{j}$ denote the indexes such that $l_{\bar{j}}$ is the maximum and $l_{\underline{j}}$ the minimum. By Proposition 3.2, it holds

$$p_h(\Delta, l_{\underline{j}}) \leq p_h(\Delta, \mathfrak{l}) \leq p_h(\Delta, l_{\bar{j}}). \quad (4.8)$$

As the (pseudo-)randomness of δ is generated by the random translation Δy along the y-axis, it is reasonable to assume that ω_j are known. Hence, if $p_h(x)$ is analytically known, it implies that $p_h(x, \mathfrak{l})$ is also analytically known on intervals of Type I. Because the right hand side of (4.7) is a weighted sum of $p_h(x)$, $p_h(x, \mathfrak{l})$ is (strictly) monotone on intervals of Type I if $p_h(x)$ is (strictly) monotone. That is, P1, P2 and S conditions are preserved on intervals of Type I, when l is regarded as a bounded random variable. P3 condition states that discontinuity of $p_h(x)$ occur at $\Delta = \frac{l}{N}$, which when considered as a point where $\lfloor \frac{l}{\Delta} \rfloor$ changes value, lies in intervals of type II. Therefore the P3 condition is also preserved by 4.7. Denote the length of intervals of Type II by

$$L_N = |\underline{\iota}_N - \overline{\iota}_{N+1}| = \frac{\overline{l} - \underline{l}}{N+1},$$

then $L_N \leq \frac{\overline{l}-\underline{l}}{3}$ and $\lim_{L_N \to 0} \underline{\iota}_N = \lim_{L_N \to 0} \overline{\iota}_{N+1} = \frac{l_t}{N+1}$.

Then consider the case where Δ comes from Type II intervals $(\overline{\iota}_{N+1}, \underline{\iota}_N]$ in detail. Let $J = J_1(\Delta) \cup J_2(\Delta)$ such that for $j \in J_1(\Delta), l_j < N\Delta$ and for $j \in J_2(\Delta), l_j \geq N\Delta$. The possible number of full scales are hence $N-2, N-1, N$, and let $\overline{p}_l, \overline{p}_m, \overline{p}_h$ be the probability of reading $N-2, N-1, N$ full scales respectively. Compared to ideal cases in chapter 3 and cases where Δ is in intervals of Type I, $\overline{p}_m$ is new and will be called the probability of the *mid reading*. Symbols of probability of high, mid, and low readings are overlined, and this is to emphasize that the discussion is for Δ from Type II intervals. Then easily it holds

$$\begin{aligned}
\overline{p}_l(\Delta, \mathfrak{l}) &= \sum_{j \in J_1(\Delta)} \omega_j (1 - p_h(\Delta, l_j)) \\
\overline{p}_m(\Delta, \mathfrak{l}) &= \sum_{j \in J_1(\Delta)} \omega_j p_h(\Delta, l_j) + \sum_{j \in J_2(\Delta)} \omega_j (1 - p_h(\Delta, l_j)) \\
\overline{p}_h(\Delta, \mathfrak{l}) &= \sum_{j \in J_2(\Delta)} w_j p_h(\Delta, l_j),
\end{aligned}$$

and these suggest that the reading of number of full scales for Type II intervals can be regarded as a combination of two simple cases. By Proposition 3.1, the following are immediate

$$\lim_{L_N \to 0} \overline{p}_l(\Delta, \mathfrak{l}) = \lim_{L_N \to 0} \overline{p}_h(\Delta, \mathfrak{l}) = 0 \qquad \lim_{L_N \to 0} \overline{p}_m(\Delta, \mathfrak{l}) = 1 \tag{4.9}$$

Now it is time to modify the measurement process with the consideration of general mis-alignments. Firstly, find out $\overrightarrow{n}$ and $\overrightarrow{m}$ by performing a scan alongside the x-axis and applying a proper algorithm on the obtained point cloud. Then compute K, $\kappa(\alpha_{\min})$

and $\kappa(\alpha_{\text{max}})$. Regardless of the tolerance range to be checked against, set a proper bound to l_t by $\underline{L} < l_t < \overline{L}$.[3] Let

$$\bar{l} = \overline{L}K\kappa(\alpha_{\text{min}}) \qquad \text{and} \qquad \underline{l} = \overline{L}K\kappa(\alpha_{\text{max}}),$$

then $\bar{l} - \underline{l}$ is an upper bound of the oscillation of l_t. If $\bar{l} - \underline{l}$ is too large, one should stop and check the fixture of the gauge object and the measurement system. Choose an $N_0 \in \mathbb{Z}_+$ and let $\Delta_0 = \frac{l_n}{N_0}$. The choice of N_0 must guarantee the condition that $\bar{l} - \underline{l} < \Delta_0$, and if possible make L_N significantly smaller than the minimum step of y-axis that can be achieved by the controller of the gantry system. During the (pseudo-)randomness shifts alongside the y-axis and the sampling process, this Δ_0 should be maintained using a proper control algorithm. Then by equation (4.2), find out $\overline{\Delta}$ and count the number of full scales. The result set is then ready for $\overline{\Delta}$.

Then theories established in chapter 3 on $p_h(\overline{\Delta}, \mathfrak{l})$ can be applied here with no modification. This is because for a general positioning of the gauge object and choice of N_0, L_N will be very small compared to the resolution of gantry axes. Thus almost all practical measurements will be for Type I intervals. In case that $\overline{\Delta}$ actually falls in Type II intervals, by equations (4.9) the result sets are most likely to be supported on a single point. The single point supported result set coincides with the case in chapter 3 in the sense that both indicate the same fact that the multiple of $\overline{\Delta}$ is extremely close to the true value of the measurand. For coherence reason, more detailed discussions for R_M supported on three points are presented at the end of the next section on randomness. The section ends with the following example:

Example 4.3. Using Micro-Epsilon `LLT2500-25` profiler, a scan of a gauge object with extrusion shows that

$$\overrightarrow{n} = (0.0119761, 0.0618767, 0.998012)$$
$$\overrightarrow{m} = (0.998322, -0.0399329, 0.0419295).$$

It implies that $\theta_n \approx 3.6°, \theta_m \approx 3.3°$, a huge mis-alignment observable by bare eyes. To test against the tolerance range $[2.7 - 0.1, 2.7 + 0.1]$, one fixes $N_0 = 13$, $\Delta_0 = 2.7/13 \approx 0.207692$ and chooses $\overline{L} = 2.9, \underline{L} = 2.5$.[4] The process of generation of pseudo-randomness guarantees that $\alpha_{\text{max}} = 5°$ and $\alpha_{\text{min}} = 2°$, then

$$\bar{l} \approx 2.8946 \qquad \underline{l} \approx 2.88515,$$

and hence $L_{13} \leq 0.0006754$. It means that the Type II interval around $\Delta = 0.207$ spans merely about 3.5‰ of the Δ-axis. □

[3] For example, one may assume that $\overline{L} = l_n + 10T$, $\underline{L} = l_n - 10T$ define a safe range; or more practically $\overline{L} = l_n + \Delta$ and $\underline{L} = l_n - \Delta$ for a chosen Δ.

[4] This choice of Δ can be achieved by using every 10^{th} beam.

4.3 Randomness and Robustness

In this section, the randomness of δ is investigated. Early in this chapter, it has been briefly stated that in the aspect of implementation, the randomness of δ would be mainly induced from random shifts of the gantry system alongside of the y-axis; however the reason behind the statement was never mentioned. Besides the man-made random shift, other random factors, such as, table vibrations, hysteresis of axes and thermal errors may also affect the distribution of δ. One of the goals of this section is to closely examine these sources of randomness and justify the use of y-axis random shift in this thesis, especially for the validation process. Through the discussion of this section it will show that PBM is robust against vibrations and other random disturbances, which are commonly treated as noises or random errors. And this is the other main goal to be achieved in this section. Because this chapter deals with real-world obstacles for validation, all theoretical discussions will be focused on the scenarios modelled in section 4.1.

The probability-based method proposed in this thesis requires to obtain p_h, the probability of high readings, and in practice f_h the frequency of the high readings. The frequency is immediate once the result set is obtained, and thus the random behavior of δ actually occurs in every sampling process. As early as 1873, A. Hall in [Hal73] reported trials to determine the value of π by throwing fine steel wires on plane wooden surface ruled with equidistant parallel lines. It is reported there that the result is improved if the surface was rotated a little bit every time before each throw. [Hal73] can be regarded as a piece of evidence showing that better result can be obtained by improving the quality of randomness during the sampling process. In terms of implementation, "throwing" the gauge object for randomness is not a good idea; because this action introduces randomness to other parameters besides δ. For example, $\overrightarrow{m}$ as defined in the previous section goes wild. More importantly, after each "throwing" the section of the extrusion changes which essentially means that the measurement work is conducted against different measurands.

Now suppose that a perfect fixture structure is designed and the placement of the gauge object is always precisely set at the same places. Ramesh in [RMP00] categorized sources of error into 4 major groups, and these sources of error influence the random behavior to δ. For example, the relative motion between machine parts (or vibration) will produce random fluctuation on the displacement between the ends of the

measurand and the laser sensor; thermal error from the machine structure causes distortion of the bed where the gauge object is put. Besides, the initial state of the whole system also contributes to the randomness of δ. If the initial position of the gantry system is (pseudo-)random, it is equivalent to think that the gauge object is randomly placed with identical initial system state. Compared to the wild random "throwing" of the gauge object, the initial position of the gantry system is controllable. For example, by shifting along the y-axis, it can be expected that all samplings are conducted against one section of the gauge object. And with proper algorithms, randomness of different distributions can be achieved. The randomness caused by the initial state of the gantry system will henceforth be known as *randomness from placement* or *placement randomness*.

Thus it is reasonable to decompose δ as

$$\delta \sim \delta_p + \delta_0 + \delta_1 + \cdots \tag{4.10}$$

where δ_p denotes the randomness from placement, and δ_i the randomness introduced by various sources of error. Although sources of error differ in each system; the combined impact on randomness is limited in the sense that the randomness is spatially bounded and has a mean of 0. Thus it is equivalent to treat all δ_i in (4.10) altogether and re-write (4.10) as

$$\delta \sim \delta_p + \delta_r. \tag{4.11}$$

For a rule of scale Δ, $\delta_p \in [0, \Delta)$ by definition and is assumed to be satisfying the conditions of Theorem 3.1. Assume $\delta_r \in [-m_r, m_r]$ for some fixed $m_r \geq 0$ and $E(\delta_r) = 0$. Then from equation (4.11) the following identity can be established

$$\delta = (\delta_p + \delta_r) - \lfloor \frac{\delta_p + \delta_r}{\Delta} \rfloor \Delta. \tag{4.12}$$

If both δ_p, δ_r are insignificant, i.e. being supported on a very narrow interval, then δ will again be supported on a very narrow interval. It means that δ behaves like a random variable of the Dirac distribution. In this case if δ and p_h satisfy the assumptions in chapter 3, PBM can be applied without modification; however, in this case PBM degenerates to the classic method in the sense of Theorem 3.2. While δ_r can hardly be manipulated; in order to avoid this degenerated case, it is possible to amplify and manipulate the randomness of δ_p using the gantry system. This is the reason why the decision to induce randomness on δ using random shifts alongside the y-axis is proposed at the end of section 4.1.

In the rest of the subsection, the discussion will be consisting of two topics — one on the implementation of pseudo-randomness of δ_p, and the other on the impact of δ_r on δ via (4.12).

Random shifts of the gantry alongside the y-axis keep the important vectors $\overrightarrow{n}$ and $\overrightarrow{m}$ intact. Although disturbances from other axes are inevitable during the movement; it is reasonable to assume that the impact is insignificant in well-designed systems and the section of extrusion under examination is unchanged. Let the random shift of the gantry along the y-axis be presented by a bounded random variable $\mathfrak{y}$ and the gauge object be fixed at position (x_0, y_0, z_0). Then it holds

$$\delta_p = \mathfrak{y} + y_0 - \lfloor \frac{\mathfrak{y} + y_0}{\Delta} \rfloor \Delta. \tag{4.13}$$

Replacing y_0 by $y_0' = y_0 - i\Delta$ for $i \in \mathbb{Z}$ in (4.13), the form remains the identical. Therefore it can always be assumed that $y_0 \in [0, \Delta)$ for a given Δ. If the distribution of $\mathfrak{y}$ is known, then the distribution of δ_p can be computed using (4.13). Thus ultimately, one needs to either generate pseudo-randomness on $\mathfrak{y}$ for desired distributions on δ or find out the distribution of the induced δ for a given $\mathfrak{y}$.

In [ISO24153], the methods of generation of (pseudo-)randomness have been categorized in three groups, the mechanical device method, table method and computer method. For this thesis, it is more convenient to adopt the computer method for the validation process. That is, a pseudo-random number will be generated by computer algorithms, and then used as $\mathfrak{y}$.

Mainly following Knuth's work [Knu97] and making reference to [ISO28640] [JISZ9031] [ISO24153], a brief review on how pseudo-randomness of certain distribution is generated will be included here. While [ISO28640] uses the term "random number" for uniformly distributed random variate, this thesis uses "random number" for random variables with any distributions. Henceforth the symbol $\mathfrak{u}$ will be used to refer to the uniformly distributed random variable on $[0, 1]$. One general approach is to firstly implement a pseudo-random real number uniformly distributed on the interval $[0, 1]$. Then for a random variable X with continuous distribution, the inverse function method can be applied. Let $F(x)$ be the cumulative distribution function of X, that is, $F(X) = P(X \leq x)$. Then for strictly increasing F, the inverse function F^{-1} is well-defined and X is obtained by $F^{-1}(\mathfrak{u})$.

For a specific distribution, better alternative algorithms exist. For example, for normal distributions the polar method (also known as Box-Müller) is well-known and suggested by [ISO28640]. This is a special case of the more general Neumann's rejection

method [Knu97]. Special algorithms are often optimized in certain cases. For example, to generate gamma distribution of integral order a, [ISO28640] recommended a simple logarithm method (inverse function method); however, this method is too slow when a is very large. Ahrens and Dieter in [AD74] compared the performance of 5 different algorithms and found that the Dieter-Ahrens GO algorithm is 10 times faster than the simple logarithm method for large a.

Unlike the generation of random variables for specific distributions, most software runtimes have an implementation of $\mathfrak{u}$. Limited by the floating-point number system, $\mathfrak{u}$ is practically implemented as

$$\mathfrak{u} = \frac{X}{m}$$

where m is a fixed positive integer and $0 \leq X < m$ is an equally weighted random integer [Knu97][ISO28640]. Thus the implementation of $\mathfrak{u}$ is supported by this X. Starting from the famous yet simple linear congruential method (LCM), M-sequences, GFSR (generalized feedback shift register) and the Mersenne twister are widely used nowadays in industry for generation of long period random sequences. Parameters used in these algorithms must be dedicatedly chosen for the quality of randomness; as these topics are of little relevance to this thesis detailed discussions are suppressed here. For further reference, one can follow Knuth's work [Knu97].

Now assume that an implementation of $\mathfrak{y}$ for a given distribution is ready. Suppose $|\mathfrak{y}| \leq M_y$ for some $M_y \in \mathbb{R}_+$ and the probability distribution of $\mathfrak{y}$ is absolutely continuous with respect to μ_L, the Lebesgue measure. Let $h_{\mathfrak{y}}$ be the Radon-Nikodym derivative of $P_{\mathfrak{y}}$. Then because

$$P(\delta_p \leq x) = P(0 \leq \delta_p \leq x) = P(0 \leq \mathfrak{y} + y_0 - \lfloor \frac{\mathfrak{y} + y_0}{\Delta} \rfloor \Delta)$$

and $\lfloor \frac{\mathfrak{y}+y_0}{\Delta} \rfloor \in \mathbb{Z}$, it holds that

$$P(\delta_p \leq x) = \sum_{i \in \mathbb{Z}} P(0 \leq \mathfrak{y} + y_0 - i\Delta \leq x). \tag{4.14}$$

As $\mathfrak{y}$ is bounded, the right hand side of (4.14) is always a finite sum. This shows that P_{δ_p} is also absolutely continuous with respect to the Lebesgue measure. Let h_{δ_p} be the be the Radon-Nikodym derivative of P_{δ_p} and it holds

$$h_{\delta_p,\Delta}(x) = \sum_{i \in \mathbb{Z}} h_{\mathfrak{y}}(x - y_0 + i\Delta). \tag{4.15}$$

While h_{δ_p} is parameterized by Δ as in chapter 3, and denoted by $h_{\delta_p,\Delta}$ whenever this fact needs to be emphasized; $h_{\mathfrak{y}}$ by the modelling is irrelevant to Δ. This is because the random shift along the y-axis is achieved by the gantry.

As a special case, if $\mathfrak{y}$ is uniformly distributed on some $[a, a+k\Delta)$ for some $k \in \mathbb{Z}_+$, then the induced $h_{\delta_p,\Delta}$ is uniform on $[0, \Delta)$.

Proposition 4.1. *If the random shift $\mathfrak{y}$ satisfies*

$$\lim_{z\to 0} \int_{\mathbb{R}} |h_{\mathfrak{y}}(x) - h_{\mathfrak{y}}(x+z)| \, \mathrm{d}\mu_L(x) = 0, \tag{4.16}$$

then the mapping $\Phi : \mathbb{R}_+ \to L^1(\mathbb{R}, \mu_L)$ by $\Delta \mapsto h_{\delta_p,\Delta}$ is continuous.

Proof. Because the right hand side of (4.15) is a finite sum, it holds

$$\begin{aligned}\lim_{\Delta_2\to\Delta_1} \left\| h_{\delta_p,\Delta_1} - h_{\delta_p,\Delta_2} \right\|_1 &= \lim_{\Delta_2\to\Delta_1} \int_{\mathbb{R}} \left| h_{\delta_p,\Delta_1} - h_{\delta_p,\Delta_2} \right| \mathrm{d}\mu_L \\ &\leq \sum_{i\in\mathbb{Z}} \lim_{\Delta_2\to\Delta_1} \int_{\mathbb{R}} |h_{\mathfrak{y}}(x - y_0 + i\Delta_1) - h_{\mathfrak{y}}(x - y_0 + i\Delta_2)| \, \mathrm{d}\mu_L(x) = 0.\end{aligned}$$

□

The condition (4.16) in Proposition 4.1 is not too strong. Indeed any bounded piecewise continuous $h_{\mathfrak{y}}$ satisfy this condition, and this covers the widely used uniform distribution, (truncated) Gaussian distribution, and Beta distribution. Proposition 4.1 says that if $\mathfrak{y}$ satisfies the condition (4.16), then the induced δ_p satisfies the conditions of Theorem 3.1, which forms the base of the discussions in this thesis. Moreover the proof of Proposition 3.1 only relies on the conditions of Theorem 3.1; therefore δ_p will always be satisfying P3 condition if $\mathfrak{y}$ satisfies the conditions of (4.16). Once h_{δ_p} is obtained, it can be checked explicitly whether the P2, P1, and S condition hold.

Now to discuss the impact of δ_r on δ via (4.12). As a reminder, the assumptions $\delta_p \in [0, \Delta)$, $\delta_r \in [-m_r, m_r]$, and $E(\delta_r) = 0$ are automatically taken from the previous discussions. Now to briefly comment on the assumption $E(\delta_r) = 0$, if $E(\delta_r) \neq 0$, by the definition of δ_p and δ_r, the object will be drifting over time towards some direction and this is usually interpreted as a result of bad positioning or loose fixture. The next assumption is that δ_p and δ_r are independent as random variables. This assumption is reasonable because δ_p is only affected by the initial position of the gauge object and the random shifts. After each random shift, it stays stationary and changes no more. However, it is worth pointing out that this assumption is not necessary. For example, it

is entirely possible that in some systems the placement of the gauge object drastically affects the vibration pattern of the machine and thus is no longer proper to be thought as independent to δ_r.

Let $\overline{\delta} = \delta_p + \delta_r$, then $\overline{\delta}$ is supported on $[-m_r, \Delta + m_r)$. By the condition of independence, the probability distribution of $\overline{\delta}$ is

$$P_{\overline{\delta}} = P_{\delta_p + \delta_r} = P_{\delta_p} * P_{\delta_r}$$

where P_{δ_r} is the probability distribution of δ_r and $*$ denotes the convolution of measures. If either P_{δ_p} or P_{δ_r} is absolutely continuous with respect to μ_L, so is $P_{\overline{\delta}}$ (Ex 7.14.(c) [AL06]). If δ_p is induced by a proper $\mathfrak{y}$, this is automatic. Now assume δ_r is also absolutely continuous with respect to the Lebesgue measure with the Radon-Nikodym derivative h_{δ_r}. Let $\overline{h}$ denote the Radon-Nikodym derivative of $\overline{\delta}$, then

$$\overline{h} = h_{\delta_p} * h_{\delta_r}$$

where $*$ means the convolution of functions on $\mathbb{R}$. Suppose $\Delta \mapsto h_{\delta_p,\Delta}$ is continuous as a function from $\mathbb{R}_+$ to $L^1(\mathbb{R}, \mu_L)$, which again is satisfied if δ_p is induced by a proper $\mathfrak{y}$. Then by the Young's inequality

$$\left\|\overline{h}_{\Delta_1} - \overline{h}_{\Delta_2}\right\|_1 = \left\|(h_{\delta_p,\Delta_1} - h_{\delta_p,\Delta_2}) * h_{\delta_r}\right\|_1 \leq \left\|h_{\delta_p,\Delta_1} - h_{\delta_p,\Delta_2}\right\|_1 \left\|h_{\delta_r}\right\|_1,$$

the mapping $\Delta \mapsto \overline{h}_\Delta$ is also continuous. Because $\delta = \overline{\delta} + \lfloor \overline{\delta}/\Delta \rfloor \Delta$, similar to arguments for (4.16), it holds

$$h_\Delta(x) = \sum_{i \in \mathbb{Z}} \overline{h}_\Delta(x + i\Delta), \tag{4.17}$$

where h_Δ is the Radon-Nikodym derivative of δ and the right hand side consists of only finitely many non-zero entries. In case $m_r \ll \Delta$, equation (4.17) expands as

$$h_\Delta(x) = \begin{cases} \overline{h}_\Delta(x) + \overline{h}_\Delta(x + \Delta) & x \in [0, m_r), \\ \overline{h}_\Delta(x) & x \in [m_r, \Delta - m_r), \\ \overline{h}_\Delta(x - \Delta) + \overline{h}_\Delta(x) & x \in [\Delta - m_r, \Delta), \\ 0 & \text{elsewhere.} \end{cases} \tag{4.18}$$

Then the following proposition holds:

Proposition 4.2. *If δ_p is induced by $\mathfrak{y}$ and the followings are true*

$$\lim_{z \to 0} \int_{\mathbb{R}} |h_{\mathfrak{y}}(x) - h_{\mathfrak{y}}(x + z)| \, \mathrm{d}\mu_L(x) = 0 \tag{4.19}$$

then for $m_r \ll \Delta$, the map $\Phi : \mathbb{R}_+ \to L^1(\mathbb{R}, \mu_L)$ as $\Delta \mapsto h_\Delta$ as (4.18) is also continuous.

Proof. Condition (4.19) is exactly condition (4.16) in Proposition 4.1; and by the arguments above, it shows that $\Delta \mapsto \overline{h}_\Delta$ is continuous. Now claim that

$$\lim_{\substack{\Delta_2 \to \Delta_1 \\ y \to 0}} \int_{\mathbb{R}} \left| \overline{h}_{\Delta_1}(x) - \overline{h}_{\Delta_2}(x+y) \right| \mathrm{d}\mu_L(x) = 0. \tag{4.20}$$

Indeed

$$\begin{aligned} &\int_{\mathbb{R}} \left| \overline{h}_{\Delta_1}(x) - \overline{h}_{\Delta_2}(x+y) \right| \mathrm{d}\mu_L(x) \leq \\ &\qquad \int_{\mathbb{R}} \left| \overline{h}_{\Delta_1}(x) - \overline{h}_{\Delta_1}(x+y) \right| \mathrm{d}\mu_L(x) + \int_{\mathbb{R}} \left| \overline{h}_{\Delta_1}(x+y) - \overline{h}_{\Delta_2}(x+y) \right| \mathrm{d}\mu_L(x), \end{aligned}$$

and $\lim_{\Delta_2 \to \Delta_1} \int_{\mathbb{R}} \left| \overline{h}_{\Delta_1}(x+y) - \overline{h}_{\Delta_2}(x+y) \right| \mathrm{d}\mu_L(x) = 0$ because of the continuity of $\Delta \mapsto \overline{h}_\Delta$. By equation (4.15), for a given Δ, the induced δ_p also satisfies

$$\lim_{z \to 0} \int_{\mathbb{R}} \left| h_{\delta_p,\Delta}(x) - h_{\delta_p,\Delta}(x+z) \right| \mathrm{d}\mu_L(x) = 0.$$

Thus to show (4.20), let τ_a be the translation operator, i.e., $(\tau_a f)(y) = f(y+a)$, then

$$\begin{aligned} \lim_{\substack{\Delta_2 \to \Delta_1 \\ y \to 0}} \int_{\mathbb{R}} \left| \overline{h}_{\Delta_1}(x) - \overline{h}_{\Delta_1}(x+y) \right| \mathrm{d}\mu_L(x) &= \lim_{y \to 0} \left\| h_{\delta_p,\Delta_1} * h_{\delta_r} - \tau_y (h_{\delta_p,\Delta_1} * h_{\delta_r}) \right\|_1 \\ &= \lim_{y \to 0} \left\| h_{\delta_p,\Delta_1} * h_{\delta_r} - (\tau_y h_{\delta_p,\Delta_1}) * h_{\delta_r} \right\|_1 \\ &\leq \lim_{y \to 0} \left\| h_{\delta_p,\Delta_1} - \tau_y h_{\delta_p,\Delta_1} \right\|_1 \left\| h_{\delta_r} \right\|_1 = 0. \end{aligned}$$

Now show $\lim_{\Delta_2 \to \Delta_1 -} \left\| h_{\Delta_1} - h_{\Delta_2} \right\|_1 = 0$.

$$\begin{aligned} \lim_{\Delta_2 \to \Delta_1 -} \left\| h_{\Delta_1} - h_{\Delta_2} \right\|_1 \leq &\lim_{\Delta_2 \to \Delta_1 -} \int_{[0, m_r)} \left| h_{\Delta_1} - h_{\Delta_2} \right| \mathrm{d}\mu_L && (4.21) \\ &+ \lim_{\Delta_2 \to \Delta_1 -} \int_{[m_r, \Delta_2 - m_r)} \left| h_{\Delta_1} - h_{\Delta_2} \right| \mathrm{d}\mu_L && (4.22) \\ &+ \lim_{\Delta_2 \to \Delta_1 -} \int_{[\Delta_2 - m_r, \Delta_1 - m_r)} \left| h_{\Delta_1} - h_{\Delta_2} \right| \mathrm{d}\mu_L && (4.23) \\ &+ \lim_{\Delta_2 \to \Delta_1 -} \int_{[\Delta_1 - m_r, \Delta_2)} \left| h_{\Delta_1} - h_{\Delta_2} \right| \mathrm{d}\mu_L && (4.24) \\ &+ \lim_{\Delta_2 \to \Delta_1 -} \int_{[\Delta_1, \Delta_2)} \left| h_{\Delta_1} - h_{\Delta_2} \right| \mathrm{d}\mu_L && (4.25) \end{aligned}$$

By the continuity of $\Delta \mapsto \overline{h}_\Delta$ and (4.20), it is easy to see that (4.21), (4.23) and (4.25) are 0. By the absolute continuity of $P_{\overline{\delta}}$ with respect to μ_L, (4.22) and (4.24) are 0. Similarly it can be shown that $\lim_{\Delta_2 \to \Delta_1 +} \left\| h_{\Delta_1} - h_{\Delta_2} \right\|_1 = 0$ and thus completes the proof. □

Combined with Proposition 4.1 and the discussion above, if $\mathfrak{y}$ satisfies the condition(4.16) in Proposition 4.1, then δ will be satisfying the conditions of Theorem 3.1 the very base of the theory and it will be satisfying the P3 condition. If $m_r \ll 1$, then δ_r is very close to the Dirac distribution. Convolution with the Dirac delta function yields identical output and this mathematical fact hints that $\overline{h}$ should be close to h_p. Consider the special case where δ_r is uniform on $[-m_r, m_r]$, then

$$\overline{h}_{\Delta,m_r}(x) = \int_{\mathbb{R}} h_{\delta_p}(y) h_r(x-y)\,\mathrm{d}\mu_L(y) = \frac{1}{2m_r}\int_{[x-m_r,x+m_r]} h_{\delta_p}(y)\,\mathrm{d}\mu_L(y),$$

and then by the Lebesgue differentiation theorem,

$$\lim_{m_r\to 0} \overline{h}_{\Delta,m_r}(x) = h_p(x). \tag{4.26}$$

Not so obvious as equation (4.26), the following discussion will investigate how p_h behaves as $m_r \to 0$. The equation (4.18) shows that h_Δ consists of three parts among which both the ends are slightly modified with the overheads. For $x \in (\frac{l}{N+1}, \frac{l}{N})$, consider a slightly shrunken range

$$\frac{l+m_r}{N+1} < x < \frac{l-m_r}{N}$$

which guarantees $m_r < l - Nx < x - m_r$. Then

$$p_h(x) = \int_0^{l-Nx} h_x(y)\,\mathrm{d}y = \int_0^{m_r} \overline{h}_x(y+x)\,\mathrm{d}y + \int_0^{l-Nx} \overline{h}_x(y)\,\mathrm{d}y \tag{4.27}$$

The absolute continuity of $P_{\overline{\delta}}$ shows that $\lim_{m_r\to 0}\int_0^{m_r} \overline{h}_x(y+x)\,\mathrm{d}y = 0$, and thus it only needs to work on the second entry on the right hand side of (4.27). By Fubini's

theorem,

$$\begin{aligned}
\int_0^{l-Nx} \overline{h}_x(y)\,\mathrm{d}y &= \int_0^{l-Nx}\int_{\mathbb{R}} h_{\delta_p,x}(z)h_r(y-z)\,\mathrm{d}z\,\mathrm{d}y \\
&= \int_0^{l-Nx}\int_{y-m_r}^{y+m_r} h_{\delta_p,x}(z)h_r(y-z)\,\mathrm{d}z\,\mathrm{d}y \\
&= \int_{m_r}^{l-Nx-m_r}\int_{z-m_r}^{z+m_r} \frac{h_{\delta_p,x}(z)}{2m_r}\,\mathrm{d}y\,\mathrm{d}z + \int_{-m_r}^{m_r}\int_0^{z+m_r} \frac{h_{\delta_p,x}(z)}{2m_r}\,\mathrm{d}y\,\mathrm{d}z \\
&\quad + \int_{l-Nx-m_r}^{l-Nx+m_r}\int_{z-m_r}^{l-Nx} \frac{h_{\delta_p,x}(z)}{2m_r}\,\mathrm{d}y\,\mathrm{d}z \\
&= \int_0^{l-Nx} h_{\delta_p,x}(z)\,\mathrm{d}z - \int_0^{m_r} h_{\delta_p,x}(z)\,\mathrm{d}z \\
&\quad - \int_{l-Nx-m_r}^{l-Nx} h_{\delta_p,x}(z)\,\mathrm{d}z + \int_0^{m_r} \frac{(z+m_r)h_{\delta_p,x}(z)}{2m_r}\,\mathrm{d}z \\
&\quad + \int_{l-Nx-m_r}^{l-Nx} \frac{(l-Nx-z+m_r)h_{\delta_p,x}(z)}{2m_r}\,\mathrm{d}z \\
&= p_{h,\delta_p}(x) + \int_0^{m_r} \frac{(z-m_r)h_{\delta_p,x}(z)}{2m_r}\,\mathrm{d}z \\
&\quad + \int_{l-Nx-m_r}^{l-Nx} \frac{(l-Nx-z-m_r)h_{\delta_p,x}(z)}{2m_r}\,\mathrm{d}z,
\end{aligned}$$

where $p_{h,\delta_p}(x)$ is the probability of high reading induced by δ_p. By absolute continuity of δ_p and Lebesgue differentiation theorem,

$$\lim_{m_r\to 0}\int_0^{m_r} \frac{(z-m_r)h_{\delta_p,x}(z)}{2m_r}\,\mathrm{d}z = \lim_{m_r\to 0}\int_{l-Nx-m_r}^{l-Nx} \frac{(l-Nx-z-m_r)h_{\delta_p,x}(z)}{2m_r}\,\mathrm{d}z = 0$$

Therefore for $x \in \left(\frac{l+m_r}{N+1}, \frac{l-m_r}{N}\right)$, it holds

$$\lim_{m_r\to 0} p_h(x) = p_{h,\delta_p}(x). \tag{4.28}$$

Similar to the case discussed in the subsection of mis-alignment, the intervals $(\frac{l+m_r}{N+1}, \frac{l-m_r}{N})$ play a similar role to the Type I intervals; and equation (4.28) links the manipulated pseudo-random shift to the final output which is combined with random system effects. The convergence also shows the robustness of PBM in the sense that as the significance of random effects from the system goes smaller, the probability of a high reading coincides with the manipulable parts.

4.3.1 3-Point-Supported Result Sets

In this subsection, detailed analysis and treatments on result sets supported on 3 points will be conducted with the consideration of randomness on $\mathfrak{l}$. As previously seen in

the section of alignment, practically instead of $p_h(x)$, the sampled probability frequencies are indeed $p_h(x, \mathfrak{l})$. Discussion in section 4.2 revealed how an interesting discrete behavior of $\mathfrak{l}$ arises from mis-alignments of sensor and the gauge object. Other factors, like random temperature changes or vibrations also change the measurand. When $\mathfrak{l}$ is a random variable that is very close to l_n, result sets that are supported on 3 points are often observed, like Example. 4.2. For example, $l_n = 150, \Delta = 3$ and $\mathfrak{l} \in [150 - 0.01, 150 + 0.01]$, result sets supported on $\{48, 49\}$ and $\{49, 50\}$ will be observed. When $\mathfrak{l} < l_n$, there are always 48 or 49 full scales; and when $\mathfrak{l} \geq l_n$, the number of full scales will be 49 or 50. Qualitatively a result set of this kind will be of the form

$$R_M = \{(N-2, c_l), (N-1, c_m), (N, c_h)\} \qquad \Delta_0 = l_n/N \tag{4.29}$$

where $c_l, c_h \ll c_m$.

To deal with result sets of this type, many statistical methods could be applied. For what will later be used in this thesis, a simple and direct method for P1+S condition will be stated here. As computed in 3.3.5, let

$$p_1 = p_h(\Delta_0, l_n + T) \qquad p_2 = p_h(\Delta_0, l_n + T)$$

then the probability for the middle reading is

$$p_m = \frac{(1 - p_1) + p_2}{2}$$

when $\mathfrak{l}$ is assumed be equally distributed on $[l_n - T, l_n + T]$. Then it is satisfactory to claim that $l_t \in [l_n - T, l_n + T]$ when the following 3 inequality hold simultaneously

$$f_m = \frac{c_m}{M} > p_m \qquad \frac{c_h}{c_m + c_h} < p_1 \qquad \frac{c_m}{c_m + c_l} > p_2.$$

4.4 Real-World Gantry

In this section, the impact from real-world gantry systems on PBM will be investigated. Although there are brief discussions on real gantries in subsection 3.3.1 and section 4.2; it has not yet been examined systematically. The gantry-scanner system modelled in earlier sections of this chapter is a typical 3-axis system, therefore general theories on multi-axis systems, like [LS03][Sch+08][ISO230-1], are of great help and can be applied directly. For a general 3-axis system, there are 21 commonly acknowledged parametric errors [LS03][SAH13]; detailed error analysis and various ways of

compensation are currently hot research topics. In the following, the impact from the inaccuracy of the 3-axis system on PBM will be investigated. The theoretic work so far assumes the fact that Δ can be perfectly set to an arbitrary value; however, this assumption fails in real-world applications. This is because the real-world axes are discrete in the sense that the combination of mechanical components, sensors and controllers can only reliably generate displacement above certain numeric threshold. This discrete behavior of gantry systems will also be analyzed for its impact on PBM.

The 21 parametric errors of a 3-axis system consists of 6 geometric errors of each axis and three squareness errors [SAH13][LS03]. Following the specification of [ISO230-1], for the x-axis there are three angular error motions, denoted by E_{AX}, E_{BX}, E_{CX} and known as roll, yaw, pitch respectively, two straightness error motions denoted by E_{YX}, E_{ZX} and one linear positioning error motion E_{XX}. The squareness of the z-axis relative to x-axis, denoted by $E_{B(0X)Z}$ refers to the difference between the inclination of the reference straight line of the trajectory of the z-axis and that of the x-axis. By fixing a point on the scanner, and using it as the functional point (§3.4.2 of [ISO230-1]) the standard ways of evaluation of error motion can be directly applied.

The work on error analysis and compensation has a long history. It has been recorded that as early as around 1830 Edward Troughton used a look-up table to compensate errors of linear dividing engine ([Eva89][SZ95]). Around 1970s, the adoption of CNC (computerized numerical control) systems made online compensation possible [STO77] [DG81]. Dufour in [DG81] established the "error matrix" method, where $(e_X, e_Y, e_Z)^T$, the error vector of the functional point, is considered as a function to many factors such as coordinate, temperature, and load etc. Then the error vector will be sampled at many different positions with various system states. When compensation at a general position is needed, a microcomputer is used to compute the interpolated data. Sata in [STO77] approximated the error vector using quadratic forms of the spatial coordinates and used a minicomputer to compensate the force-related error. For complicated structures, the error vector is analyzed by rigid body kinematics, using homogeneous coordinates and coordinate transformation matrices [Hoc+77][FL86][LE93]; moreover this approach has been proven to be effective even in 5-axis systems [LS03][HW07]. In this thesis, it is quite enough to express the error vector as

$$\overrightarrow{e} = (e_X, e_Y, e_Z)^T$$

where e_X, e_Y, e_Z are functions of coordinates. Because the gantry is of finite volume, each component of $\overrightarrow{e}$ is supported on a compact set; in a well-designed and calibrated

system, it can be assumed that $|e_i| \ll 1, i = X, Y, Z$. Kinematic analysis suggests further that the assumption of e_i all being continuous is reasonable [LE93] [KF93] [YYF11].

As analyzed in the previous section of randomness, equation (4.12) can be slightly modified to

$$\delta = (\delta_p + \delta_r + e_Y) - \lfloor \frac{\delta_p + \delta_r + e_Y}{\Delta} \rfloor \Delta$$

and this expression stresses the presence of e_Y. By considering $\delta_r + e_Y$ together as one entry and the fact that $|e_Y| \ll 1$, the role of e_Y is no more than another random error and its impact is limited to what has been analyzed in the previous section. Besides e_Y, e_X slightly changes the section of the extrusion under examination, and e_Z slightly changes the relative distance between the scanner and the gauge object. As the modelling in this chapter uses a laser triangulation scanner, the variation introduced by e_Z will certainly impact Δ (Fig. 4.1[b]). For very small turbulence of Δ, because of Proposition 3.1, the impact on p_h is limited and methods established in chapter 3 can be applied with little modification. For larger turbulence of Δ, the theoretic analysis will be merged with the discussion of the discrete behavior of axes in the rest of this section.

Although the motion of sliders, stages, and joints are continuous; due to the limits in encoders, actuators, and controllers, there is a minimal displacement gap, usually known as the minimum step/advance/increment [NK17][NP17][PI18]. This restricts the possible value of the function point to a lattice

$$\mathcal{L} = \{(x_0, y_0, z_0) + (l\Delta_x, m\Delta_y, n\Delta_z) | l, m, n \in \mathbb{Z}\}$$

where (x_0, y_0, z_0) represents an initial position and $\Delta_x, \Delta_y, \Delta_z$ denote the possible minimum increments in motion alongside the x, y and z-axis respectively. The numeric value of the scale Δ is a function of the gantry coordinate, and thus is discrete.

Suppose the object is examined in the effective scanning area of the laser profiler as illustrated by Fig. 4.12. Let h denote the distance between the top surface of the object and the top edge of the trapezoid scanning area. Then Δ is a function of h, explicitly written as

$$\Delta = \Delta(h) = \frac{h}{H_S}(\Delta_M - \Delta_m) + \Delta_m. \tag{4.30}$$

Let (x, y, z) be the coordinate of a fixed point on the laser profile and use this point as the functional point. Then the difference between h and z is a constant depending only

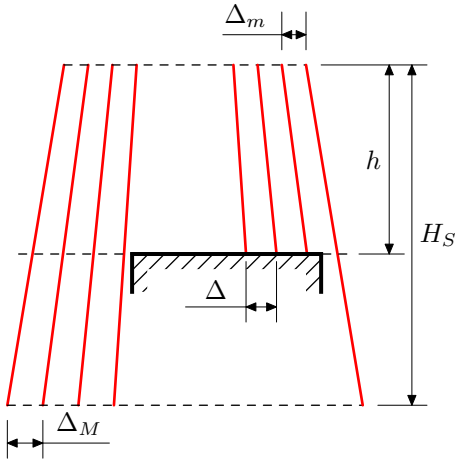

Figure 4.12: The relation between Δ and the height of the scanning surface

on the choice of the origin of the coordinate system. For this reason, henceforth the usage of h and z will be interchangeable; and as a result, h in equation (4.30) makes sense even in mis-aligned cases where $\overrightarrow{n}$ is not parallel to $\overrightarrow{e_3}$. Thus by (4.30), the minimum increment for Δ is

$$m_m = \frac{\Delta_z(\Delta_M - \Delta_m)}{H_S}.$$

In the following a brief retrospect of the discussions from subsection 3.3.1 to 3.3.5 will be conducted. Before diving into the details, a clarification to the process of setting Δ to some specific value Δ_0 will be made. After carefully adjusting the gantry alongside the z-axis, it could be expected that the actual value of the scale is at $\Delta_0 + \delta_m$, where $\delta_m \in (-m_m, m_m)$. It is reasonable to assume that the value $\Delta_0 + \delta_m$ is known, because it can be computed using all points in the sampled profile. The reason why δ_m is assumed to be within a symmetric interval is that the hysteresis of axis is considered to be random and the process of adjustment consists of motion of the z-axis in both directions.

4.4.1 P3, P2 and P2+S Condition

As discussed in chapter 3, for p_h satisfying only the P3 condition, more information/ assumption on p_h must be provided for detection of discontinuity. For p_h satisfying the P2 condition and m_m known, one could define the oscillation of p_h as follows

$$\Omega = \Omega(p_h, m_m) = \sup_{\substack{x,y \in (\frac{l}{N+1}, \frac{l}{N}) \\ |x-y| \leq m_m}} |p_h(x) - p_h(y)|.$$

Then the search of discontinuity is possible in the situation of the following proposition:

Proposition 4.3. *If* $\Omega(p_h, m_m) < \frac{1}{3}$ *and* $p_h(\Delta) < \frac{1}{3}$*, and* $p_h(\Delta + m_m) > \frac{2}{3}$*, then there's a discontinuity in* $(\Delta, \Delta + m_m)$.

Now consider the case satisfying the P2(+S) condition. The method discussed in subsection 3.3.2 remains valid. The minimum increment of Δ sets restrictions on the fineness of the search sequence. With the same symbols and conventions used in subsection 3.3.2, any sequences must satisfy

$$x_{i+1} - x_i \geq m_m.$$

And by equation (3.19), the finest estimation of l_t one can obtain is within a interval whose length is capped by m_m.

4.4.2 P1 and P1+S Condition

For small m_m, replacing Δ_0 by $\Delta_0' = \Delta_0 + \delta_m$ it can be checked that the arguments conducted in subsections 3.3.4 and 3.3.5 remain identical and valid, because of the continuity of $p_h(x, l)$ as a function of l on every $l \in (Nx, (N+1)x), N \in \mathbb{Z}_+$. However if m_m is relatively large, things are different. For example, let $\Delta_0 = \frac{l_n}{N}$ for a large integer N so that m_m is of the same magnitude of Δ_0, then

$$\lfloor \frac{l_n}{\Delta_0'} \rfloor = \lfloor \frac{l_n}{\Delta_0 + \delta_m} \rfloor \tag{4.31}$$

may value other than N and $N-1$. This implies that the support of the result sets (of two points) can be different to $\{N-1, N\}$ and $\{N-2, N-1\}$. To avoid this situation, (4.31) must be valuing within the range $[N-1, N]$, the following inequality must be satisfied

$$N - 1 \leq \frac{l_n}{\Delta_0 + \delta_m} < N + 1,$$

which implies

$$-\frac{l_n}{N(N+1)} < \delta_m \leq \frac{l_n}{(N-1)N}.$$

Therefore

$$m_m < \frac{l_n}{N(N+1)} \tag{4.32}$$

is a sufficient condition which guarantees that the discussions in chapter 3 remain valid and need no change. Because the value of m_m is usually determined by the hardware configuration and software implementation in a given system; what equation (4.32) suggests is that the choice of N should never be too large.

4.5 Summary

In this chapter, the modelling of a measurement system and gauge object is established. Under this modelling, three topics are investigated — mis-alignments, randomness and real-world gantry systems. In the discussion of mis-alignments, trigonometric errors are computed and more importantly a discrete random behavior of the measurand is discovered. Detailed examination of the sources of randomness in the sampling process justifies the use of synthetic random shifts for the validation process and shows the robustness of PBM against random errors in the sense of the convergence described by (4.28). Finally, the discreteness of Δ, as an impact from real-world gantries, is investigated and its effects on PBM established in chapter 3 are examined. All the discussions pave the way towards the real world validation.

5 Experiment and Validation

This chapter gives a detailed presentation to various engineering works that support the validation process either directly or directly, and validates the theoretical works by real-world experiments. The essence of the process of validation is a real-world attempt to solve Problem 3.1 proposed at the beginning of chapter 3 with different numeric settings using the probability-based method. The overall setup of hardware follows the modelling in section 4.1. A description of the physical build of the system will be given, including the hardware and the software. To better support the validation process, a slight modification to the modelling of the gauge object in section 4.1 is conducted. The validation process consists of three parts — preparation, sampling, and evaluation as shown by Fig. 5.1. The flow of the whole validation process will be clearly defined and exhibited, and the data sampling and analyzing processes will be explained. Then real-world experiment data will be presented and examined, through which the validity of the theory shall be proven.

Figure 5.1: Overview of the validation process

5.1 The Laboratory Setup

The gantry-profiler system (Fig. 5.2) used for the validation in this thesis was originally built for the EU Micro-Fast project[5]. Micro-Fast is the acronym of the collaborative project with grant agreement number 608720 which enables an increase the manufacturing flexibility and high-quality micro components by adopting the latest powder-sintering technologies. It aims to provide components of various raw-materials including metals, ceramics and cermets. The linear motions are implemented by 3 linear stages, and controlled by a 3-channel controller all from the Newmark Systems, inc. The laser triangulation scanner is from Micro-Epsilon and is directly controlled by software. Detailed model and key specifications of the key parts are listed in Table 5.1.

The assembled whole system is illustrated by Fig. 5.2. To serve the original purpose of usage, the 3-axis system is mounted on another long axis Fig. 5.2[a][b], which is not used in this thesis. In the original design, an endoscope was also attached to the gantry

[5]project website address: http://www.micro-fast.eu/

Table 5.1: Key parts and specifications

Description	Model	Specification
x-axis y-axis	`NLE-50-A`	travel 50mm; motor resolution 0.1μm; encoder resolution 0.1μm; accuracy $\pm 3\mu$m; repeatability $\pm 0.5\mu$m
z-axis	`NLE-100-A`	travel 100mm; motor resolution 0.1μm; encoder resolution 0.1μm; accuracy $\pm 3\mu$m; repeatability $\pm 0.5\mu$m
controller	`NSC-G3-E`	spec with encoder; 3-axis control; RS-232 and Ethernet connections
profiler	`scanCONTROL 2900-25`	height resolution 2μm, linearity $\pm 0.16\%$; in width 1280 points/profile; profile frequency 200Hz; laser power 8mW (class 2M)

system with a dedicated structure for rotation (Fig. 5.2[a]), and is removed during the validation process (Fig. 5.2[b]).

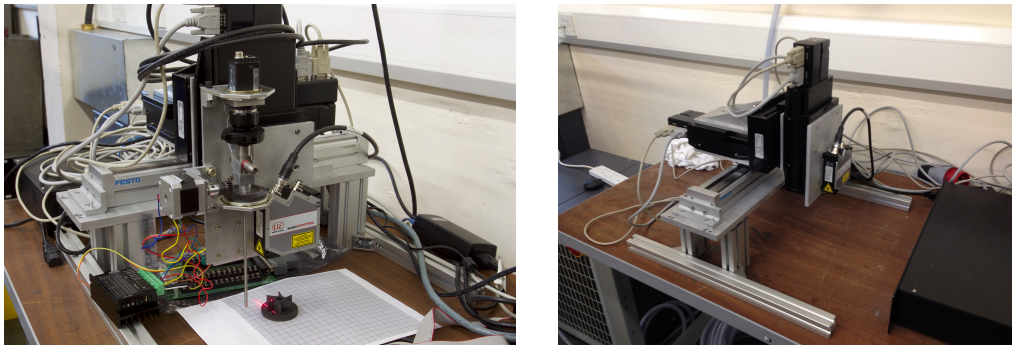

[a] [b]

Figure 5.2: Laboratory setup: **[a]** original design for the EU Micro-Fast project, equipped with an endoscope and a laser scanner; **[b]** for the validation of this thesis

The connections of the hardware are illustrated by Fig. 5.3. Both the stepper motor and the internal encoder of every linear stage are directly connected to the controller. Then the controller is connected to the serial port of the host PC. The laser scanner is connected to the host PC using a CAT6e Ethernet cable with Power-over-Ethernet (PoE) enabled. Inside of the Newmark controller, a DMC-21xx series controller from Galil Motion Control, Inc. implements the functions of the CNC commands and conducts the interpretation and motion control.

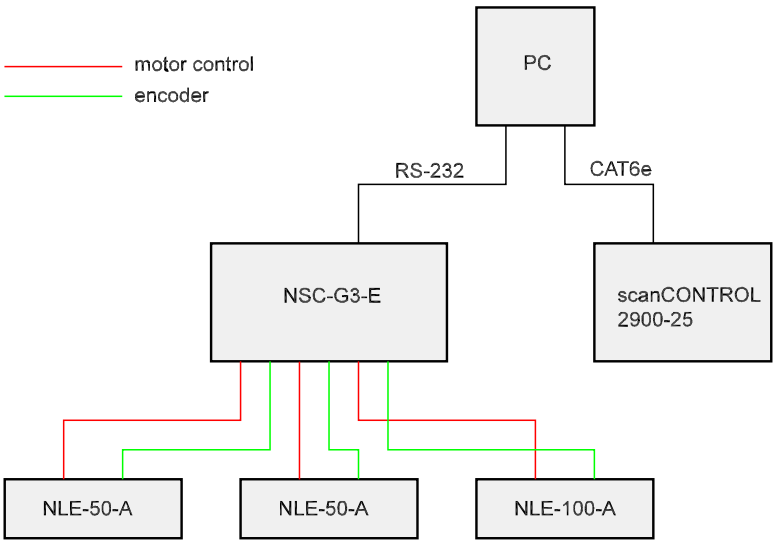

Figure 5.3: Connection of hardware

The design of the gauge block and photo of the manufactured pieces are as shown in Fig. 5.4. The most significant difference to the gauge object modelled in chapter 4 is that there are two parallel extrusions of different widths on the top surface. For a given tolerance ranges $[l_n - T, l_n + T]$ and a chosen Δ_0, both extrusions will be examined at the same time and the results analyzed and compared. For contrast, the tolerance range will be set in a way so that one of the extrusion is within the range and the other not. The reason having two extrusions side by side is to control the impact of trigonometric errors in the sense that the angular mis-alignments of both extrusions are managed to be as identical as possible. The 0.5mm side grooves are used as position indicators so that one can confirm that the work is conducted on the middle of extrusions. The 2mm chamfer is used as an direction indicator so that one can easily distinguish the width of the extrusions.

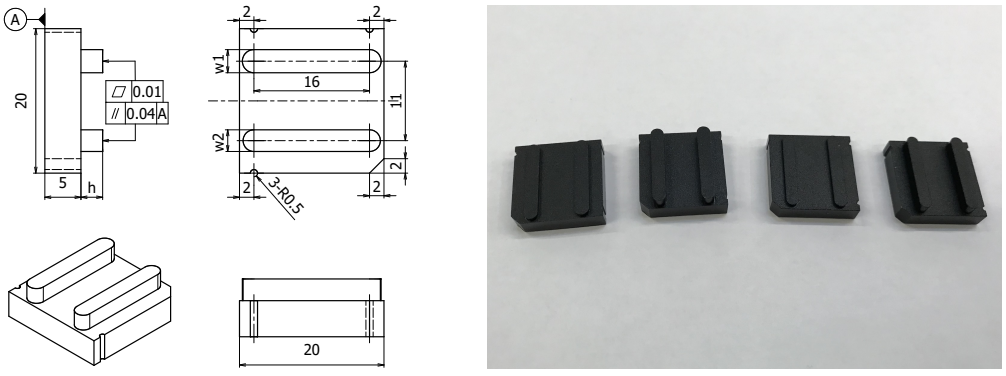

Figure 5.4: Gauge object designs and the manufactured pieces. ($1 =$ 1mm)

As a conclusion of this section, a brief remark to the software system is conducted. For the validation purpose, it is possible to use the software designed for the Micro-Fast project. Actually the software for the Micro-Fast project was designed to be with two plug-in frameworks, one for the overall behavior control and the other for data evaluation, feedback and presentation. Fig. 5.5[a] is a screenshot of the software after scanning a gauge object. To simplify the validation process — more specifically, to avoid redundant API callbacks and focus on static analysis — a new software is designed and used for all the validation works in this thesis. This software re-used a great portion of the legacy code, including the abstract interfaces for devices and plug-ins. Instead of online visual presentation, a lot of the effort has been put on a logging system for the purpose of data integrity. A screenshot of the software is shown by Fig. 5.5[b]. Sampled data are stored and then analyzed by other tools, and the details are to be revealed in the following sections.

5.2 The Software Design

5.2.1 The Overview

The software used for the validation process can be divided into two groups. One group (G1) is for the data sampling and control of the validation process; and the newly developed software briefly introduced at the end of the previous subsection belongs to this group. The name of this software is `PhDSampline` [6], and it is the main software within this group and is installed and executed on the host PC (Fig. 5.3). The software belonging to the other group (G2) focus on the data analysis and post processing, and will be introduced following this chapter when they are used. There are many small tools in this group for different but specific purposes. Usually they take input from the software in G1 or outputs from other tools in G2. Some open source/free software will also be used for non-validation purposes, for example, `gnuplot` is used for drawing plots. The development and testing of software and tools in the G1 and G2 groups are conducted by the author of this thesis.

Fig. 5.6 illustrates a typical work flow with the collaboration of all the software and tools; and it also shows how data are generated and processed in the work flow. Usually `PhDSampline` generates two types of outputs the log files and binary data files. The

[6] `PhDSampline` is for PhD Sampling for Line(s).

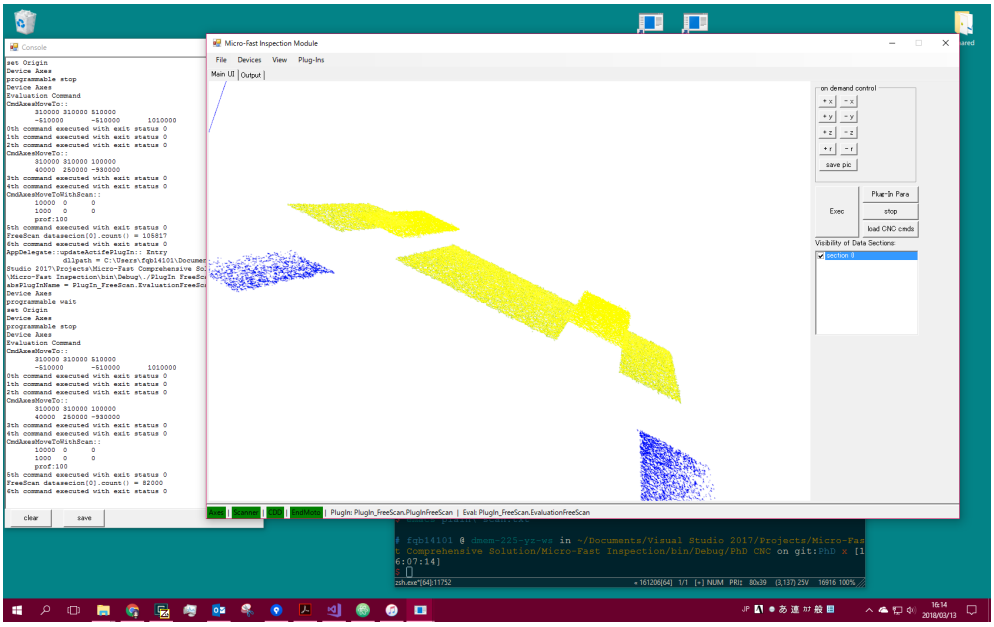

[a]

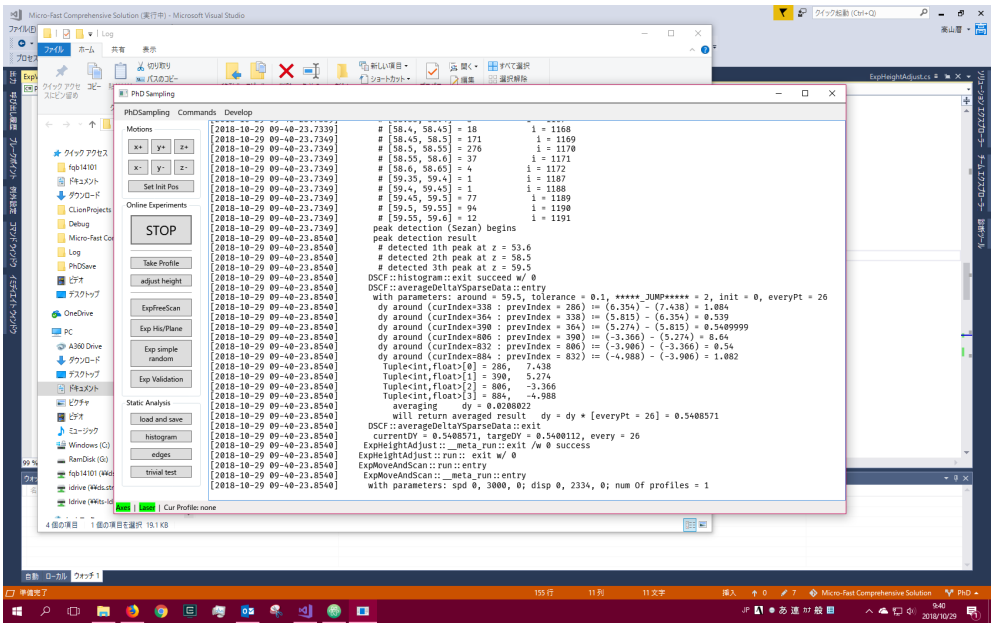

[b]

Figure 5.5: Screenshots of the software: **[a]** the Micro-Fast version showing the point cloud from a scan of the gauge block; **[b]** `PhDSampline` with detailed logs

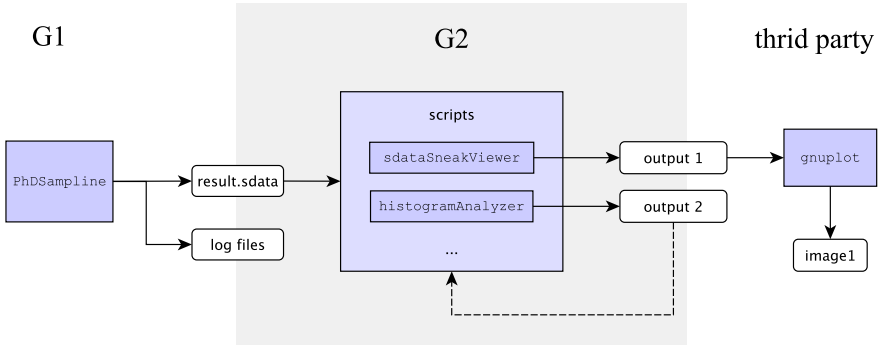

Figure 5.6: Work flow of the software

log file records the operations of the `PhDSampline` software that is either performed by operators using mouse and keyboard or by programmatic calls that are automatically triggered. Records and logs from validation experiments are also contained in these logs files for data integrity, traceability and audit purposes. Binary data files (the `result.sdata` file, as shown in Fig. 5.6) are usually generated by various experiments with the point cloud data and processed by tools in G2. The specification of the `sdata` format can be found in B.1. Fig. 5.7 shows sample contents of the log file and the `sdata` file.

Although the tools in G2 can work independently; as shown in Fig. 5.6, they are more often assembled in shell scripts and collaborate with each other and even other shell commands. For example, `sdataSneakViewer` is a tool from G2 that can strip data from an `sdata` files in various ways and echo the result. Detailed options and the usage instruction of `sdataSneakViewer` can be found in B.7. `histogramAnalyzer` from G2, which analyzes the histogram of the input and detects the peaks, this is an example that it mainly aims to provide auxiliary information for other tools. Detailed options and the usage instruction of `sdataSneakViewer` can be found in B.6. Figs. 5.8[a][b] are sample outputs from tools in G2; and Figs. 5.8[c][d] are visual presentations of the outputs.

5.2.2 Detailed Design of the Main Software

A detailed description of the software designs in `PhDSampline`, the main software, will be presented. The goal of this subsection is to prove the feasibility of the validation experiments in the sense that all controls and data sampling processes can be realized by the design of `PhDSampline`. Henceforth the word *experiments* will be used to refer to

processes of specific purpose, including but not limited to sequences of motion controls, data sampling, and evaluations. For example, to gather data for output like Fig. 5.8[c], an experiment can be designed to repeatedly advance the gantry for a fixed amount and then take the sample of a profile using the laser scanner and finally after many loops store all the data to an `sdata` file. As `PhDSampline` re-uses some of the source code from the Micro-Fast project, for legacy reasons, it is implemented using `C#` under the `.NET` framework in Windows 10. In the following, sample codes and interface designs

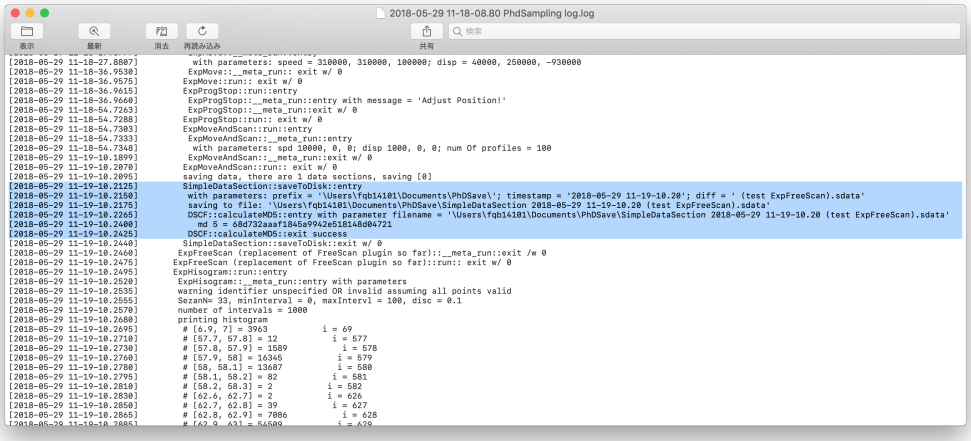

[a]

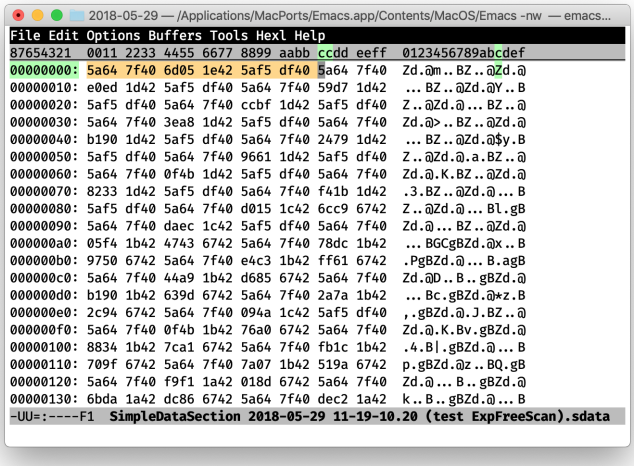

[b]

Figure 5.7: Sample outputs from G1: **[a]** segments of a log file with highlighted lines clearly documenting the generation of an `sdata` file with the `md5` hash tags; **[b]** head sections of the generated `sdata` file and the highlighted part reads 3.990, 39.505, 6.998

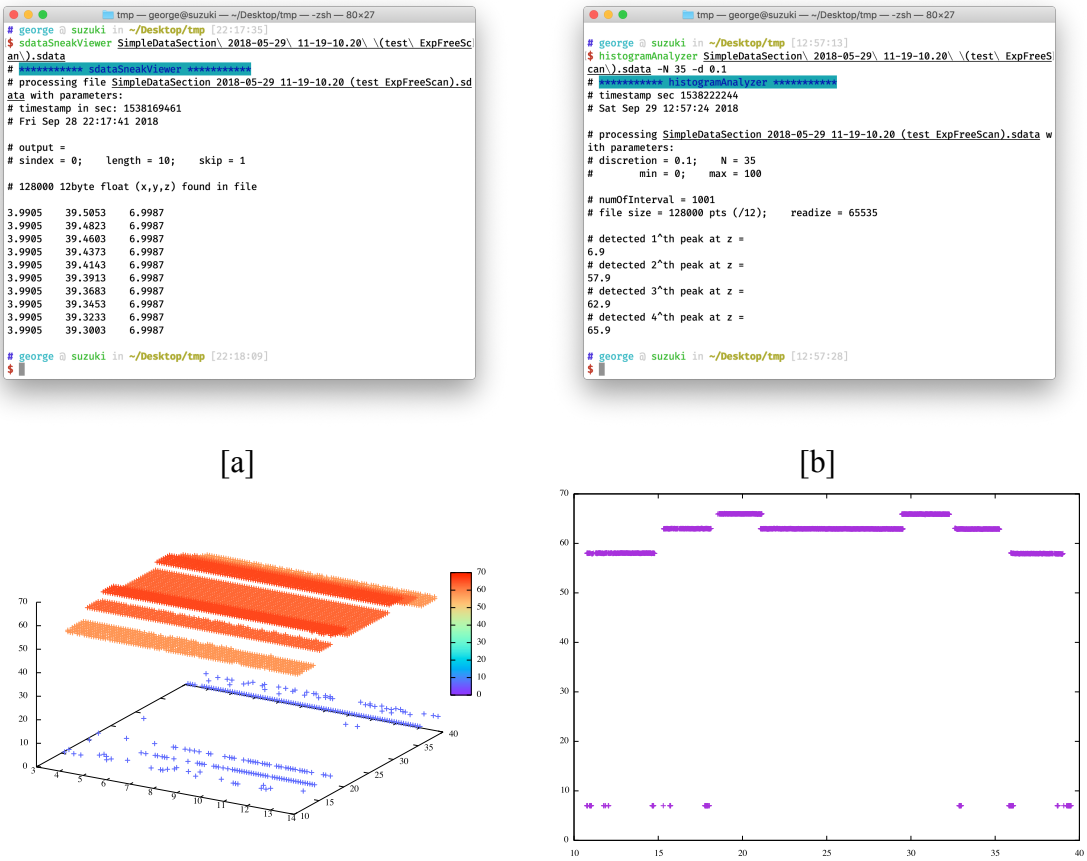

Figure 5.8: Sample output from tools in G2: **[a]** `sdataSneakViewer` prints the first 10 triples of the floats in an `sdata` file; **[b]** `histogramAnalyzer` prints detected peaks of the histogram of an `sdata` file; **[c]** figure of cloud points filtered by `sdataSneakViewer`, plotted by `gnuplot`; **[d]** figure of the first profile (first 1280 points) of an `sdata` file filtered out by `sdataSneakViewer`, plotted by `gnuplot`

will be using the `C#` language.

There is a common abstraction for all the *devices* used in the laboratory setup, including 3 axes and a laser profiler. The key interfaces are `open`, `close`, `read`, and `write`. The `open` interface initializes a device to a usable state and the `close` interface on the contrary sets a device to the idle state and releases all resources it holds. The `read` interface generally retrieves signals, and processed data from the underlying device, for example, profile data from the laser profiler or the current position of the axes from the controller. The `write` interface enables a user to send signals for the purposes of control, for example, to simply set analogue outputs or to issue complicated CNC commands. This abstraction is also as an isolation layer which grants neutrality in hardware. The key interfaces and the relations are as shown in the UML modeling diagram (Fig. 5.9).

There is an `AbsDeviceCfg` class for various configurations needed by different devices, such as, IP addresses, axis directions, resolutions etc.

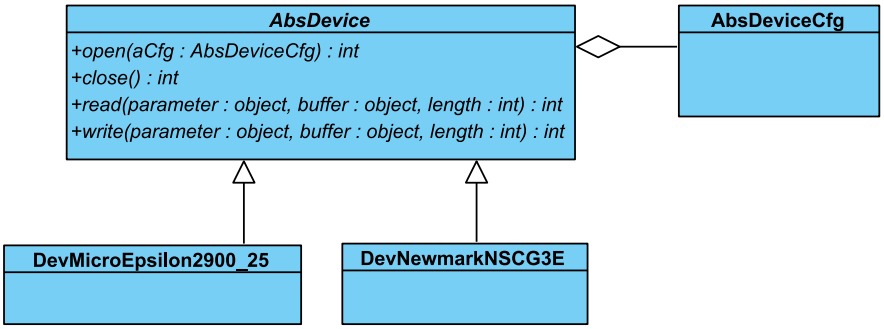

Figure 5.9: Class diagram of devices

The implementation of the `DevMicroEpsilon2900_25` class (or the laser class) wraps the LLT driver from Micro-Epsilon, where the marshallings are defined and provided. The realization of `read` of the laser class implements a buffer of the `float[]` type and the profile data are stored sequentially as $y_1, z_1, y_2, z_2, \cdots$, where y_i represents the lateral coordinate and z_i the the height coordinate of a point. The implementation of the `DevNewmarkNSCG3E` class (or the axes class) wraps the GalilTools Communication Library provided by the Galil Motion Control, Inc. In terms of functionality ([Suh+08]), this wrapping links the MMI (man machine interface) unit and the NCK (numerical control kernel) unit of the CNC system. Inside the Newmark `NSC-G3-E` controller, the DMC 2000 series controller conducts the actual work of NCK [Gal05a] with pre-defined internal function calls ([Gal05b]) and handles the work of interpretation and interpolation. The axes class acts as an adapter and enables the design of a set of CNC commands dedicated for this thesis. The realization of `write` of the axes class has two parameters — `parameter` of the `object` type and `buffer` of the `int[3]` type — and they are interpreted as speeds and displacements for directions along each axis.

The data storage interfaces are defined by the `AbsDataSections` class, which enables sequential writings and random readings (Fig. 5.10). Because during a general data sampling process the data flow is mainly from the sensor to memory, the sequential writing design provides good performance with simplicity. Henceforth the terms *sections* or *data sections* will be used to refer to instances of this class. The first design and implementation of this class was in the Micro-Fast project, where each section is responsible to store and visually present the segmented images. In `PhDSampline` for the validation purpose, only `sdata` files will be used as containers. Thus a specific subclass of the `AbsDataSections` called `SimpleDataSection` is implemented. There is also

a DSCF class (data section common function) designed alongside the AbsDataSections class to provide common algorithmic and procedure functionalities. For example, the fitPlane call in DSCF conducts multi-variable fitting to find the best estimated plane for an input data section. The purpose of DSCF class is to achieve loose coupling between data sections formats and the procedures on them; for example, the fitPlane and autoEdge can be toggled between using the calls from the gsl library (GNU Scientific Library) and using the calls implemented by the author.

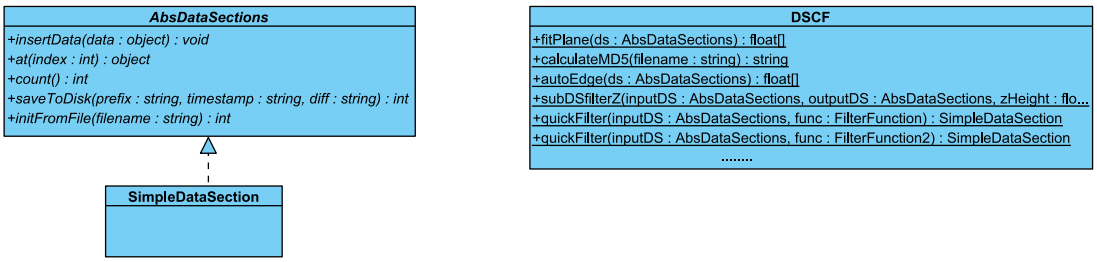

Figure 5.10: Class diagram of data section design showing the key interfaces

To implement various experiments for development, testing, and validation purposes, the design of AbsExperiment class uses the command pattern (p233 [Gam+94]) in a style of the template method pattern (p325 [Gam+94]). This design is a simplification to the plug-in framework design used in the Micro-Fast project. As shown in Fig. 5.11, the template method run of AbsExperiment provides a public access point. Inside of run, it executes the actions defined by __meta_run and more importantly hooks back to the user interface (UI). One of the important reasons behind this design is that it allows user interventions to be issued during the execution of run, for example, to pause or to force terminate poorly designed or very long calls of __meta_run. Fig. 5.11 illustrates some of the subclasses of the AbsExperiment class. Some of the subclasses define simple operations. For example, ExpMove simply moves the gantry and ExpMoveAndScan repeatedly advances the gantry and samples a profile. Others implement complicated algorithms and sequences of operations. For example, ExpHistogram performs histogram generation and peak detection and ExpFreeScan sequentially executes 6 sub-experiments. To support these complicated functionalities, a composite pattern (p163 [Gam+94]) is implemented in AbsExperiment. Although on Fig. 5.11 the aggregation is realized as a linked list by next of AbsExperiment; the actual implementation also uses template containers.

Although most of the experiment classes come from the research project Micro-Fast with minimum necessary modifications; as a simplified design, PhDSampline does not

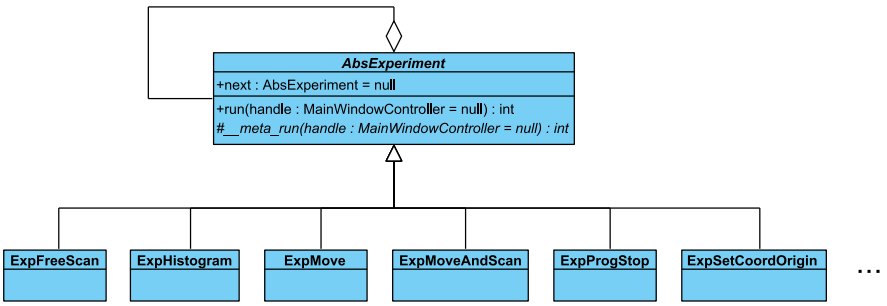

Figure 5.11: Class diagram of experiments design showing the key interfaces

support external text scripts. Instead of parsing scripts and instantiate an object of `AbsExperiment`, in `PhDSampline` the creation of experiments are through constructors and their handy overloads. For example, besides the default constructor, `ExpMove` provides another constructor where all parameters can be specified by the user. For those parameters that are better to be provided online, a graphical user interface (GUI) is used for better experience. For example, `ExpPreparation` has a constructor with GUI for inputs, because some of the parameters like `yDivision` depends on how the gauge object is placed.

Detailed explanation to the functionality and design of each experiment class will be conducted when they are actually used. This keeps the thesis tidy and concise yet not compromising much on being self-explanatory and easy to follow. The same policy will be applied to the small tools of G2 as well. Thus concludes the section of software.

5.3 Validation

The validation process is summarized by the flowcharts Figs. 5.12 5.13 5.14; and in the rest of this section the explanation will be made following these charts. Before going into the details, it begins with the clarification of the convention and usage of symbols in the flow charts. The nodes starting with `S` represent a step that conducts either an operation or data processing. For example, `S6` (also being referred to as node `S6` or step `S6`) in Fig. 5.12 represents an action to perform an edge detection algorithm and node `S10` in Fig. 5.13 represents an action to conduct a gantry motion. The nodes starting with `D` represent data, which might be user input, sampled data, or derived outputs from `S` nodes. For example, `D13` (also being referred to as node `D13` or data `D13`) contains sampled data from the laser profiler stored in the `sdata` format and `D2` in Fig. 5.12 are generated by the peak detection algorithm in `S2`. All symbols in the flowcharts follow

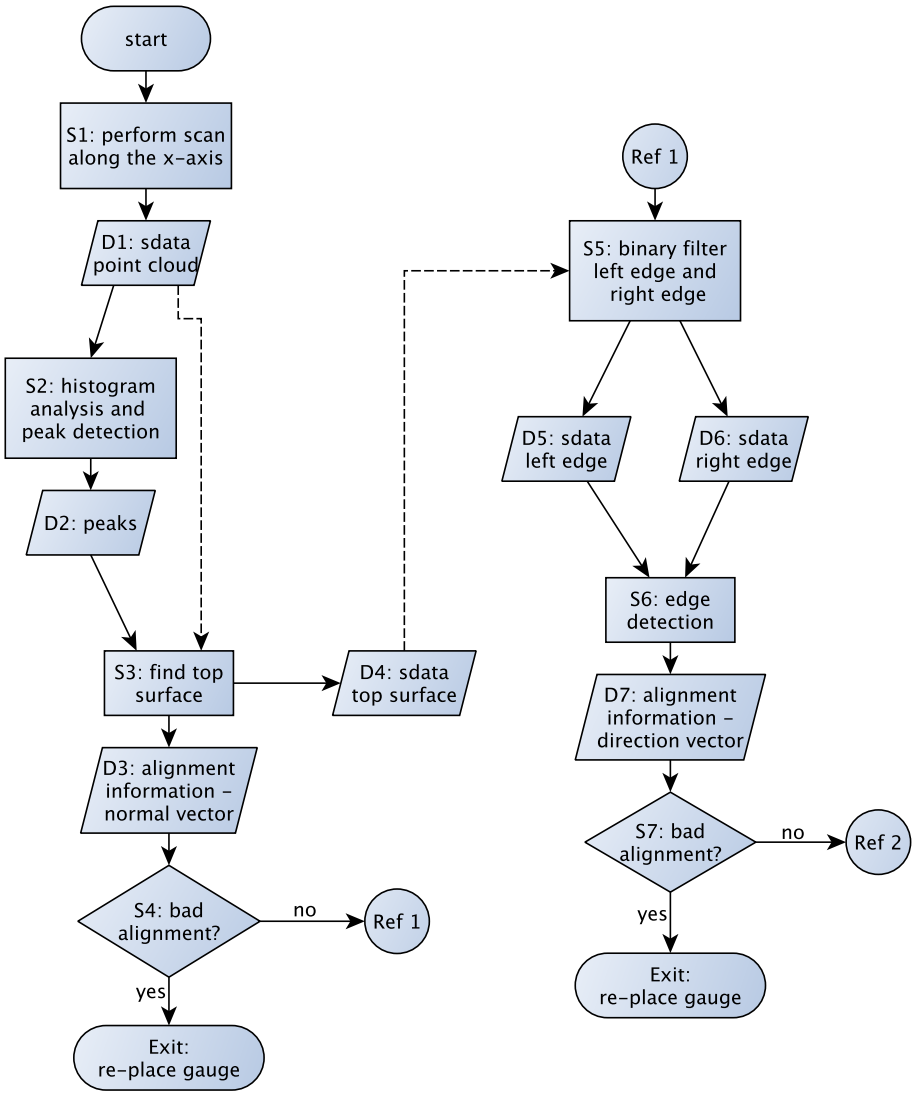

Figure 5.12: Validation process flowchart part 1: Preparation

the [ISO5807] standard except explicit distinctions on data type, format, and storage. The validation process will be solving a problem similar to Problem 3.1 with different numeric settings, and will be stated in detail later in this section.

The whole flow chart of the validation process is intentionally split into three pieces. Fig. 5.12 presents the necessary preparation of a single validation and the main output (`D4`) is a scan of the gauge object along the x-axis. By `S7`, it is expected to find out whether the gauge object is well-placed and placement related parameters lie within acceptable range. Fig. 5.13 presents the procedures to randomly sample data for the actual validation, it uses the outputs generated in Fig. 5.12 and outputs profiles of random scans for detailed analysis. By `Ref3`, the end of Fig. 5.13, the procedures are online

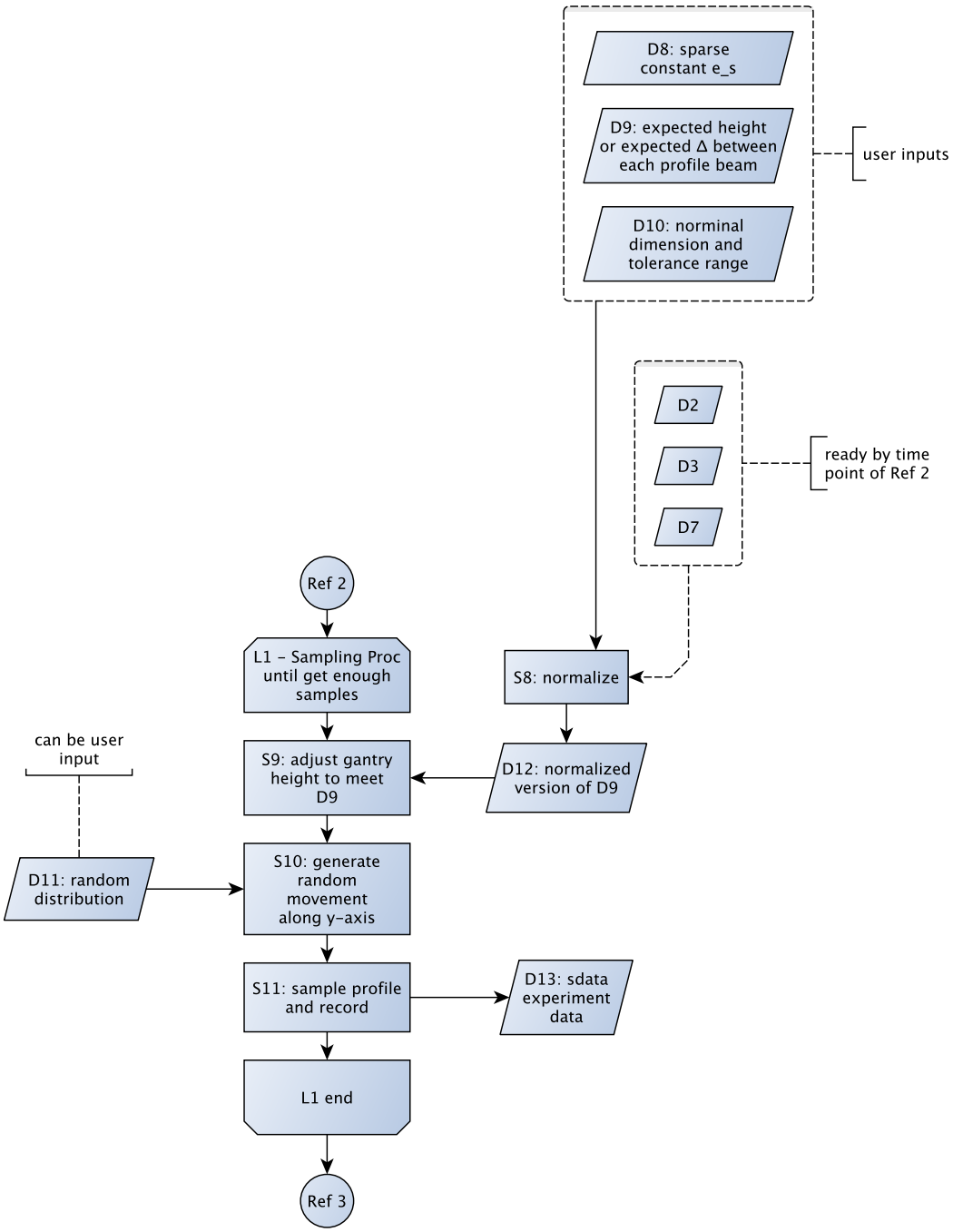

Figure 5.13: Validation process flowchart part 2: Data Sampling

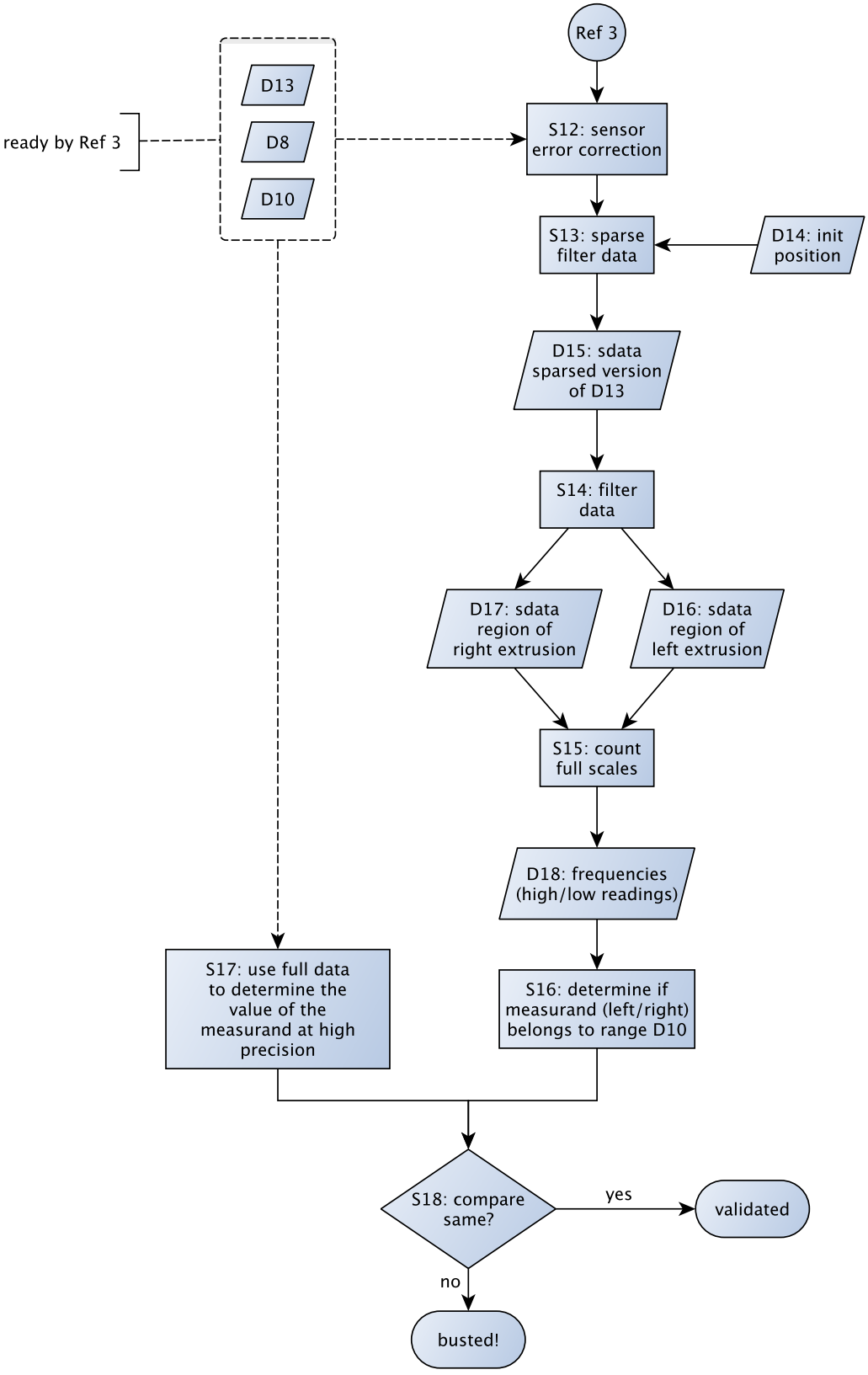

Figure 5.14: Validation process flowchart part 3: Evaluation

using the laboratory set up. The last chart Fig. 5.14 presents the actual validation of the method where frequencies of the high/low reading will be counted and claims on whether the measurand lies within the tolerance range conducted. The claims will be compared to the direct measurements to verify the validity of PBM. In the following, detailed explanation of the flow charts will be conducted.

It begins with the formal statement of the modified version of Problem 3.1. A brief summary of the parameters of the devices and the dimensions of the gauge object is included here. For the dimensions of the gauge object (Fig. 5.4), w_1, w_2, the width of the extrusions value either $w_1 = 3.2\text{mm}, w_2 = 3.0\text{mm}$ or $w_1 = 2.9\text{mm}, w_2 = 2.7\text{mm}$; and h, the height of the extrusion values either 1mm or 3mm. The effective scanning area of the laser triangulation profiler has the following parameters

$$N_S = 1280 \qquad \Delta_m \approx 18.3\mu\text{m} \qquad \Delta_M \approx 22.8\mu\text{m} \qquad H_S = 25\text{mm},$$

which is more than enough to find out the width of the extrusions at sub-millimeter level. The nominal dimension and tolerance range used to test the extrusions typically look like 2.7 ± 0.1mm or 3.2 ± 0.1mm. This means that the laser profiler in the laboratory set up will be too precise (laterally) for validation. To make the validation meaningful, only the data from every e_s^{th} beam in a sampled profile will be used; and this e_s is specified by the input `D8` in Fig. 5.13. In detail, it means that for the validation of PBM, only the data from beams

$$\{\mathfrak{b}_{i_0+ke_s} | k = 0, 1, 2, 3, \cdots\} \tag{5.1}$$

will be used; and Fig. 5.15 gives a visual illustration to this approach. A thinned out profile using beams in the set of type (5.1) will be called a *sparse profile* or an e_s*-sparse profile*. This e_s is known as the *sparse index* or *sparse constant*. The initial index i_0 will be specified by `D14`, and it is always assumed that $0 \leq i_0 < e_s$. By doing so, it virtually sets up a *spars laser profiler*, whose Δ_m, Δ_M, denoted by $\Delta_{m,e_s}, \Delta_{M,e_s}$, are e_s times of the origin. For example, fixing $e_s = 26$, the 26-sparse virtual laser profiler has the specification that

$$\Delta_{m,26} = 26\Delta_m \approx 0.4758\text{mm} \qquad \Delta_{M,26} = 26\Delta_M \approx 0.5928\text{mm}.$$

By doing so, the validation is meaningful because the scale is much larger than the tolerance range to be checked. Thus the problem to be solved for validation of PBM is stated as follows:

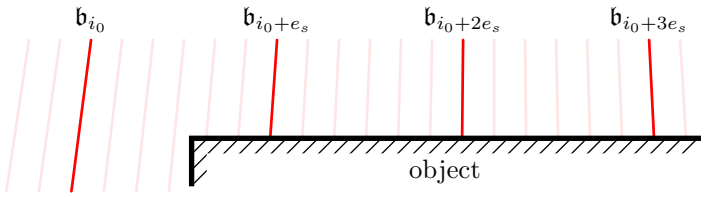

Figure 5.15: Sparse laser profiles

Problem 5.1. For a given gauge object with two extrusions of width w_1, w_2, determine whether the widths belong to a given tolerance range $l_n \pm T$ using a sparse laser profiler with a pre-selected sparse constant e_s, which makes $\Delta_{m,e_s} > T$.

With the problem formally defined by Problem 5.1, the explanation to the validation process now begins following the flow charts Fig. 5.12 5.13 5.14. To make the expression vivid and easy to follow, the following will be using a gauge piece with $w_1 = 2.7\text{mm}, w_2 = 2.9\text{mm}, h = 1\text{mm}$ and the gauge block will be placed in a way that the w_1 extrusion is on the "left" and w_2 on the "right" side[7]. The data used for the explanation comes from a real-world validation experiment which is logged by `F18102903` in the master log file.

5.3.1 Step S1 to S7

The `S1` step in Fig. 5.12 is achieved by an experiment defined by the `ExpFreeScan` class. It is a congregation of 6 experiments and sequentially executes `ExpMove`, `ExpWait`, `ExpSetCoordOrigin`, `ExpMove`, `ExpProgStop`, and `ExpMoveAndScan`. The detailed functionality and purpose of these sub-steps are explained as follows:

1) `ExpMove`, moves the gantry by a specified displacement and speed. The first execution of `ExpMove` resets the axes to one of the ends. By doing so, it simplifies the consequential programming work in the sense that all displacement related parameters can be set constant without the worry about the gauge object falling outside of the effective scanning area of the laser scanner.

2) `ExpWait` intentionally makes `PhDSampline` to wait for a short period. This step is necessary because the initial position of the gantry is unknown and one must wait several seconds for the completion of `ExpMove` if the gantry is at worst initial positions.

[7]The y coordinate of the left part is less than that on the right.

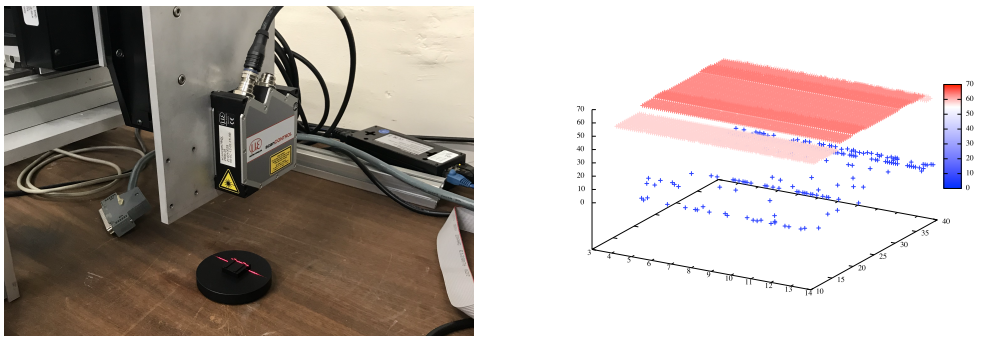

[a] [b]

Figure 5.16: **[a]** photo of the set up after the action of `ExpProgStop`, cropped from `F18102917`; **[b]** point cloud `D1` produced by `S1`, plotted using original data `F18102905` (every 20 points). ($1 = 1$mm)

3) `ExpSetCoordOrigin` performs a coordinate translation by setting the current position to a given coordinate. Although this functionality is common in modern CNC systems, there is another reason for it to be implemented in `PhDSampline` . After each initialization of the `NSC-G3-E` controller, the inner coordinates are randomly assigned. This step in `ExpFreeScan` guarantees consistent coordinate for positioning in the consequential experiments.

4) The second `ExpMove` moves the gantry to the desired position so that the extrusions are contained in the scanning area of the laser profiler.

5) `ExpProgStop` causes a programmable stop, which prompts a dialog box and communicates with the operator. Unlike `ExpWait`, user interventions are needed for the program to continue. This step in `ExpFreeScan` asks the user to examine and adjust the position of the gauge object. Fig. 5.16[a] shows the gauge object with the laboratory set up, when the experiment is paused at this step.

6) `ExpMoveAndScan` repeatedly moves the gantry and then records a profile. The sampled profiles are then stored in a given `AbsDataSections` container. It is the actual experiment in which `ExpFreeScan` conducts the work of "scan and profiling"; and here a special container of type `SimpleDataSection` is used to catch all the point cloud data.

`S1` in experiment `F18102903` recorded 100 profiles with about 0.1mm spacing along the x-axis between adjacent profiles. The output `D1` is recorded by `F18102905` and shown by Fig. 5.16[b].

The step S2 is realized by ExpHisogram. ExpHisogram takes an AbsDataSections as input where a cloud point is contained and then builds a histogram on the z coordinate of the points. After that it executes an automatic peak detection algorithm from Sezan ([Sez90]) and generates the output. The interval length for statistics can be specified by assigning the desired values to the discretion variable of the class and similar the Sezan constant N. The histogram is shown by Fig. 5.17 and the detected peaks are summarized in Table. 5.2.

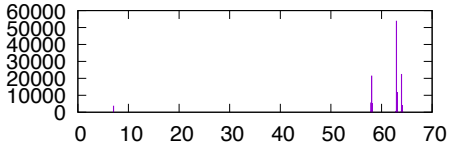

Figure 5.17: Histogram of z coordinate of points, using data F18102905; interval width 0.1, horizontal axis in mm, vertical frequency count

index	height (mm)	frequency
1	7	3522
2	58	21371
3	62.9	53692
4	63.9	22307

Table 5.2: Detected peaks in the histogram, with Sezan constant 23, result quoted from log file F18102903

S3 is achieved by subDSfilterZ and fitPlane as a static calls of the DSCF class. subDSfilterZ simply filters the points and finds out those whose z coordinate is within a specified range. Then fitPlane performs a least square fitting using the filtered points for the equation of the top surface. D4, the top surface obtained from F18102905 as D1, is recorded by F18102906 and visually presented as Fig. 5.18. The equation of the top surface is

$$0.000722x - 0.003113y + 64.04971 = z.$$

The normal vector is

$$\overrightarrow{n} = (-0.000721996, 0.00311298, 0.999995)$$

and the included angle θ_n between $\overrightarrow{n}$ and $\overrightarrow{e_3}$ is about 0.00319 rad or $0.18°$. These are all computed and logged in F18102903; and these data show an acceptable alignment which clears S4.

As stated earlier in this chapter, two extrusions are prepared on each gauge object for direct comparison of difference in high/low reading frequencies. To fulfill this, flow charts of the validation process sometimes splits for each of the extrusions. S5 filters D4 into two parts and the "left" part refers to the extrusion with smaller y coordinates. It is realized by quickFilter, a static call in the DSCF class. For flexibility the call takes

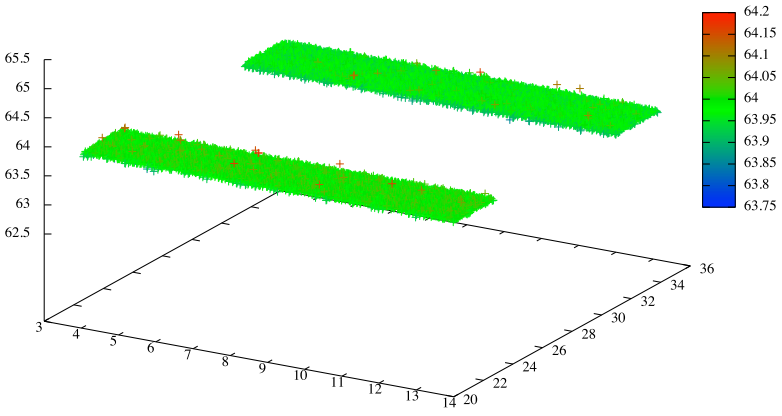

Figure 5.18: Top surface `D4`, visualized using original data `F18102906` (every 2 points); filtration keeps only the points whose z coordinate is within 63.9 ± 0.3. ($1 = 1$mm)

a function pointer (or delegate) for the criterion of filtration. The point clouds for the left and right extrusions are shown in Fig. 5.19.

Step `S6` is achieved by `autoEdges`, a static call of the `DSCF` class. The algorithm processes on the point cloud of an extrusion on the top surface (Fig. 5.19[a][b]). It firstly finds out the projected edges on the xOy plane using least square fittings; then with the equation of the top surface the actual directional vector is calculated. For each point cloud, two vectors will be obtained and their arithmetic mean will be used as $\overrightarrow{m}$ the alignment vector defined in chapter 4. In terms of implementation, the `autoEdges`

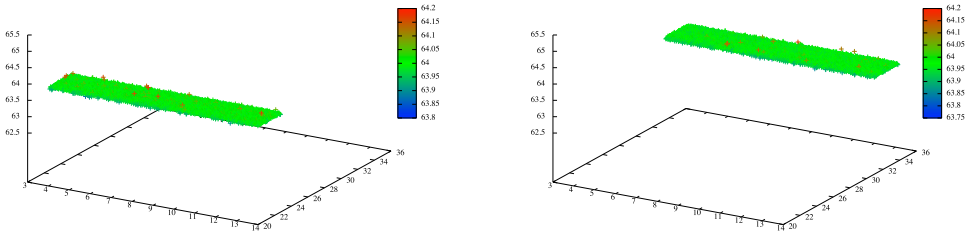

[a] [b]

Figure 5.19: Split top surfaces using the top surface data `F18102906`, severed by the plane $y = 25$: **[a]** `D5` the left extrusion (`F18102907`); **[b]** `D6` the right extrusion (`F18102908`)

call has two overloads — one focuses on computing the equation of the projected lines and the other computes the actual directional vector. From the log file `F18102903`, the computed directional vectors are summarized in Table. 5.3. These data indicates that θ_m are about 0.0074 rad and 0.0055 rad respectively. These suggests a good placement and hence clears `S7`.

Table 5.3: Direction vector of the edges of extrusions

side	index	vector
left	1	$(0.9999679,\ 0.007990315,\ 0.0006969193)$
	2	$(0.9999766,\ 0.006810424,\ 0.0007007758)$
right	1	$(0.9999839,\ 0.005633586,\ 0.0007042463)$
	2	$(0.9999859,\ 0.005279162,\ 0.0007057879)$

So far all steps in Fig. 5.12, the first part of the flowchart, have been covered. Indeed, all these steps are encapsulated in `ExpPreparation`, which holds a dedicatedly designed UI for easy initialization. As the name of `ExpPreparation` suggests, what has been done so far are preparations for the actual sampling process. With better fixture and vice tools, these procedures can be greatly simplified.

5.3.2 Step S8 to S11

In Fig. 5.13, `D8` the sparse constant e_s, `D9` the expected scale Δ_0, and `D10` the nominal dimension and tolerance range are all specified by the user through a dedicatedly designed UI. The procedures on the flow chart 5.13 will be conducting actions for the "left" extrusion, while sampling also the "right" extrusion. For example, the information provided by `D10` is by default understood to be used for the "left" part. In the experiment recorded by `F18102903`, l_n is specified to be 2.7mm and the tolerance range $T = 0.1$mm. Then by choosing $N_0 = 5$, `D9` is specified as

$$\Delta_0 = \frac{l_n}{N_0} = 0.54\text{mm}.$$

To achieve this choice of Δ_0, `D8`, the sparse constant is specified to 26.

The `S8` procedure computes the alignment related parameters which have been discussed intensively in section 4.2. In experiment `F18102903`, with $\alpha_0 = 6.5°$, it holds that

$$\theta_s \approx 0.178° \qquad K(\overrightarrow{n}, \overrightarrow{m}) \approx 1.000023 \qquad \kappa(\overrightarrow{n}, \overrightarrow{m}, \alpha) \in [0.9996453, 1.000355)$$

Compared to $T = 0.1$, the impact from mis-alignment is negligible — discussions similar to Example 4.1 and Example 4.3 show no big impact. To see this in detail, with the assumption that $\overline{L} = 3.7, \underline{L} = 1.7$, it follows that

$$L_5 \leq 0.000437658$$

which means that the Type II interval around $\Delta_0 = 0.54$ occupies no more than 0.081% of the Δ-axis. And the fact that $0.9996 < K\kappa < 1.0004$ indicates that the trigonometric error from mis-alignments is less than 0.04%. K and κ are multiplied to the specified Δ_0 to make the necessary alignment-related compensation; and henceforth in this section Δ_0 will be used to refer to this corrected value if no ambiguity arises.

The main random sampling procedure is contained in loop `L1`; and for each run `S9` adjusts the height of the laser profiler so that the specified Δ_0 is maintained. Then the gantry moves along the y-axis for a random amount as discussed in section 4.3 of chapter 4. After that the profile is recorded and advances to the next run of the loop.

The height adjustment is implemented in `ExpHeightAdjust`, which performs a close-loop proportional control. Because the effective scanning area of the laser profiler is trapezoidal, the linear relation by equation (4.30) guarantees the effectiveness of the P-control. To extract the current value of Δ, `ExpHeightAdjust` directly reads from the profiler, and then extract peak information by calling `DSCF.histogram`. Like `ExpHistogram`, `DSCF.histogram` firstly builds histogram and then applies Sezan's peak detection algorithm. Then `DSCF.averageDeltaYSparseData` is called to compute the arithmetic mean of Δ on the top surface. The whole control algorithm only uses e_s-sparse data from the raw profile.

The random engine used in the validation process is Mersenne Twister[8], and the random shifts along the y-axis are uniform. `S10` is implemented by directly calling `genrand_N` of the Mersenne Twister class.

In `S11`, instead of recording scanned profiles in each run of the loop, all profiles are recorded in one `sdata` file. To distinguish each profile, a coordinate transformation is performed at the beginning of each loop by setting the origin back 0.1mm along the x-axis. `S11` is realized by `ExpMoveAndScan` and the coordinate transformation by `ExpSetCoordOrigin`. In the validation experiment recorded by `F18102903`, 100 random samples are recorded in an `sdata` file with ID `F18102909`, which is `D13` in the flow chart

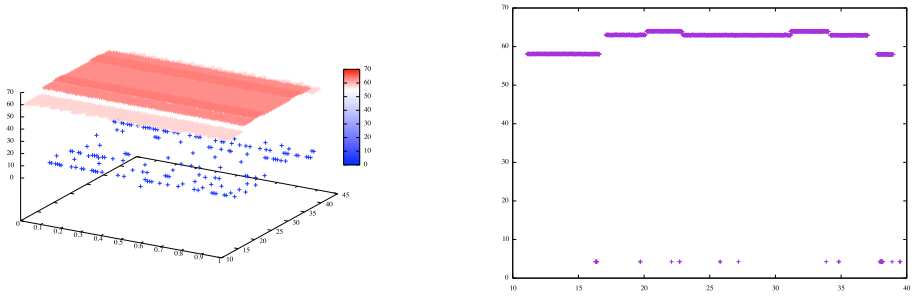

[a] [b]

Figure 5.20: Visualization of `D13` identified by `F18102909`: [a] 100 randomly sampled profile as a whole plotted (using every 20 points); [b] the first profile in `F18102909`

Fig. 5.13. The visualization of the whole `D13` and the first sampled profile are illustrated by Fig. 5.20.

Now all steps in Fig. 5.13 have been covered, and thus finishes the explanation to the part two of the flow chart of the whole validation. `ExpValidation` encapsulates all the steps so far, and indeed it even owns an `ExpPreparation` for all the steps by `S8`. So far most of the designs are part of `PhDSampline` and belong to the G1 group. Because the result set and the frequency counts are determined by this point, the rest of the validation process are offline.

5.3.3 Step 12 to End

The first procedure needed after random sampling is to identify some errors and make necessary corrections for later procedures. `S12` is the step where all these happen. In order to provide a good explanation, it begins with the description of the Micro-Epsilon `scanCONTROL 2900-25` laser profiler. Optical triangulation relies on tracking the laser spots on the surface of the object; and this non-contact method sometimes fails due to various reasons. For example, a laser spot might fall out of the field of view of the camera; or the surface of the object might be well-polished and shimmering; or the object itself might be transparent. In case of such failures, the `scanCONTROL 2900-25` laser profiler will return with height 0 which is significantly smaller than the valid readings. The blue points on Fig. 5.16[b] and points on bottom of the profile graph Fig. 5.20[b] reflect such failures. It is theoretically hard to fix all these failures, however, with the shape of the gauge object known, the validation process fixes one kind of these failures

[8] source code by Makoto Matsumoto and Takuji Nishimura, ported to `C#` by stlalv

Table 5.4: 10 points from the first sampled profile in `F18102909`

index	244	245	246
(y, z)	$(33.2754, 63.9291)$	$(33.2534, 63.9441)$	$(33.2314, 63.9521)$
index	247	*248*	249
(y, z)	$(33.2114, 63.9541)$	$(33.8644, 4.2541)$	$(33.1694, 63.9561)$
index	250	251	252
(y, z)	$(33.1484, 63.9571)$	$(33.1264, 63.9701)$	$(33.1054, 63.9771)$
index	253		
(y, z)	$(33.0844, 63.9801)$		

that occur on the top surface. Data in Table. 5.4 are retrieved from the first sampled profile in `F18102909` (Fig. 5.20[b]). The point with index 248 is easily identified as a failure of the sensor[9], because it is between correctly recognized top surface points. `S12` only fixes failure of this kind on the top surface and the correction is conducted by `sensorErrorCorrection`, a tool from the G2 group. Detailed options and the usage instruction of `sensorErrorCorrection` can be found in B.8. An execution of `sensorErrorCorrection` on `F18102909` with properly set parameters[10] corrected 70 points in 60 profiles, among which 45 had one failure and the remaining 15 two. The output `sdata` file is identified by `F18103001` in the master log file.

The output of `S12` is immediately fed into `S13` to be thinned out. In order to fully benefit from the random samplings, `D14`, an integer for the starting index is included in the validation process. For example, with $e_s = 26$ and `D14` set to 3, only points from beams $\mathfrak{b}_3, \mathfrak{b}_{29}, \mathfrak{b}_{55}, \ldots, \mathfrak{b}_{1277}$ remain in `D15` after `S13`; and if `D14` is set to 4, the points from beams $\mathfrak{b}_4, \mathfrak{b}_{30}, \mathfrak{b}_{56}, \ldots, \mathfrak{b}_{1278}$ remain. The tool `binaryPtFilterSparse` from G2 conducts the actual filtering work. Detailed options and the usage instruction of `binaryPtFilterSparse` can be found in B.4. Setting `D14` to 0 and thin out `F18103001` for every 26 points, `D15` is obtained and will be referred to as `F18103101`. Fig. 5.21 shows clearly the difference before and after the filtration. This thinned out data is what actually generates the result sets and frequency counts. Together with the fact that `S9` only used thinned out data for height adjustment, it is clear that the validation is performed on an e_s-sparse virtual laser profiler with all restrictions in Problem 5.1.

`S14` then separates `D15` into two `sdata` files containing the left and right top surfaces. Again the word "left" means that the y coordinate of the points are smaller. The small tool `binaryPtFilter` from the G2 group handles this work. Detailed options

[9] The coordinate 4.2541mm is obtained by adding gantry coordinates

[10] parameters: `-H 64 -T 0.4 -t 10`

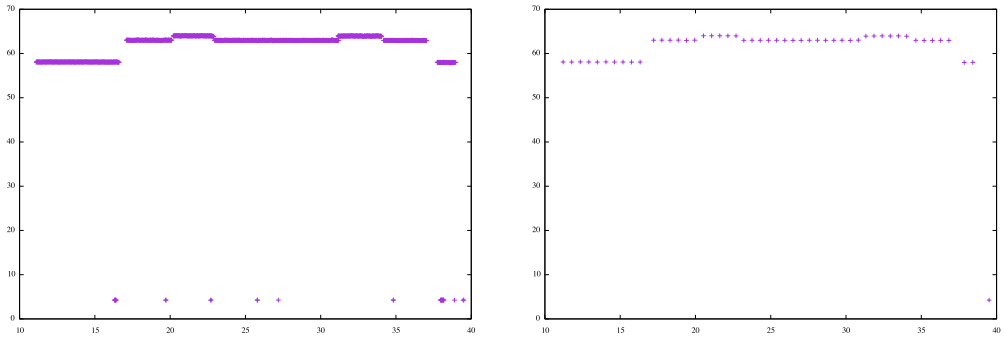

[a] [b]

Figure 5.21: Comparison of dense data and thinned out data: **[a]** first sampled profile in `F18103001` with correction; **[b]** the thinned out profile, staring from index 0 and using every 26 points in `F18103001`

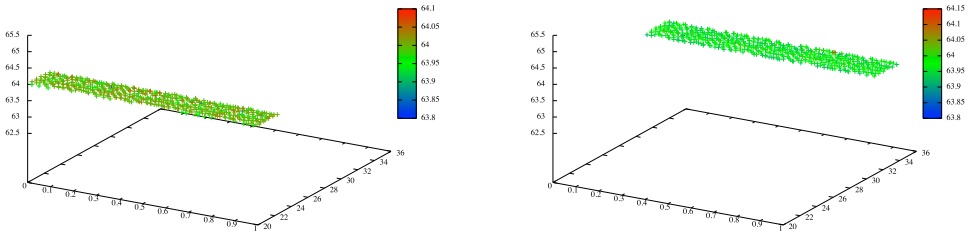

[a] [b]

Figure 5.22: Severed top surfaces using data `F18103101`: **[a]** `D16` the left part; **[b]** the right part.

and the usage instruction of `binaryPtFilter` can be found in B.3. An execution with input `F18103101` and proper parameters[11] produces outputs `D16` and `D17`, identified by `F18103102` and `F18103103` respectively on the master log file. Fig. 5.22 presents these data visually.

The `S15` is a simple procedure, which counts the number of full scales and then reports the result. The tool `fullScaleStatistics` does this humble work. Detailed options and the usage instruction of `fullScaleStatistics` can be found in B.5. An execution with default parameters yields the result sets as shown in Table. 5.5.

[11] parameters: `-H 63.95 -t 0.5 -Y 25 -m 20 --not-drop-point`

Table 5.5: Result sets from `D16` and `D17`

	`D16` — left extrusion	`D17` — right extrusion
result set	$R_{100}^{(\text{left})} = \{(4, 99), (5, 1)\}$	$R_{100}^{(\text{right})} = \{(4, 69), (5, 31)\}$

Table 5.6: Actual width measured in `S17` using `F18102909` (`D13`)

left extrusion			right extrusion		
frequency	length (mm)	corrected (mm)	frequency	length (mm)	corrected (mm)
1	2.65	2.67	39	2.84	2.86
49	2.67	2.69	6	2.85	2.87
44	2.69	2.71	31	2.86	2.88
6	2.71	2.73	19	2.87	2.89
			5	2.89	2.91

With the result sets, `S16` is the step where methods discussed in chapter 3 is applied. Because the random displacement is uniform, it is actually working for the P1+S case. Thus compute

$$p_1 = p_h(\Delta_0, l_n + T) \approx 0.185$$
$$p_2 = p_h(\Delta_0, l_n - T) \approx 0.815.$$

Data in Table. 5.5 gives

$$f_h^{(\text{left})} = 0.01 < p_1 \qquad \text{and} \qquad f_h^{(\text{right})} = 0.31 > p_1$$

Therefore the left part is claimed to be within the range 2.7 ± 0.1mm and the right part is not. Further more, because $f_h^{(\text{left})}$ is near 0, it implies that the true value l_t is larger than $l_n = 2.7$.

Although the dimension of the manufactured gauge block agrees with the result from PBM, a much more precise result can be obtained by `S17`. The tool `actualWidths` accomplishes this task by analysing the original profile data and making direct measurements. Detailed options and the usage instruction of `actualWidths` can be found in B. 2. The algorithm actually computes the difference of y coordinates of end points on the top surfaces, and hence has at least an error $(-2\Delta_0/e_s, 0]$.[12] All results from `actualWidths` will be later corrected by adding Δ_0/e_s to them. An execution of `actualWidths` using `D13` with proper parameters[13] gives the details of the 100 samples, and together with the corrected values are presented in Table. 5.6.

The average of the left and the right extrusions are 2.71mm and 2.88mm respectively through direct measurements. This is consistent with the statement from PBM that the left extrusion is within the range 2.7 ± 0.1mm and the right is not; and furthermore it confirms the claim that $l_t < l_n = 2.7$mm. Thus PBM is verified to be valid in this case. Now all contents on the third part of the validation flow chart are covered and the whole procedure of validation is fully explained.

[12] The Δ_0 is understood here as from the virtual sparse profiler.
[13] parameters: `-H 63.95 -T 0.5 -S 100`

5.4 Experiments and Analysis

In this section, experiment data is exhibited with descriptions and comments. The result of the experiments are summarized in eight tables (from Table 5.7 to 5.14) at the end of this chapter. In total eight sets of validation experiments are conducted on four different gauge objects with different parameter settings, and each set will be referred to as `SETX`, where `X` values from 1 to 8. Each table represents a set of validation experiments, and the sampled data are then used for e_s individual tests. A total number of 213 tests are conducted following the discussions in this thesis, and all these practical results show consistency with the theoretic predictions.

`SET1`, `SET2`, `SET3` and `SET4` are conducted on gauge objects with $w_1 = 2.9$mm, $w_2 = 2.7$mm; while the rest are conducted on gauge objects with $w_1 = 3.2$mm, $w_2 = 3.0$mm. Parameters of `SET5` to `SET8` are set in a way similar to experiments `SET1` to `SET4` only with different widths of extrusions. Thus it is enough to make comments on `SET1` to `SET4`.

`SET1` and `SET2` are exactly the situation described by Problem 5.1 with different choices of Δ_0. In `SET3` and `SET4`, the nominal length l_n is intentionally set to be different than the size of the extrusions. The result shows that correct conclusions can nevertheless be drawn. In `SET1`, `SET2` and `SET3` the "left" extrusion is within the tolerance range and in `SET4` the "right" extrusion is within the range. All these results impartially show the validity of PBM.

As a reminder, the 3-point-supported result sets like `ENT22` and `ENT26` are treated in the way discussed in 4.3.1.

5.5 Summary

In this chapter, the design of the hardware and the software for the validation has been presented, starting from the design of the gauge object, hardware specification, software structure, as well as the design patterns in `PhDSampline` , the main software. The whole validation process, presented by 3 flow charts (Figs. 5.125.135.14), is fully explained. 8 sets of experiments with over 200 tests are conducted, through which the validity and feasibility of PBM are proven. The whole validation process also shows that PBM can be applied on existing machines and devices if the software can be properly updated.

Table 5.7: SET1: Experiment records for validation for the tolerance range 2.7 ± 0.1mm with $\Delta_0 = 0.54$mm

ID	log ID	Gauge and Placement lft. (mm)	rt. (mm)	ht. (mm)	θ_n (rad)	θ_m (rad)	$K(\vec{n}, \vec{m})$	l_n (mm)	T (mm)	Δ_0	e_s	true value (S17) lft. (mm)	rt. (mm)	D14	$R_{100}^{(\text{left})}$	$R_{100}^{(\text{right})}$	in range? lft.	rt.	verified?
ENT0														0	$\{(4,99),(5,1))\}$	$\{(4,69),(5,31))\}$	y	n	Y
ENT1														1	$\{(4,99),(5,1)\}$	$\{(4,68),(5,32)\}$	y	n	Y
ENT2														2	$\{(4,99),(5,1)\}$	$\{(4,70),(5,30)\}$	y	n	Y
ENT3														3	$\{(4,97),(5,3)\}$	$\{(4,72),(5,28)\}$	y	n	Y
ENT4														4	$\{(4,99),(5,1)\}$	$\{(4,72),(5,28)\}$	y	n	Y
ENT5														5	$\{(4,96),(5,4)\}$	$\{(4,65),(5,35)\}$	y	n	Y
ENT6														6	$\{(4,99),(5,1)\}$	$\{(4,64),(5,36)\}$	y	n	Y
ENT7														7	$\{(4,98),(5,2)\}$	$\{(4,62),(5,38)\}$	y	n	Y
ENT8														8	$\{(4,99),(5,1)\}$	$\{(4,62),(5,38)\}$	y	n	Y
ENT9														9	$\{(4,97),(5,3)\}$	$\{(4,63),(5,37)\}$	y	n	Y
ENT10														10	$\{(4,96),(5,4)\}$	$\{(4,62),(5,38)\}$	y	n	Y
ENT11														11	$\{(4,97),(5,3)\}$	$\{(4,63),(5,37)\}$	y	n	Y
ENT12	F18102903	2.7	2.9	1	0.00319	0.0074	1.000023	2.7	0.1	0.54	26	avg 2.71	avg 2.88	12	$\{(4,99),(5,1)\}$	$\{(4,65),(5,35)\}$	y	n	Y
ENT13														13	$\{(4,98),(5,2)\}$	$\{(4,69),(5,31)\}$	y	n	Y
ENT14														14	$\{(4,97),(5,3)\}$	$\{(4,71),(5,29)\}$	y	n	Y
ENT15														15	$\{(4,97),(5,3)\}$	$\{(4,68),(5,32)\}$	y	n	Y
ENT16														16	$\{(4,97),(5,3)\}$	$\{(4,71),(5,29)\}$	y	n	Y
ENT17														17	$\{(4,97),(5,3)\}$	$\{(4,71),(5,29)\}$	y	n	Y
ENT18														18	$\{(4,98),(5,2)\}$	$\{(4,70),(5,30)\}$	y	n	Y
ENT19														19	$\{(4,100)\}$	$\{(4,68),(5,32)\}$	y	n	Y
ENT20														20	$\{(4,96),(5,4)\}$	$\{(4,68),(5,32)\}$	y	n	Y
ENT21														21	$\{(4,96),(5,4)\}$	$\{(4,63),(5,37)\}$	y	n	Y
ENT22														22	$\{(3,1),(4,97),(5,2)\}$	$\{(4,65),(5,35)\}$	y	n	Y
ENT23														23	$\{(4,97),(5,3)\}$	$\{(4,65),(5,35)\}$	y	n	Y
ENT24														24	$\{(4,99),(5,1)\}$	$\{(4,69),(5,31)\}$	y	n	Y
ENT25														25	$\{(4,100)\}$	$\{(4,65),(5,35)\}$	y	n	Y

The detailed experiment output by PhDSampline is logged in F18102903, other related materials including scanned raw data can be found in the master log file by following records of F18102903. The gauge block used is of nominal dimension $w_1 = 2.7$mm, $w_2 = 2.9$mm, $h = 1$mm; and is placed in a way that the left side is of 2.7mm and the right side 2.9mm. $l_n \pm T$, the targeted testing range is set to be 2.7 ± 0.1mm; and Δ_0 is set to $l_n/5 = 0.54$(mm). e_s is set to 26 so that $\Delta_0/e_s \approx 0.0208$mm which is possible using the laser profile. 100 samples are obtained with uniform randomness, and $p_1 \approx 0.185$, $p_2 \approx 0.815$ for the P1+S case.

Table 5.8: SET2: Experiment records for validation for the tolerance range 2.7 ± 0.1mm with $\Delta_0 = 0.45$mm

ID	log ID	Gauge and Placement lft. (mm)	rt. (mm)	ht. (mm)	θ_n (rad)	θ_m (rad)	$K(\vec{n}, \vec{m})$	l_n (mm)	T (mm)	Δ_0	e_s	true value (S17) lft. (mm)	rt. (mm)	D14	$R_{100}^{(\text{left})}$	$R_{100}^{(\text{right})}$	in range? lft.	rt.	verified?
ENT26														0	$\{(4,1),(5,97),(6,2)\}$	$\{(5,44),(6,56)\}$	y	n	Y
ENT27														1	$\{(4,1),(5,99)\}$	$\{(5,50),(6,50)\}$	y	n	Y
ENT28														2	$\{(4,1),(5,98),(6,1)\}$	$\{(5,45),(6,55)\}$	y	n	Y
ENT29														3	$\{(4,3),(5,97)\}$	$\{(5,46),(6,54)\}$	y	n	Y
ENT30														4	$\{(4,2),(5,98)\}$	$\{(5,44),(6,56)\}$	y	n	Y
ENT31														5	$\{(5,99),(6,1)\}$	$\{(5,46),(6,54)\}$	y	n	Y
ENT32														6	$\{(4,1),(5,98),(6,1)\}$	$\{(5,47),(6,53)\}$	y	n	Y
ENT33														7	$\{(4,1),(5,97),(6,2)\}$	$\{(5,49),(6,51)\}$	y	n	Y
ENT34														8	$\{(4,3),(5,96),(6,1)\}$	$\{(5,50),(6,50)\}$	y	n	Y
ENT35														9	$\{(5,100)\}$	$\{(5,47),(6,53)\}$	y	n	Y
ENT36	F18110203	2.7	2.9	1	0.00320	0.01646	1.00013	2.7	0.1	0.45	22	avg 2.71	avg 2.93	10	$\{(4,1),(5,98),(6,1)\}$	$\{(5,53),(6,47)\}$	y	n	Y
ENT37														11	$\{(5,99),(6,1)\}$	$\{(5,47),(6,53)\}$	y	n	Y
ENT38														12	$\{(4,1),(5,99)\}$	$\{(5,48),(6,52)\}$	y	n	Y
ENT39														13	$\{(4,4),(5,96)\}$	$\{(5,50),(6,50)\}$	y	n	Y
ENT40														14	$\{(4,1),(5,98),(6,1)\}$	$\{(5,52),(6,48)\}$	y	n	Y
ENT41														15	$\{(4,1),(5,97),(6,2)\}$	$\{(5,50),(6,50)\}$	y	n	Y
ENT42														16	$\{(4,2),(5,97),(6,1)\}$	$\{(5,51),(6,49)\}$	y	n	Y
ENT43														17	$\{(4,1),(5,98),(6,1)\}$	$\{(5,48),(6,52)\}$	y	n	Y
ENT44														18	$\{(4,1),(5,96),(6,3)\}$	$\{(5,47),(6,53)\}$	y	n	Y
ENT45														19	$\{(5,98),(6,2)\}$	$\{(5,49),(6,51)\}$	y	n	Y
ENT46														20	$\{(4,5),(5,93),(6,2)\}$	$\{(5,46),(6,54)\}$	y	n	Y
ENT47														21	$\{(4,1),(5,97),(6,2)\}$	$\{(5,43),(6,57)\}$	y	n	Y

The detailed experiment output by PhDSampline is logged in F18110203, other related materials including scanned raw data can be found in the master log file by following records of F18110203. The gauge block used is of nominal dimension $w_1 = 2.7$mm, $w_2 = 2.9$mm, $h = 1$mm; and is placed in a way that the left side is of 2.7mm and the right side 2.9mm. $l_n \pm T$, the targeted testing range is set to be 2.7 ± 0.1mm; and Δ_0 is set to $l_n/6 = 0.45$(mm). e_s is set to 22 so that $\Delta_0/e_s \approx 0.0205$mm which is possible using the laser profile. 100 samples are obtained with uniform randomness, and $p_1 \approx 0.222$, $p_2 \approx 0.778$ for the P1+S case.

Table 5.9: SET3: Experiment records for validation for the tolerance range 2.74 ± 0.1mm with $\Delta_0 = 0.548$mm

ID	log ID	Gauge and Placement lft. (mm)	rt. (mm)	ht. (mm)	θ_n (rad)	θ_m (rad)	$K(\vec{n}, \vec{m})$	l_n (mm)	T (mm)	Δ_0	e_s	true value (S17) lft. (mm)	rt. (mm)	D14	$R_{100}^{(\text{left})}$	$R_{100}^{(\text{right})}$	in range? lft.	rt.	verified?
ENT48														0	$\{(3,1),(4,99)\}$	$\{(4,74),(5,26)\}$	y	n	Y
ENT49														1	$\{(3,2),(4,97),(5,1)\}$	$\{(4,77),(5,23)\}$	y	n	Y
ENT50														2	$\{(3,2),(4,98)\}$	$\{(4,77),(5,23)\}$	y	n	Y
ENT51														3	$\{(3,1),(4,99)\}$	$\{(4,70),(5,30)\}$	y	n	Y
ENT52														4	$\{(4,100)\}$	$\{(4,68),(5,32)\}$	y	n	Y
ENT53														5	$\{(4,100)\}$	$\{(4,66),(5,34)\}$	y	n	Y
ENT54														6	$\{(3,1),(4,99)\}$	$\{(4,67),(5,33)\}$	y	n	Y
ENT55														7	$\{(3,3),(4,97)\}$	$\{(4,73),(5,27)\}$	y	n	Y
ENT56														8	$\{(3,2),(4,98)\}$	$\{(4,70),(5,30)\}$	y	n	Y
ENT57														9	$\{(3,6),(4,94)\}$	$\{(4,69),(5,31)\}$	y	n	Y
ENT58														10	$\{(3,7),(4,93)\}$	$\{(4,71),(5,29)\}$	y	n	Y
ENT59														11	$\{(3,4),(4,96)\}$	$\{(4,70),(5,30)\}$	y	n	Y
ENT60	F18110902	2.7	2.9	3	0.00637	0.00077	0.99998	2.74	0.1	0.548	26	avg 2.73	avg 2.90	12	$\{(3,3),(4,97)\}$	$\{(4,68),(5,32)\}$	y	n	Y
ENT61														13	$\{(3,3),(4,97)\}$	$\{(4,67),(5,33)\}$	y	n	Y
ENT62														14	$\{(3,3),(4,97)\}$	$\{(4,62),(5,38)\}$	y	n	Y
ENT63														15	$\{(3,1),(4,99)\}$	$\{(4,62),(5,38)\}$	y	n	Y
ENT64														16	$\{(3,2),(4,98)\}$	$\{(4,63),(5,37)\}$	y	n	Y
ENT65														17	$\{(3,1),(4,99)\}$	$\{(4,63),(5,37)\}$	y	n	Y
ENT66														18	$\{(3,2),(4,98)\}$	$\{(4,63),(5,37)\}$	y	n	Y
ENT67														19	$\{(3,4),(4,96)\}$	$\{(4,63),(5,37)\}$	y	n	Y
ENT68														20	$\{(3,7),(4,93)\}$	$\{(4,72),(5,28)\}$	y	n	Y
ENT69														21	$\{(3,4),(4,96)\}$	$\{(4,74),(5,26)\}$	y	n	Y
ENT70														22	$\{(3,4),(4,96)\}$	$\{(4,78),(5,22)\}$	y	n	Y
ENT71														23	$\{(4,100)\}$	$\{(4,80),(5,20)\}$	y	n	Y
ENT72														24	$\{(3,1),(4,99)\}$	$\{(4,74),(5,26)\}$	y	n	Y
ENT73														25	$\{(3,3),(4,97)\}$	$\{(4,77),(5,23)\}$	y	n	Y

The detailed experiment output by PhDSampline is logged in F18110902, other related materials including scanned raw data can be found in the master log file by following records of F18110902. The gauge block used is of nominal dimension $w_1 = 2.7$mm, $w_2 = 2.9$mm, $h = 1$mm; and is placed in a way that the left side is of 2.7mm and the right side 2.9mm. $l_n \pm T$, the targeted testing range is set to be 2.74 ± 0.1mm; and Δ_0 is set to $l_n/5 = 0.548$(mm). e_s is set to 26 so that $\Delta_0/e_s \approx 0.0211$mm which is possible using the laser profile. 100 samples are obtained with uniform randomness, and $p_1 \approx 0.182$, $p_2 \approx 0.818$ for the P1+S case.

Table 5.10: SET4: Experiment records for validation for the tolerance range 2.95 ± 0.15mm with $\Delta_0 = 0.59$mm

ID	log ID	Gauge and Placement lft. (mm)	rt. (mm)	ht. (mm)	θ_n (rad)	θ_m (rad)	$K(\vec{n}, \vec{m})$	l_n (mm)	T (mm)	Δ_0	e_s	true value (S17) lft. (mm)	rt. (mm)	D14	$R_{100}^{(\text{left})}$	$R_{100}^{(\text{right})}$	in range? lft.	rt.	verified?
ENT74														0	$\{(3,38),(4,62)\}$	$\{(3,6),(4,94)\}$	n	y	Y
ENT75														1	$\{(3,40),(4,60)\}$	$\{(3,7),(4,93)\}$	n	y	Y
ENT76														2	$\{(3,42),(4,58)\}$	$\{(3,8),(4,92)\}$	n	y	Y
ENT77														3	$\{(3,43),(4,57)\}$	$\{(3,5),(4,95)\}$	n	y	Y
ENT78														4	$\{(3,46),(4,54)\}$	$\{(3,3),(4,97)\}$	n	y	Y
ENT79														5	$\{(3,44),(4,56)\}$	$\{(3,4),(4,96)\}$	n	y	Y
ENT80														6	$\{(3,42),(4,58)\}$	$\{(3,6),(4,94)\}$	n	y	Y
ENT81														7	$\{(3,42),(4,58)\}$	$\{(3,7),(4,93)\}$	n	y	Y
ENT82														8	$\{(3,42),(4,58)\}$	$\{(3,7),(4,93)\}$	n	y	Y
ENT83														9	$\{(3,40),(4,60)\}$	$\{(3,8),(4,92)\}$	n	y	Y
ENT84														10	$\{(3,38),(4,62)\}$	$\{(3,6),(4,94)\}$	n	y	Y
ENT85														11	$\{(3,36),(4,64)\}$	$\{(3,8),(4,92)\}$	n	y	Y
ENT86														12	$\{(3,36),(4,64)\}$	$\{(3,10),(4,90)\}$	n	y	Y
ENT87														13	$\{(3,30),(4,70)\}$	$\{(3,15),(4,85)\}$	n	y	Y
ENT88	F18111403	2.7	2.9	3	0.00629	0.00597	0.999998	2.95	0.15	0.59	29	avg 2.73	avg 2.91	14	$\{(3,31),(4,69)\}$	$\{(3,11),(4,89)\}$	n	y	Y
ENT89														15	$\{(3,32),(4,68)\}$	$\{(3,6),(4,94)\}$	n	y	Y
ENT90														16	$\{(3,34),(4,66)\}$	$\{(3,2),(4,98)\}$	n	y	Y
ENT91														17	$\{(3,39),(4,61)\}$	$\{(3,3),(4,97)\}$	n	y	Y
ENT92														18	$\{(3,41),(4,59)\}$	$\{(3,5),(4,95)\}$	n	y	Y
ENT93														19	$\{(3,42),(4,58)\}$	$\{(3,7),(4,93)\}$	n	y	Y
ENT94														20	$\{(3,40),(4,60)\}$	$\{(3,3),(4,97)\}$	n	y	Y
ENT95														21	$\{(3,40),(4,60)\}$	$\{(3,4),(4,96)\}$	n	y	Y
ENT96														22	$\{(3,42),(4,58)\}$	$\{(3,2),(4,98)\}$	n	y	Y
ENT97														23	$\{(3,42),(4,58)\}$	$\{(3,2),(4,98)\}$	n	y	Y
ENT98														24	$\{(3,42),(4,58)\}$	$\{(3,5),(4,95)\}$	n	y	Y
ENT99														25	$\{(3,41),(4,59)\}$	$\{(3,4),(4,96)\}$	n	y	Y
ENT100														26	$\{(3,43),(4,57)\}$	$\{(3,5),(4,95)\}$	n	y	Y
ENT101														27	$\{(3,40),(4,60)\}$	$\{(3,6),(4,94)\}$	n	y	Y
ENT102														28	$\{(3,38),(4,62)\}$	$\{(3,6),(4,94)\}$	n	y	Y

The detailed experiment output by PhDSampline is logged in F18111403, other related materials including scanned raw data can be found in the master log file by following records of F18111403. The gauge block used is of nominal dimension $w_1 = 2.7$mm, $w_2 = 2.9$mm, $h = 3$mm; and is placed in a way that the left side is of 2.7mm and the right side 2.9mm. $l_n \pm T$, the targeted testing range is set to be 2.95 ± 0.15mm; and Δ_0 is set to $l_n/5 = 0.59$(mm). e_s is set to 29 so that $\Delta_0/e_s \approx 0.0203$mm which is possible using the laser profile. 100 samples are obtained with uniform randomness, and $p_1 \approx 0.254$, $p_2 \approx 0.746$ for the P1+S case.

Table 5.11: SET5: Experiment records for validation for the tolerance range 3.0 ± 0.1mm with $\Delta_0 = 0.5$mm

ID	log ID	Gauge and Placement lft. (mm)	rt. (mm)	ht. (mm)	θ_n (rad)	θ_m (rad)	$K(\vec{n}, \vec{m})$	l_n (mm)	T (mm)	Δ_0	e_s	true value (S17) lft. (mm)	rt. (mm)	D14	$R_{100}^{(\text{left})}$	$R_{100}^{(\text{right})}$	in range? lft.	rt.	verified?
ENT103														0	$\{(5,87),(6,13)\}$	$\{(5,49),(6,51)\}$	y	n	Y
ENT104														1	$\{(5,88),(6,12)\}$	$\{(5,45),(6,55)\}$	y	n	Y
ENT105														2	$\{(5,91),(6,9)\}$	$\{(5,45),(6,55)\}$	y	n	Y
ENT106														3	$\{(5,91),(6,9)\}$	$\{(5,45),(6,55)\}$	y	n	Y
ENT107														4	$\{(5,87),(6,13)\}$	$\{(5,46),(6,54)\}$	y	n	Y
ENT108														5	$\{(5,82),(6,18)\}$	$\{(5,47),(6,53)\}$	y	n	Y
ENT109														6	$\{(5,87),(6,13)\}$	$\{(5,49),(6,51)\}$	y	n	Y
ENT110														7	$\{(5,90),(6,10)\}$	$\{(5,47),(6,53)\}$	y	n	Y
ENT111														8	$\{(5,92),(6,8)\}$	$\{(5,51),(6,49)\}$	y	n	Y
ENT112														9	$\{(5,90),(6,10)\}$	$\{(5,53),(6,47)\}$	y	n	Y
ENT113														10	$\{(5,92),(6,8)\}$	$\{(5,54),(6,46)\}$	y	n	Y
ENT114	F18111205	3.0	3.2	1	0.00286	0.00979	1.00004	3.0	0.1	0.5	24	avg 3.06	avg 3.25	11	$\{(5,88),(6,12)\}$	$\{(5,54),(6,46)\}$	y	n	Y
ENT115														12	$\{(5,89),(6,11)\}$	$\{(5,51),(6,49)\}$	y	n	Y
ENT116														13	$\{(5,91),(6,9)\}$	$\{(5,55),(6,45)\}$	y	n	Y
ENT117														14	$\{(5,90),(6,10)\}$	$\{(5,55),(6,45)\}$	y	n	Y
ENT118														15	$\{(5,93),(6,7)\}$	$\{(5,58),(6,42)\}$	y	n	Y
ENT119														16	$\{(5,91),(6,9)\}$	$\{(5,53),(6,47)\}$	y	n	Y
ENT120														17	$\{(5,87),(6,13)\}$	$\{(5,53),(6,47)\}$	y	n	Y
ENT121														18	$\{(5,87),(6,13)\}$	$\{(5,51),(6,49)\}$	y	n	Y
ENT122														19	$\{(5,89),(6,11)\}$	$\{(5,53),(6,47)\}$	y	n	Y
ENT123														20	$\{(5,93),(6,7)\}$	$\{(5,48),(6,52)\}$	y	n	Y
ENT124														21	$\{(5,93),(6,7)\}$	$\{(5,46),(6,54)\}$	y	n	Y
ENT125														22	$\{(5,93),(6,7)\}$	$\{(5,46),(6,54)\}$	y	n	Y
ENT126														23	$\{(5,88),(6,12)\}$	$\{(5,47),(6,53)\}$	y	n	Y

The detailed experiment output by PhDSampline is logged in F18111205, other related materials including scanned raw data can be found in the master log file by following records of F18111205. The gauge block used is of nominal dimension $w_1 = 3.0$mm, $w_2 = 3.2$mm, $h = 1$mm; and is placed in a way that the left side is of 3.0mm and the right side 3.2mm. $l_n \pm T$, the targeted testing range is set to be 3.0 ± 0.1mm; and Δ_0 is set to $l_n/6 = 0.5$(mm). e_s is set to 24 so that $\Delta_0/e_s \approx 0.0208$mm which is possible using the laser profile. 100 samples are obtained with uniform randomness, and $p_1 \approx 0.2$, $p_2 \approx 0.8$ for the P1+S case.

Table 5.12: SET6: Experiment records for validation for the tolerance range 3.0 ± 0.1mm with $\Delta_0 = 0.6$mm

ID	log ID	Gauge and Placement lft. (mm)	rt. (mm)	ht. (mm)	θ_n (rad)	θ_m (rad)	$K(\vec{n}, \vec{m})$	l_n (mm)	T (mm)	Δ_0	e_s	true value (S17) lft. (mm)	rt. (mm)	D14	$R_{100}^{(\text{left})}$	$R_{100}^{(\text{right})}$	in range? lft.	rt.	verified?
ENT127														0	$\{(4,89),(5,11)\}$	$\{(4,65),(5,35)\}$	y	n	Y
ENT128														1	$\{(4,88),(5,12)\}$	$\{(4,68),(5,32)\}$	y	n	Y
ENT129														2	$\{(4,85),(5,15)\}$	$\{(4,66),(5,34)\}$	y	n	Y
ENT130														3	$\{(4,91),(5,9)\}$	$\{(4,65),(5,35)\}$	y	n	Y
ENT131														4	$\{(4,91),(5,9)\}$	$\{(4,64),(5,36)\}$	y	n	Y
ENT132														5	$\{(4,90),(5,10)\}$	$\{(4,62),(5,38)\}$	y	n	Y
ENT133														6	$\{(4,90),(5,10)\}$	$\{(4,63),(5,37)\}$	y	n	Y
ENT134														7	$\{(4,90),(5,10)\}$	$\{(4,66),(5,34)\}$	y	n	Y
ENT135														8	$\{(4,92),(5,8)\}$	$\{(4,64),(5,36)\}$	y	n	Y
ENT136														9	$\{(4,93),(5,7)\}$	$\{(4,61),(5,39)\}$	y	n	Y
ENT137														10	$\{(4,93),(5,7)\}$	$\{(4,56),(5,44)\}$	y	n	Y
ENT138														11	$\{(4,90),(5,10)\}$	$\{(4,55),(5,45)\}$	y	n	Y
ENT139														12	$\{(4,90),(5,10)\}$	$\{(4,55),(5,45)\}$	y	n	Y
ENT140														13	$\{(4,92),(5,8)\}$	$\{(4,52),(5,48)\}$	y	n	Y
ENT141	F18111206	3.0	3.2	1	0.00287	0.00973	1.00004	3.0	0.1	0.6	29	avg 3.06	avg 3.25	14	$\{(4,94),(5,6)\}$	$\{(4,53),(5,47)\}$	y	n	Y
ENT142														15	$\{(4,97),(5,3)\}$	$\{(4,51),(5,49)\}$	y	n	Y
ENT143														16	$\{(4,95),(5,5)\}$	$\{(4,53),(5,47)\}$	y	n	Y
ENT144														17	$\{(4,94),(5,6)\}$	$\{(4,49),(5,51)\}$	y	n	Y
ENT145														18	$\{(4,93),(5,7)\}$	$\{(4,51),(5,49)\}$	y	n	Y
ENT146														19	$\{(4,95),(5,5)\}$	$\{(4,50),(5,50)\}$	y	n	Y
ENT147														20	$\{(4,92),(5,8)\}$	$\{(4,51),(5,49)\}$	y	n	Y
ENT148														21	$\{(4,91),(5,9)\}$	$\{(4,53),(5,47)\}$	y	n	Y
ENT149														22	$\{(4,92),(5,8)\}$	$\{(4,54),(5,46)\}$	y	n	Y
ENT150														23	$\{(4,94),(5,6)\}$	$\{(4,55),(5,45)\}$	y	n	Y
ENT151														24	$\{(4,93),(5,7)\}$	$\{(4,54),(5,46)\}$	y	n	Y
ENT152														25	$\{(4,91),(5,9)\}$	$\{(4,56),(5,44)\}$	y	n	Y
ENT153														26	$\{(4,91),(5,9)\}$	$\{(4,58),(5,42)\}$	y	n	Y
ENT154														27	$\{(4,92),(5,8)\}$	$\{(4,63),(5,37)\}$	y	n	Y
ENT155														28	$\{(4,92),(5,8)\}$	$\{(4,65),(5,35)\}$	y	n	Y

The detailed experiment output by PhDSampline is logged in F18111206, other related materials including scanned raw data can be found in the master log file by following records of F18111206. The gauge block used is of nominal dimension $w_1 = 3.0$mm, $w_2 = 3.2$mm, $h = 1$mm; and is placed in a way that the left side is of 3.0mm and the right side 3.2mm. $l_n \pm T$, the targeted testing range is set to be 3.0 ± 0.1mm; and Δ_0 is set to $l_n/5 = 0.6$(mm). e_s is set to 29 so that $\Delta_0/e_s \approx 0.0207$mm which is possible using the laser profile. 100 samples are obtained with uniform randomness, and $p_1 \approx 0.167$, $p_2 \approx 0.833$ for the P1+S case.

Table 5.13: SET7: Experiment records for validation for the tolerance range 3.04 ± 0.1mm with $\Delta_0 \approx 0.5067$mm

ID	log ID	Gauge and Placement lft. (mm)	rt. (mm)	ht. (mm)	θ_n (rad)	θ_m (rad)	$K(\vec{n},\vec{m})$	l_n (mm)	T (mm)	Δ_0	e_s	true value (S17) lft. (mm)	rt. (mm)	D14	$R^{(\text{left})}_{100}$	$R^{(\text{right})}_{100}$	in range? lft.	rt.	verified?
ENT156														0	$\{(4,5),(5,95)\}$	$\{(5,47),(6,53)\}$	y	n	Y
ENT157														1	$\{(4,6),(5,94)\}$	$\{(5,49),(6,51)\}$	y	n	Y
ENT158														2	$\{(4,5),(5,95)\}$	$\{(5,55),(6,45)\}$	y	n	Y
ENT159														3	$\{(4,5),(5,95)\}$	$\{(5,59),(6,41)\}$	y	n	Y
ENT160														4	$\{(4,1),(5,99)\}$	$\{(5,64),(6,36)\}$	y	n	Y
ENT161														5	$\{(4,2),(5,98)\}$	$\{(5,72),(6,28)\}$	y	n	Y
ENT162														6	$\{(4,4),(5,96)\}$	$\{(5,69),(6,31)\}$	y	n	Y
ENT163														7	$\{(4,7),(5,93)\}$	$\{(5,70),(6,30)\}$	y	n	Y
ENT164														8	$\{(4,2),(5,98)\}$	$\{(5,70),(6,30)\}$	y	n	Y
ENT165														9	$\{(4,10),(5,90)\}$	$\{(5,67),(6,33)\}$	y	n	Y
ENT166														10	$\{(4,7),(5,93)\}$	$\{(5,73),(6,27)\}$	y	n	Y
ENT167														11	$\{(4,7),(5,93)\}$	$\{(5,67),(6,33)\}$	y	n	Y
ENT168	F18111302	3.0	3.2	3	0.00261	0.00141	0.999998	3.04	0.1	0.5067	26	avg 3.02	avg 3.24	12	$\{(4,11),(5,89)\}$	$\{(5,64),(6,36)\}$	y	n	Y
ENT169														13	$\{(4,7),(5,93)\}$	$\{(5,65),(6,35)\}$	y	n	Y
ENT170														14	$\{(4,3),(5,97)\}$	$\{(5,64),(6,36)\}$	y	n	Y
ENT171														15	$\{(4,5),(5,95)\}$	$\{(5,64),(6,36)\}$	y	n	Y
ENT172														16	$\{(4,10),(5,90)\}$	$\{(5,66),(6,34)\}$	y	n	Y
ENT173														17	$\{(4,9),(5,91)\}$	$\{(5,62),(6,38)\}$	y	n	Y
ENT174														18	$\{(4,11),(5,89)\}$	$\{(5,58),(6,42)\}$	y	n	Y
ENT175														19	$\{(4,11),(5,89)\}$	$\{(5,58),(6,42)\}$	y	n	Y
ENT176														20	$\{(4,6),(5,94)\}$	$\{(5,55),(6,45)\}$	y	n	Y
ENT177														21	$\{(4,11),(5,89)\}$	$\{(5,55),(6,45)\}$	y	n	Y
ENT178														22	$\{(4,7),(5,93)\}$	$\{(5,56),(6,44)\}$	y	n	Y
ENT179														23	$\{(4,5),(5,95)\}$	$\{(5,54),(6,46)\}$	y	n	Y
ENT180														24	$\{(4,4),(5,96)\}$	$\{(5,52),(6,48)\}$	y	n	Y
ENT181														25	$\{(4,5),(5,95)\}$	$\{(5,49),(6,51)\}$	y	n	Y

The detailed experiment output by PhDSampline is logged in F18111302, other related materials including scanned raw data can be found in the master log file by following records of F18111302. The gauge block used is of nominal dimension $w_1 = 3.0$mm, $w_2 = 3.2$mm, $h = 3$mm; and is placed in a way that the left side is of 3.0mm and the right side 3.2mm. $l_n \pm T$, the targeted testing range is set to be 3.04 ± 0.1mm; and Δ_0 is set to $l_n/6 \approx 0.5067$(mm). e_s is set to 26 so that $\Delta_0/e_s \approx 0.0195$mm which is possible using the laser profile. 100 samples are obtained with uniform randomness, and $p_1 \approx 0.197$, $p_2 \approx 0.803$ for the P1+S case.

Table 5.14: SET8: Experiment records for validation for the tolerance range 3.25 ± 0.15mm with $\Delta_0 = 0.65$mm

ID	log ID	Gauge and Placement			θ_n (rad)	θ_m (rad)	$K(\vec{n}, \vec{m})$	l_n (mm)	T (mm)	Δ_0	e_s	true value (S17)		D14	$R_{100}^{(\text{left})}$	$R_{100}^{(\text{right})}$	in range?		verified?
		lft. (mm)	rt. (mm)	ht. (mm)								lft. (mm)	rt. (mm)				lft.	rt.	
ENT182														0	$\{(3,37),(4,63)\}$	$\{(3,1),(4,99)\}$	n	y	Y
ENT183														1	$\{(3,39),(4,61)\}$	$\{(3,1),(4,96),(5,3)\}$	n	y	Y
ENT184														2	$\{(3,38),(4,62)\}$	$\{(3,1),(4,98),(5,1)\}$	n	y	Y
ENT185														3	$\{(3,41),(4,59)\}$	$\{(3,1),(4,98),(5,1)\}$	n	y	Y
ENT186														4	$\{(3,42),(4,58)\}$	$\{(3,2),(4,98)\}$	n	y	Y
ENT187														5	$\{(3,42),(4,58)\}$	$\{(3,3),(4,97)\}$	n	y	Y
ENT188														6	$\{(3,40),(4,60)\}$	$\{(4,97),(5,3)\}$	n	y	Y
ENT189														7	$\{(3,40),(4,60)\}$	$\{(3,2),(4,98)\}$	n	y	Y
ENT190														8	$\{(3,45),(4,55)\}$	$\{(3,2),(4,96),(5,2)\}$	n	y	Y
ENT191														9	$\{(3,47),(4,53)\}$	$\{(3,1),(4,99)\}$	n	y	Y
ENT192														10	$\{(3,47),(4,53)\}$	$\{(3,2),(4,97),(5,1)\}$	n	y	Y
ENT193														11	$\{(3,46),(4,54)\}$	$\{(3,3),(4,97)\}$	n	y	Y
ENT194														12	$\{(3,51),(4,49)\}$	$\{(3,4),(4,94),(5,2)\}$	n	y	Y
ENT195														13	$\{(3,50),(4,50)\}$	$\{(3,4),(4,95),(5,1)\}$	n	y	Y
ENT196														14	$\{(3,53),(4,47)\}$	$\{(3,2),(4,98)\}$	n	y	Y
ENT197	F18111402	3.0	3.2	3	0.00354	0.01524	1.00011	3.25	0.15	0.65	31	avg 2.96	avg 3.24	15	$\{(3,51),(4,49)\}$	$\{(3,1),(4,99)\}$	n	y	Y
ENT198														16	$\{(3,57),(4,43)\}$	$\{(3,4),(4,96)\}$	n	y	Y
ENT199														17	$\{(3,58),(4,42)\}$	$\{(3,1),(4,97),(5,2)\}$	n	y	Y
ENT200														18	$\{(3,54),(4,46)\}$	$\{(3,1),(4,99)\}$	n	y	Y
ENT201														19	$\{(3,52),(4,48)\}$	$\{(3,3),(4,97)\}$	n	y	Y
ENT202														20	$\{(3,52),(4,48)\}$	$\{(3,2),(4,98)\}$	n	y	Y
ENT203														21	$\{(3,49),(4,51)\}$	$\{(3,1),(4,97),(5,2)\}$	n	y	Y
ENT204														22	$\{(3,50),(4,50)\}$	$\{(3,1),(4,98),(5,1)\}$	n	y	Y
ENT205														23	$\{(3,48),(4,52)\}$	$\{(3,1),(4,99)\}$	n	y	Y
ENT206														24	$\{(3,49),(4,51)\}$	$\{(4,100)\}$	n	y	Y
ENT207														25	$\{(3,49),(4,51)\}$	$\{(3,1),(4,99)\}$	n	y	Y
ENT208														26	$\{(3,45),(4,55)\}$	$\{(3,2),(4,98)\}$	n	y	Y
ENT209														27	$\{(3,45),(4,55)\}$	$\{(3,1),(4,99)\}$	n	y	Y
ENT210														28	$\{(3,46),(4,54)\}$	$\{(3,3),(4,96),(5,1)\}$	n	y	Y
ENT211														29	$\{(3,44),(4,56)\}$	$\{(4,99),(5,1)\}$	n	y	Y
ENT212														30	$\{(3,37),(4,63)\}$	$\{(3,1),(4,99)\}$	n	y	Y

The detailed experiment output by PhDSampline is logged in F18111402, other related materials including scanned raw data can be found in the master log file by following records of F18111402. The gauge block used is of nominal dimension $w_1 = 3.0$mm, $w_2 = 3.2$mm, $h = 3$mm; and is placed in a way that the left side is of 3.0mm and the right side 3.2mm. $l_n \pm T$, the targeted testing range is set to be 3.25 ± 0.15mm; and Δ_0 is set to $l_n/5 = 0.65$(mm). e_s is set to 31 so that $\Delta_0/e_s \approx 0.0210$mm which is possible using the laser profile. 100 samples are obtained with uniform randomness, and $p_1 \approx 0.231$, $p_2 \approx 0.769$ for the P1+S case.

6 Conclusions and Discussions

As the final chapter of the thesis, concluding comments on PBM and remarks on the potential for future works are made. The first section summarizes the thesis, including a quick review of PBM as well as other validated discoveries. Comments on the limitations are also included in this section. The validation of feasibility conducted in chapter 5 utilized a laser profiler and a 3-axis gantry system; however this is only one of the many possible scenarios where PBM can be applied. In the second section, there are comments on possible alternative implementations of PBM for future work. Scattered over previous chapters, there are interesting theoretical topics and findings in experiments that deserve more in-depth discussion. These topics also set a good starting point for future research and will be summarized in the last section of this chapter in the hope that they will provide help to future researchers.

6.1 Conclusions, Contributions and Limitations

The thesis proposed a probability-based measurement method, established and proved the theory mathematically, and then justified the validity and feasibility on a laboratory set up. The contribution is clearly shown by solving Problem 3.1 (defined on page 24), where the scale of ruler is larger than the tolerance range to be checked. Indeed, in the series of validation experiments in chapter 5, Δ, the scale of ruler, was intentionally set to be more than twice of the difference of the measurands; nevertheless, the results clearly prove the effectiveness of the new method. From a theoretic perspective, PBM utilizes probability as indicators. A jump of p_h from 0 to 1 indicates that the measurand is very close to integral multiples of the current Δ. Traditionally, this phenomenon of being close to scale marks — measurand being an integral multiple of scale — was judged by bare eyes or other means rather than using probabilities.

The probability-based method does not rely on the alignment of ends of measurands, and all the theoretic analysis is developed on this fact. This frees people from designing complicated fixtures for different samples, tedious procedures of aligning or finding certain starting points for measurement. It also sheds light on scenarios where alignment of the sample is hardly possible. Without the information of alignment, multiple random samplings are required; and this can somehow be regarded as a "fair trade" for a general measurement. Theorem. 3.1 and Example. 3.6 serve as negative answers to the question that asks if simply averaging the sampled data would be enough for

measurement. PBM covers these scenarios. The discussions made in chapter 4 are for pragmatic applications. The topics are carefully chosen and they cover more than the laboratory set up used for validation. It is expected that these discussions could provide help in future designs and implementations.

One obvious limitation of the PBM approach presented in this thesis is that it does not work for measurands smaller than the pixel resolution of the ruler. As a concrete example, the discussion on PBM in thesis does not give an answer to Problem 3.1 (defined on page 24) if the line segment in is claimed to be within 1 ± 0.4mm. Because in such cases, full scales do not exist. In practice, one should expect help from engineering works and other subsystems, for example, lens systems to magnify the measurands in sampled images.

6.2 Other Implementations for Future Work

The implementation of PBM for validation in this thesis uses a device created for an EU project, where the trapezoidal effective scanning area of the laser profiler together with the motion of the 3-axis gantry make adjustable scale feasible. There are other possible situations where PBM can be applied. A pin hole camera (Fig. 3.1) or any projective camera is capable of providing an adjustable scale once they are attached to a gantry system. Suppose there is an effective algorithm identifying the points from the area of interest, like the points on the "top surface" of the extrusion, then all discussions in chapter 4 hold true and PBM is applicable to the scenario. Instead of relying on an external gantry system for motion, manipulation of a lens system can be conducted to adjust the magnification. In this case, adjacent pixels will represent different spacial distance. This situation is commonly seen in microscopes.

In this thesis, the measurands are extracted using the height coordinates which are from the laser profiler using the triangulation method. Depending on the application and device, various methods can be used to extract the feature of interest. For example, the silhouette produced by diffuse backlight illuminators can be used to measure dimensions of boundaries. With adjustable magnification, the probability-based approach should be applicable. Equation (2.8) indicates that the camera model used in triangulation measurements is rational polynomial [HS97a]. Proper rational polynomial camera (RPC) models encode 3D coordinates into 2D images and reconstruction

can be conducted for certain scenarios [HS97b]. It indicates a potential for application of PBM to systems of this kind, for example, satellite imaging with RPC systems [GD03].

The randomness of sampling in the validations of this thesis is induced by random shifts alongside the y-axis. The amount of the random displacement along the y-axis was determined by pseudo-randomness algorithms. In many real world cases, instead of synthetic randomness of this kind, vibration and other disturbance can be used as sources of randomness. Many measurement and machining systems today utilize an external stabilizer to cancel vibration; if the pattern of vibration is well-studied, its induced impact on δ can be calculated.

6.3 Other Theoretic and Practical Considerations for Future Work

In this section, some of the theoretical topics are presented in the hope of setting up starting points for future researches on this probability-based method. These topics are either hints revealing deeper facts behind the scattered discoveries presented in the previous chapters or thoughts inspired by the practice of validation which potentially improve future implementation of PBM. These contents are not presented in previous chapters for various reasons. For example, some of them are not closely relevant to the content of this thesis in the sense of discussing situations away from Problem 3.1, some of them incline too much towards the engineering practice and are considered to be improper to be put in previous chapters. Although early works has been conducted, these topics are still distant from being complete.

6.3.1 Estimation Using Result Sets

One might have noticed that, unlike the nominal length l_n, T the tolerance range is irrelevant to the measurement process. Result sets R_M can be obtained once $\Delta_0 = l_n/N$ is specified, and then f_h, the frequency of the high readings. Assume M is sufficiently large and f_h approximates p_h satisfactorily. Then as discussed in subsection 3.3.5, f_h is compared against p_1 and p_2 to test whether the true value l_t is within $l_n \pm T$. As a reminder, p_1 and p_2 are computed as

$$p_1 = p_h(\Delta_0, l_n + T) \qquad\qquad p_2 = p_h(\Delta_0, l_n - T).$$

Table 6.1: Comparison of true value estimation using result sets and direct measure on the left extrusion of `F18111206` (Table. 5.11): **[a]** estimation using the 29 result sets; **[b]** results of direct measure using `actualWidths`

frequency	T_m(mm)	$T_m + l_n$(mm)
1	0.018	3.018
2	0.030	3.030
3	0.036	3.036
4	0.042	3.042
6	0.048	3.048
5	0.054	3.054
5	0.060	3.060
1	0.066	3.066
1	0.072	3.072
1	0.090	3.090

[a]

frequency	length (mm)	corrected (mm)
4	3.00	3.02
1	3.01	3.03
32	3.02	3.04
21	3.03	3.05
28	3.04	3.06
11	3.05	3.07
1	3.06	3.08
2	3.07	3.09

[b]

Instead of fixing T from the beginning, one may solve

$$p_h(\Delta_0, l_n + T) = f_h \tag{6.1}$$

for the smallest T if f_h is near 0, or

$$p_h(\Delta_0, l_n - T) = f_h \tag{6.2}$$

if f_h is near 1. Theoretically, this $l_n + T$ or $l_n - T$ will be l_t, and empirically close to l_n. Denote the solution to (6.1) or (6.2) by T_m. Using data from Table. 5.11, the computed T_m and measured true values are illustrated in Table 6.1[a][b]. Direction comparison shows consistency in the variation range of the results and the extreme values. The consistency of data also indicates that the probability-based measurement method can be integrated into the probability framework ([SA96][Ros14]).

6.3.2 Joint Distribution of $(\delta, \mathfrak{l})$

The discussion of randomness has widened from δ to l_t, the measurand, since chapter 4. It has been seen for many scenarios where l_t is better to be treated as a random variable $\mathfrak{l}$. For example, under external turbulence the state of the measurand might be constantly changing. Even in a stationary, perfect environment, mis-alignments will cause discrete randomness behavior of $\mathfrak{l}$ and this has been discussed in 4.2 of chapter 4.

Let $h_\Delta(x, y)$ be the probability density function of the random vector $(\delta, \mathfrak{l})$, where $0 \leq \delta < \Delta$ and $\underline{l} \leq \mathfrak{l} \leq \bar{l}$. For simplicity, assume that $h_\Delta(x, y)$ is induced by a

compactly supported smooth function $H_\Delta(x,y)$ on $\mathbb{R}^2$, that is, $h_\Delta \equiv H$ on the area $[0,\Delta)\times[\underline{l},\bar{l}]$. Then the possible values of the number of full scales are described by equation (4.6), and as a reminder

$$\left\{\lfloor\frac{\mathfrak{l}-\delta}{\Delta}\rfloor|\mathfrak{l}\in[\underline{l},\bar{l}],\delta\in[0,\Delta)\right\}=\left\{\lfloor\frac{\mathfrak{l}}{\Delta}\rfloor|\mathfrak{l}\in[\underline{l},\bar{l}]\right\}\cup\left\{\lfloor\frac{\mathfrak{l}}{\Delta}\rfloor-1|\mathfrak{l}\in[\underline{l},\bar{l}]\right\}.$$

This means that instead of high and low readings, there are cases where result sets are supported on three or more points. Restricting to the case that $\bar{l}-\underline{l}<\Delta$, then for Δ in the interval of Type I, the high and low readings can be defined. Define areas

$$\begin{aligned}\overline{\triangle}_N(\Delta)&=\{(x,y)|y-x\geq N\Delta,\Delta>x\geq 0,y<(N+1)\Delta\}\\ \underline{\triangle}_N(\Delta)&=\{(x,y)|y-x<N\Delta,\Delta>x\geq 0,y\geq N\Delta\}\\ \mathfrak{R}(\Delta)&=\{(x,y)|0\leq x<\Delta,\underline{l}\leq y\leq\bar{l}\}\end{aligned}$$

then for $\Delta\in(\underline{\iota}_N,\bar{\iota}_N]$, it holds

$$p_h(\Delta,\mathfrak{l})=\int_{\mathfrak{R}(\Delta)\cap\overline{\triangle}_N(\Delta)}h_\Delta(x,y)\,\mathrm{d}x\,\mathrm{d}y+\int_{\mathfrak{R}(\Delta)\cap\underline{\triangle}_{N+1}(\Delta)}h_\Delta(x,y)\,\mathrm{d}x\,\mathrm{d}y.$$

And the following proposition on continuity of p_h can be proven.

Proposition 6.1. *If $\Delta\mapsto H_\Delta(x,y)$ is continuous as a mapping from $\mathbb{R}_+$ to $L^1(\mathbb{R}^2,\mu_L)$ and $|H_\Delta|\leq M$ for all Δ, then $p_h(\Delta,\mathfrak{l})$ is continuous as a function of Δ on $(\underline{\iota}_N,\bar{\iota}_N]$.*

Proof. It is enough to prove that the two parts of $p_h(\Delta,\mathfrak{l})$

$$\begin{aligned}F(\Delta)&=\int_{\mathfrak{R}(\Delta)\cap\overline{\triangle}_N(\Delta)}h_\Delta(x,y)\,\mathrm{d}x\,\mathrm{d}y\\ G(\Delta)&=\int_{\mathfrak{R}(\Delta)\cap\underline{\triangle}_{N+1}(\Delta)}h_\Delta(x,y)\,\mathrm{d}x\,\mathrm{d}y\end{aligned}$$

are continuous. Show the continuity of $G(\Delta)$ as an example. For arbitrary Δ_1,Δ_2 with

Δ_2 being close to D_1, it holds

$$
\begin{aligned}
&|G(\Delta_1) - G(\Delta_2)| \\
=& \left| \int_{\Re(\Delta_1)\cap\triangleq_{N+1}(\Delta_1)} H_{\Delta_1}(x,y)\,\mathrm{d}x\,\mathrm{d}y - \int_{\Re(\Delta_2)\cap\triangleq_{N+1}(\Delta_2)} H_{\Delta_2}(x,y)\,\mathrm{d}x\,\mathrm{d}y \right| \\
\leq& \left| \int_{(\Re(\Delta_1)\cap\triangleq_{N+1}(\Delta_1))\cap(\Re(\Delta_2)\cap\triangleq_{N+1}(\Delta_2))} H_{\Delta_1}(x,y) - H_{\Delta_2}(x,y)\,\mathrm{d}x\,\mathrm{d}y \right| \\
&+ \left| \int_{(\Re(\Delta_1)\cap\triangleq_{N+1}(\Delta_1))\setminus(\Re(\Delta_2)\cap\triangleq_{N+1}(\Delta_2))} H_{\Delta_1}(x,y)\,\mathrm{d}x\,\mathrm{d}y \right| \\
&+ \left| \int_{(\Re(\Delta_2)\cap\triangleq_{N+1}(\Delta_2))\setminus(\Re(\Delta_1)\cap\triangleq_{N+1}(\Delta_1))} H_{\Delta_2}(x,y)\,\mathrm{d}x\,\mathrm{d}y \right| \\
\leq& \int_{\mathbb{R}^2} |H_{\Delta_1} - H_{\Delta_2}|\,\mathrm{d}x\,\mathrm{d}y + M \int_{(\Re(\Delta_1)\cap\triangleq_{N+1}(\Delta_1))\setminus(\Re(\Delta_2)\cap\triangleq_{N+1}(\Delta_2))} \mathrm{d}x\,\mathrm{d}y \\
&+ M \int_{(\Re(\Delta_2)\cap\triangleq_{N+1}(\Delta_2))\setminus(\Re(\Delta_1)\cap\triangleq_{N+1}(\Delta_1))} \mathrm{d}x\,\mathrm{d}y.
\end{aligned}
$$

By the continuity of $\Delta \mapsto H_\Delta$, $|G(\Delta_1) - G(\Delta_2)| \to 0$ as $\Delta_2 \to \Delta_1$. Similarly one can prove the continuity of $F(\Delta)$ and hence the continuity of $p_h(\Delta, \mathfrak{l})$ follows. □

This proposition states a fact that has been discovered in chapter 4. That is, p_h is continuous on Type I intervals. Although the conclusions are identical, the assumptions behind the scenes are different. The joint distribution of δ and $\mathfrak{l}$ in chapter 4 is discrete in $\mathfrak{l}$, while the joint distribution here is absolutely continuous with respect to the Lebesgue measure. Future work should therefore be developed on the basis of joint distributions of $\delta, \mathfrak{l}$ that unifies these discussions meaningfully.

6.3.3 2D Cases

One of the fundamental assumptions made in Problem 3.1 (on page 24) is that one holds a ruler with adjustable scales. It makes sense to ask what happens if one has a planar grid ruler with adjustable scales on two orthogonal directions. A rasterized image grabber with a lens system is an equipment of this kind. Although the thesis intentionally restricts the discussion to the one dimensional case, so far there is no evidence preventing the probability-based method to be applied to 2D cases. One question for the 2D cases is about randomness. Should the sample be completely randomly thrown into the view of the measurement system like Hall did in [Hal73], or only make randomly

translation to the measurement system? In the former case, the obvious random variables are $(\delta_x, \delta_y, \theta)$, where δ_x, δ_y are similarly defined as δ and θ represents the random angular discrepancy of the sample to some fixed direction; and in the latter case, only (δ_x, δ_y) are involved. It is reasonable to expect more interesting results in 2D cases, not only because there are two rulers on orthogonal directions but also the fact that many existing pattern recognition algorithms for images might be helpful identifying the features on the measurand.

References

[AD74] J. H. Ahrens and U. Dieter. “Computer methods for sampling from gamma, beta, poisson and bionomial distributions”. In: *Computing* 12.3 (Sept. 1, 1974), pp. 223–246.

[Ada65] Ernest W. Adams. “Elements of a Theory of Inexact Measurement”. In: *Philosophy of Science* 32.3/4 (1965), pp. 205–228.

[AL06] Krishna B Athreya and Soumendra N Lahiri. *Measure theory and probability theory*. Springer Science & Business Media, 2006.

[BH69] Robert E. Brooks and Lee O. Heflinger. “Moiré Gauging Using Optical Interference Patterns”. In: *Appl. Opt.* 8.5 (May 1969), pp. 935–939.

[BIP+08] BIPM et al. “Evaluation of measurement data—guide for the expression of uncertainty in measurement. JCGM 100: 2008”. In: *Citado en las* (2008), p. 167.

[BIP+09] BIPM et al. “The 2007 International Vocabulary of Metrology (VIM), JCGM 200: 2008 [ISO/IEC Guide 99]: Meeting the need for intercontinentally understood concepts and their associated intercontinentally agreed terms”. In: *Clinical biochemistry* 42.4 (2009), pp. 246–248.

[BIP06] BIPM. *The International System of Units (SI brochure (EN)): 8th edition*. 2006.

[Cam40] Norman Robert Campbell. “Final report, Committee of the British Association for Advancement of Science on the problem of measurement”. In: *London: British Association* (1940).

[Cam57] Norman Robert Campbell. *Physics the Elements, 1920; reprinted as Foundations of Science*. Cambridge University Press, 1957.

[Car66] Rudolf Carnap. *Philosophical foundations of physics*. Vol. 966. Basic Books New York, 1966.

[CB80] CIPM and BIPM. *Report on the BIPM enquiry on error statements*. Mar. 1980.

[CBW73] P. J. Campion, J. E. Burns, and A. Williams. *Code of practice for the detailed statement of accuracy*. Her Majesty's Stationery Office, Jan. 1973.

[CL96] Jenq Shyong Chen and Cheng Chang Ling. “Improving the machine accuracy through machine tool metrology and error correction”. In: *The International Journal of Advanced Manufacturing Technology* 11.3 (May 1, 1996), pp. 198–205.

[Cox+08] Maurice G Cox et al. “A probabilistic approach to the analysis of measurement processes”. In: *Metrologia* 45.5 (2008), p. 493.

[CSS11] Horst Czichos, Tetsuya Saito, and Leslie E Smith. *Springer handbook of metrology and testing*. Springer Science & Business Media, 2011.

[DB08] Richard C. Dorf and Robert H. Bishop. *Modern Control Systems*. Eleventh Edition. Addison-wesley, 2008.

[DC01] J. Davis and Xing Chen. "A laser range scanner designed for minimum calibration complexity". In: *3-D Digital Imaging and Modeling, 2001. Proceedings. Third International Conference on*. 2001, pp. 91–98.

[Deb58] Gerard Debreu. "Stochastic Choice and Cardinal Utility". In: *Econometrica* 26.3 (1958), pp. 440–444.

[DG81] Paolo Dufour and Roberto Groppetti. "Computer Aided Accuracy Improvement in Large NC Machine Tools". In: *Proceedings of the Twenty-First International Machine Tool Design and Research Conference*. Ed. by J. M. Alexander. London: Macmillan Education UK, 1981, pp. 611–618.

[DG94] Leslie Deck and Peter de Groot. "High-speed noncontact profiler based on scanning white-light interferometry". In: *Appl. Opt.* 33.31 (Nov. 1994), pp. 7334–7338.

[Dil87] Oswald Ashton Wentworth Dilke. *Mathematics and Measurement (Reading the Past, Vol. 2)*. University of California Press, 1987.

[DIN95] DIN. *Basic concepts in metrology - General concepts*. Tech. rep. DIN Deutsches Institut für Normung e.V., Berlin, 1995.

[Ete81] N. Etemadi. "An elementary proof of the strong law of large numbers". In: *Zeitschrift für Wahrscheinlichkeitstheorie und Verwandte Gebiete* 55.1 (Feb. 1, 1981), pp. 119–122.

[Eva89] Chris Evans. *Precision engineering: an Evolutionary View*. Cranfield University Press, 1989.

[Fal02] Jean-Claude Falmagne. *Elements of Psychophysical Theory (Oxford Psychology Series)*. Oxford University Press, 2002.

[Fal76] Jean-Claude Falmagne. "Random conjoint measurement and loudness summation." In: *Psychological Review* 83.1 (1976), pp. 65–79.

[Fal80] Jean-Claude Falmagne. "A Probabilistic Theory of Extensive Measurement". In: *Philosophy of Science* 47.2 (1980), pp. 277–296.

[Fan97] K-C Fan. "A non-contact automatic measurement for free-form surface profiles". In: *Computer Integrated Manufacturing Systems* 10.4 (1997), pp. 277–285.

[Fei91] Yetai Fei. *Error Theory and Data Processing - (5th Edition)*. Machinery, 1991.

[FL86] Placid M. Ferreira and C.Richard Liu. "An analytical quadratic model for the geometric error of a machine tool". In: *Journal of Manufacturing Systems* 5.1 (1986), pp. 51–63.

[Fra15] Jacob Fraden. *Handbook of Modern Sensors: Physics, Designs, and Applications*. Springer, 2015.

[Gal05a] Inc. Galil Motion Control. *DMC-21x2/21x3 Manual Rev. 1.0e*. Tech. rep. Galil Motion Control, Inc., 2005.

[Gal05b] Inc. Galil Motion Control. *Optima/Econo DMC-2xxx Series, Command Reference Manual Rev. 1.0p*. Tech. rep. Galil Motion Control, Inc., 2005.

[Gam+94] Erich Gamma et al. *Design Patterns: Elements of Reusable Object-Oriented Software*. Addison-Wesley Professional, 1994.

[Gao+08] Feng Gao et al. "Surface measurement errors using commercial scanning white light interferometers". In: *Measurement Science and Technology* 19.1 (2008), p. 015303.

[GD03] Jacek Grodecki and Gene Dial. "Block Adjustment of High-Resolution Satellite Images Described by Rational Polynomials". In: *Photogrammetric Engineering & Remote Sensing* 69.1 (2003), pp. 59–68.

[Gol+11] Joseph Goldstein et al. *Scanning Electron Microscopy and X-Ray Microanalysis: A Text for Biologists, Materials Scientists, and Geologists*. Springer, 2011.

[GS71] Philip Babcock Gove and Merriam-Webster Editorial Staff, eds. *Webster's third new international dictionary of the English language, unabridged*. G. & C. Merriam Co, 1971.

[GTJ13] Feng Gao, Dawei Tang, and Xiang Jiang. "White Light Spectral Interferometry for Real Time Surface Profile Measurement". Nov. 2013.

[Hal14] Paul R. Halmos. *Measure Theory (Graduate Texts in Mathematics)*. Springer, 2014.

[Hal73] Asaph Hall. "On an experimental determination of π". In: *Messeng. Math* 2 (1873), pp. 113–114.

[Har16] Kevin Harding, ed. *Handbook of Optical Dimensional Metrology (Series in Optics and Optoelectronics)*. CRC Press, 2016.

[Har93] Richard I Hartley. "Camera calibration using line correspondences". In: *Proc. DARPA Image Understanding Workshop*. 1993, pp. 361–366.

[Har95] Richard I. Hartley. "A linear method for reconstruction from lines and points". In: *Proceedings of IEEE International Conference on Computer Vision*. June 1995, pp. 882–887.

[Hec16] Eugene Hecht. *Optics, Global Edition*. Pearson Higher Education, 2016.

[Hel87] H von Helmholtz. "An epistemological analysis of counting and measurement". In: *Selected Writings of Hermann von Helmholtz, Wesleyan University Press, Connecticut* (1887).

[Hoc+77] R Hocken et al. "Three dimensional metrology". In: *Annals of the CIRP* 26.2 (1977), pp. 403–408.

[Höl01] O. Hölder. "Die Axiome der Quantität und die Lehre vom Maß". In: *Ber. Verh. Sächs. Akad. Wiss. Leipzig Math. Phys. Kl.* 53 (1901), pp. 1–64.

[How+08] Preben Howarth et al. ""metrology--in short" 3rd edition". In: *EURAMET project* 1011 (2008).

[HS97a] Richard I Hartley and Tushar Saxena. “The cubic rational polynomial camera model”. In: *Image Understanding Workshop*. Vol. 649. 1997, p. 653.

[HS97b] Richard I Hartley and Peter Sturm. “Triangulation”. In: *Computer vision and image understanding* 68.2 (1997), pp. 146–157.

[HW07] Y.Y. Hsu and S.S. Wang. “A new compensation method for geometry errors of five-axis machine tools”. In: *International Journal of Machine Tools and Manufacture* 47.2 (2007), pp. 352–360.

[IEEE754] “IEEE Standard for Floating-Point Arithmetic”. In: *IEEE Std 754-2008* (Aug. 2008), pp. 1–70.

[ISO230-1] ISO. *Test code for machine tools - Part 1: Geometric accuracy of machines operating under no-load or quasi-static conditions*. Standard. Geneva, CH: International Organization for Standardization, 2012.

[ISO24153] BS ISO. *Random sampling and randomization procedures*. Standard. Geneva, CH: International Organization for Standardization, 2009.

[ISO28640] ISO. *Random variate generation methods*. Standard. Geneva, CH: International Organization for Standardization, 2010.

[ISO3534-1] ISO. *Statistics - Vocabulary and symbols - Part 1: General statistical terms and temrs used in probability*. ISO 3534-1: 2006. Geneva, Switzerland: International Organization for Standardization, 2006.

[ISO5807] ISO. *Information processing - Documentation symbols and conventions for data, program and system flowcharts, program network charts and system resources charts*. Standard. Geneva, CH: International Organization for Standardization, 1985.

[ISO98-1] ISO. *Uncertainty of measurement -- Part 1: Introduction to the expression of uncertainty in measurement*. ISO 98-1: 2009. Geneva, Switzerland: International Organization for Standardization, 2009.

[Jac05] Karsten Jacobsen. “High resolution satellite imaging systems-an overview”. In: *Photogrammetrie Fernerkundung Geoinformation* 2005.6 (2005), p. 487.

[Jia+10] Xiangqian Jiang et al. “Fast surface measurement using wavelength scanning interferometry with compensation of environmental noise”. In: *Appl. Opt.* 49.15 (May 2010), pp. 2903–2909.

[JISZ9031] JIS. *Procedure for random number generation and randomization*. Standard. Japanese Industrial Standards Committee, 2012.

[Kal60] Rudolph Emil Kalman. “A new approach to linear filtering and prediction problems”. In: *Journal of basic Engineering* 82.1 (1960), pp. 35–45.

[KC90] Gordon S. Kino and Stanley S. C. Chim. “Mirau correlation microscope”. In: *Appl. Opt.* 29.26 (Sept. 1990), pp. 3775–3783.

[KF93] V. Kiridena and P.M. Ferreira. “Mapping the effects of positioning errors on the volumetric accuracy of five-axis CNC machine tools”. In: *International Journal of Machine Tools and Manufacture* 33.3 (1993), pp. 417–437.

[KIN86] Hisao Kikuta, Koichi Iwata, and Ryo Nagata. “Distance measurement by the wavelength shift of laser diode light”. In: *Appl. Opt.* 25.17 (Sept. 1986), pp. 2976–2980.

[Knu97] Donald E. Knuth. *Art of Computer Programming, Volume 2: Seminumerical Algorithms (3rd Edition)*. Addison-Wesley Professional, 1997.

[Kor+97] Y.E. Korchev et al. “Scanning ion conductance microscopy of living cells”. In: *Biophysical Journal* 73.2 (1997), pp. 653–658.

[KSL71] David H Krantz, Patrick Suppes, and Robert Duncan Luce. *Foundations of measurement: Additive and Polynomial Representation*. Vol. 1. Academic Press, 1971.

[Kun+05] H. Kunzmann et al. “Productive Metrology - Adding Value to Manufacture”. In: *CIRP Annals* 54.2 (2005), pp. 155–168.

[KY97] Susumu Kuwamura and Ichirou Yamaguchi. “Wavelength scanning profilometry for real-time surface shape measurement”. In: *Appl. Opt.* 36.19 (July 1997), pp. 4473–4482.

[LE93] P.D. Lin and K.F. Ehmann. “Direct volumetric error evaluation for multi-axis machines”. In: *International Journal of Machine Tools and Manufacture* 33.5 (1993), pp. 675–693.

[Lew07] Mark Edward Lewis. *The Early Chinese Empires: Qin and Han (History of Imperial China)*. Belknap Press of Harvard University Press, 2007.

[Lir02] I Lira. *Evaluating the Measurement Uncertainty: Fundamentals and Practical Guidance (Series in Measurement Science and Technology)*. CRC Press, 2002.

[LS03] Y. Lin and Y. Shen. “Modelling of Five-Axis Machine Tool Metrology Models Using the Matrix Summation Approach”. In: *The International Journal of Advanced Manufacturing Technology* 21.4 (Feb. 1, 2003), pp. 243–248.

[LS90] Byron S. Lee and Timothy C. Strand. “Profilometry with a coherence scanning microscope”. In: *Appl. Opt.* 29.26 (Sept. 1990), pp. 3784–3788.

[Luc56] R. Duncan Luce. “Semiorders and a Theory of Utility Discrimination”. In: *Econometrica* 24.2 (1956), pp. 178–191.

[Mar05] Luca Mari. “The problem of foundations of measurement”. In: *Measurement* 38.4 (2005). The logical and philosophical aspects of measurement, pp. 259–266.

[Mat86] Hirokazu Matsumoto. “Synthetic interferometric distance-measuring system using a CO2 laser”. In: *Appl. Opt.* 25.4 (Feb. 1986), pp. 493–498.

[ME96] Joel Michell and Catherine Ernst. “The Axioms of Quantity and the Theory of Measurement: Translated from Part I of Otto Hölder's German Text “Die Axiome der Quantität und die Lehre vom Mass””. In: *Journal of Mathematical Psychology* 40.3 (1996), pp. 235–252.

[Mei+09] K Meiners-Hagen et al. “Multi-wavelength interferometry for length measurements using diode lasers”. In: *Measurement Science Review* 9.1 (2009), pp. 16–26.

[Mic04] Joel Michell. “History and Philosophy of Measurement: A Realist View”. In: *10th IMEKO TC7 International Symposium* (2004).

[Mic05] Joel Michell. “The logic of measurement: A realist overview”. In: *Measurement* 38.4 (2005). The logical and philosophical aspects of measurement, pp. 285–294.

[Mic18] Micro-Epsilon, ed. *Catalogue scanCONTROL*. 2018.

[Mic93] Joel Michell. “The origins of the representational theory of measurement: Helmholtz, Hölder, and Russell”. In: *Studies in History and Philosophy of Science Part A* 24.2 (1993), pp. 185–206.

[MM05] K. W. Morton and D. F. Mayers. *Numerical Solution of Partial Differential Equations: An Introduction*. Cambridge University Press, 2005.

[MR95] R.C. Michelini and G.B. Rossi. “Measurement uncertainty: A probabilistic theory for intensive entities”. In: *Measurement* 15.3 (1995), pp. 143–157.

[MS05] Zacarias Malacara and Manuel Servín. *Interferogram Analysis For Optical Testing, Second Edition (Optical Engineering)*. CRC Press, 2005.

[Muh13] Hussam Muhamedsalih. “Investigation of Wavelength Scanning Interferometry for Embedded Metrology”. May 2013.

[NH31] Ernest Nagel and C. G. Hempel. “Measurement”. In: *Erkenntnis* 2.1 (Dec. 1, 1931), pp. 313–335.

[NK17] *RT-5 Series Rotary Stage*. Tech. rep. Newmark Systems Inc., 2017.

[NP17] *XM Series Ultra-Precision Linear Motor Stages*. Tech. rep. Newports, 2017.

[NP33] Jerzy Neyman and Egon S Pearson. “On the problem of the most efficient tests of statistical hypotheses”. In: *Philosophical Transactions of the Royal Society of London. Series A, Containing Papers of a Mathematical or Physical Character* 231 (1933), pp. 289–337.

[PI18] *PILine Linear Stage - Compact Linear Stage with Ultrasonic Piezo Motor - U-521*. Tech. rep. Physik Instrumente (PI) GmbH, 2018.

[RMP00] R Ramesh, M.A Mannan, and A.N Poo. “Error compensation in machine tools — a review: Part I: geometric, cutting-force induced and fixture-dependent errors”. In: *International Journal of Machine Tools and Manufacture* 40.9 (2000), pp. 1235–1256.

[Ros03] Giovanni B. Rossi. “A probabilistic model for measurement processes”. In: *Measurement* 34.2 (2003), pp. 85–99.

[Ros06] Giovanni Battista Rossi. “A probabilistic theory of measurement”. In: *Measurement* 39.1 (2006), pp. 34–50.

[Ros14] Giovanni Battista Rossi. “Measurement and probability”. In: *Meteorology and Atmospheric Physics* (2014).

[Rud76] Walter Rudin. *Principles of Mathematical Analysis (International Series in Pure and Applied Mathematics)*. McGraw-Hill Education, 1976.

[Rus09] Bertrand Russell. *Principles of Mathematics (Routledge Classics)*. Routledge, 2009.

[SA96] Vladimir Sobolev and Olli Aumala. “Metrological automatic support of measurement results in intelligent measurement systems”. In: *Measurement* 17.3 (1996), pp. 151–159.

[Sad11] Yoshiki Sadamatsu. “"Reliability" of the terms related to analytical reliability”. In: *Creative* 10 (2011), pp. 39–41.

[SAH13] Mohsen Soori, Behrooz Arezoo, and Mohsen Habibi. “Dimensional and geometrical errors of three-axis CNC milling machines in a virtual machining system”. In: *Computer-Aided Design* 45.11 (2013), pp. 1306–1313.

[San+11] Jorge Santolaria et al. “A crenellated-target-based calibration method for laser triangulation sensors integration in articulated measurement arms”. In: *Robotics and Computer-Integrated Manufacturing* 27.2 (2011). Translational Research – Where Engineering Meets Medicine, pp. 282–291.

[Sav+16] E. Savio et al. “Economic benefits of metrology in manufacturing”. In: *CIRP Annals* 65.1 (2016), pp. 495–498.

[Sch+08] H. Schwenke et al. “Geometric error measurement and compensation of machines—An update”. In: *CIRP Annals* 57.2 (2008), pp. 660–675.

[Sch94] C. M. Schwarz. *The Chambers Dictionary*. W & R Chambers Ltd, 1994.

[Sez90] M. Ibrahim Sezan. “A peak detection algorithm and its application to histogram-based image data reduction”. In: *Computer Vision, Graphics, and Image Processing* 49.1 (1990), pp. 36–51.

[SH38] Stevens Stanley Smith and Davis Hallowell. *Hearing: its psychology and physiology.* John Wiley & Sons, Inc., 1938.

[SI11] LI SI. *Mathematical Statistics and Data Analysis - the original book version 3(Chinese Edition)*. Machinery Industry Pub. Date :2011-6-1, 2011.

[SK06] Patrick Suppes and David H Krantz. *Foundations of measurement: Geometrical, Threshold, and Probabilistic Representations*. Vol. 2. Courier Corporation, 2006.

[Son72] A. Sona. “Lasers in Metrology Distance Measurements”. In: *Laser Handbook*. Ed. by F. T. Arecchi and E. O. Schulz-Dubois. 2 vols. North-Holland Publishing Company - Amsterdam, 1972. Chap. F1, pp. 1457–1486.

[SPP10] M Sokovic, D Pavletic, and K Kern Pipan. “Quality improvement methodologies--PDCA cycle, RADAR matrix, DMAIC and DFSS”. In: *Journal of achievements in materials and manufacturing engineering* 43.1 (2010), pp. 476–483.

[SS58] Dana Scott and Patrick Suppes. “Foundational Aspects of Theories of Measurement”. In: *The Journal of Symbolic Logic* 23.2 (1958), pp. 113–128.

[Ste36] Stanley Smith Stevens. “A scale for the measurement of a psychological magnitude: loudness.” In: *Psychological Review* 43.5 (1936), p. 405.

[Ste46] Stanley Smith Stevens. “On the theory of scales of measurement”. In: *Science* 103.2684 (1946), pp. 677–680. eprint: `https://science.sciencemag.org/content/103/2684/677.full.pdf`.

[STO77] Toshio Sata, Yoshimi Takeuchi, and Nobuyuki Okubo. “Improvement of Working Accuracy of a Machining Center by Computer Control Compensation”. In: *Proceedings of the Seventeenth International Machine Tool Design and Research Conference: held in Birmingham 20th -- 24th September, 1976*. Ed. by S. A. Tobias. London: Macmillan Education UK, 1977, pp. 93–99.

[Sug07] Nubuo Suga. *Metrology Handbook: The Science of Measurement*. Mitutoyo (UK) Ltd, 2007.

[Suh+08] Suk-Hwan Suh et al. *Theory and Design of CNC Systems (Springer Series in Advanced Manufacturing)*. Springer, 2008.

[Sup51] Patrick Suppes. “A Set of Independent Axioms for Extensive Quantities”. In: *Portugaliae Mathematica* 10.4 (1951), pp. 163–172.

[SVN37] Stanley Smith Stevens, John Volkmann, and Edwin B Newman. “A scale for the measurement of the psychological magnitude pitch”. In: *The Journal of the Acoustical Society of America* 8.3 (1937), pp. 185–190.

[SW55] Patrick Suppes and Muriel Winet. “An Axiomatization of Utility Based on the Notion of Utility Differences”. In: *Management Science* 1.3-4 (1955), pp. 259–270. eprint: `https://doi.org/10.1287/mnsc.1.3-4.259`.

[SZ62] Patrick Suppes and Joseph L Zinnes. *Basic measurement theory*. Institute for mathematical studies in the social sciences, 1962.

[SZ95] S. Sartori and G.X. Zhang. “Geometric Error Measurement and Compensation of Machines”. In: *CIRP Annals* 44.2 (1995), pp. 599–609.

[Tru+98] E. Trucco et al. “Calibration, data consistency and model acquisition with laser stripers”. In: *International Journal of Computer Integrated Manufacturing* 11.4 (1998), pp. 293–310. eprint: http://dx.doi.org/10.1080/095119298130642.

[UW03] Michał K. Urbanski and Janusz Wąsowski. “Fuzzy approach to the theory of measurement inexactness”. In: *Measurement* 34.1 (2003). Fundamental of Measurement, pp. 67–74.

[Wan+02] Guoyu Wang et al. “Modelling and calibration of the laser beam-scanning triangulation measurement system”. In: *Robotics and Autonomous Systems* 40.4 (2002), pp. 267–277.

[Wya02] James C. Wyant. “White light interferometry”. In: *Proc. SPIE* 4737 (2002), pp. 98–107.

[Yos09] Toru Yoshizawa, ed. *Handbook of Optical Metrology: Principles and Applications*. CRC Press, 2009.

[YYF11] 要小鹏 et al. “五轴数控机床的空间误差建模与解耦补偿分析”. In: 高技术通讯 10 (Mar. 2011), pp. 1084–1089.

[ZCS02] Li Zhang, B. Curless, and S.M. Seitz. “Rapid shape acquisition using color structured light and multi-pass dynamic programming”. In: *3D Data Processing Visualization and Transmission, 2002. Proceedings. First International Symposium on*. 2002, pp. 24–36.

A Examples

This appendix contains extra examples.

Example A.1. This is an example illustrating that a non-uniformly distributed δ is still capable of making $E_{AB} = l$ for all $x \in (0, \frac{l}{2})$. Choose an integer $N \geq 2$ and let

$$\psi(\Delta) = \min\{\frac{1}{2}, (\Delta - \frac{l}{N+1})(\frac{l}{N} - \Delta)\}.$$

Let the Radon-Nikodym derivative of $P_{\delta,\Delta}$ with respect to the Lebesgue measure be

$$h_\Delta(x) = \begin{cases} \frac{1}{\Delta} & x \in [0, l - N\Delta], \\ -\frac{2\psi(\Delta)(x-(l-N\Delta))}{(\Delta-(l-N\Delta))\Delta} + \frac{1+\psi(\Delta)}{\Delta} & x \in (l - N\Delta, \Delta), \\ 0 & \text{elsewhere.} \end{cases} \quad \text{for } \Delta \in (\frac{l}{N+1}, \frac{l}{N})$$

$$h_\Delta(x) = \begin{cases} \frac{1}{\Delta} & x \in [0, \Delta), \\ 0 & \text{elsewhere.} \end{cases} \quad \text{for } \Delta \notin (\frac{l}{N+1}, \frac{l}{N})$$

Then for $x \in (\frac{l}{N+1}, \frac{l}{N})$, it holds

$$\begin{aligned} E_{AB}(x) =& \int_{[0,x)} \left(\lfloor \frac{l-\delta}{x} \rfloor x + x \right) h_x \, \mathrm{d}\delta \\ =& (N+1)x \int_{[0,l-Nx)} h_x \, \mathrm{d}\delta + Nx \int_{[l-Nx,x)} h_x \, \mathrm{d}\delta \\ =& (N+1)x \frac{l-Nx}{x} + Nx \left(1 + N - \frac{l}{x}\right) = l. \end{aligned}$$

□

Example A.2. Here an example will be constructed where the monotonicity of $p_h(x)$ fails. Let $l = 150, n = 10, x_1 = 14$, consider

$$h_x(y) = \begin{cases} \frac{1}{x} & y \in (0, x), \\ 0 & \text{elsewhere.} \end{cases} \quad \text{for } x > 0 \text{ and } x \notin (\frac{l}{n+1}, \frac{l}{n})$$

$$h_x(y) = \begin{cases} \frac{1}{x - \frac{x - \frac{l}{n+1}}{x_1 - \frac{l}{n+1}}(l - nx_1)} & y \in [\frac{x - \frac{l}{n+1}}{x_1 - \frac{l}{n+1}}(l - nx_1), x), \\ 0 & \text{elsewhere.} \end{cases} \quad \text{for } x \in (\frac{l}{n+1}, x_1)$$

$$h_x(y) = \begin{cases} \frac{1}{x - \left(\frac{\frac{l}{n} - x}{\frac{l}{n} - x_1}\right)^{10}(l - nx_1)} & y \in [\left(\frac{\frac{l}{n} - x}{\frac{l}{n} - x_1}\right)^{10}(l - nx_1), x), \\ 0 & \text{elsewhere.} \end{cases} \quad \text{for } x \in [x_1, \frac{l}{n})$$

This $h_x(y)$ describes a δ with uniform distribution when $x \notin (\frac{l}{n+1}, \frac{l}{n})$. And within the range $(\frac{l}{n+1}, \frac{l}{n})$, the support of the uniform firstly shrinks as x increases from $\frac{l}{n+1}$ to

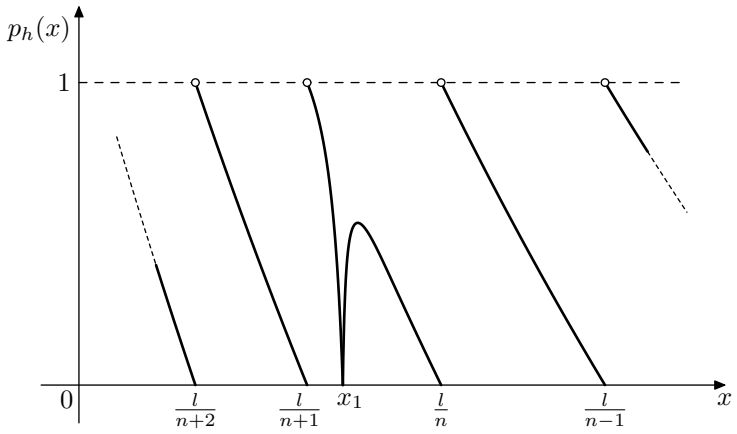

Figure A.1: Graph of p_h in Example A.2

x_1, and then extrudes back as x increases from x_1 to $\frac{l}{n}$. It is obvious that $x \mapsto h_x$ is continous and the fact

$$p_h(13.5) \approx 0.87 \qquad p_h(x_1) = 0 \qquad p_h(14.5) \approx 0.34$$

shows that $p_h(x)$ is not monotone on the interval $(\frac{l}{n+1}, \frac{l}{n})$. Indeed the graph of $p_h(x)$ is shown in Fig. A.1. □

Example A.3. This example constructs a δ so that p_h vibrates between 0 and 1 in a given $(\frac{l}{N+1}, \frac{l}{N})$. Let $x_0 = \frac{l}{N+1}, x_{2M+1} = \frac{l}{N}$ for any given $M \in \mathbb{Z}_+$, and choose $x_1, \ldots, x_{2M}$ such that

$$x_0 < x_1 < x_2 < \cdots < x_{2M} < x_{2M+1}.$$

Now let real functions $C(x), D(x)$ be defined on $[\frac{l}{N+1}, \frac{l}{N}]$ in a way such that

$$\begin{array}{llll} C(x_{2k-1}) = l - Nx_{2k-1} & C(x_{2k}) = 0 & \text{for } k = 1, 2, \ldots, M \\ D(x_{2k-1}) = x_{2k-1} & D(x_{2k}) = l - Nx_{2k} & \text{for } k = 1, 2, \ldots, M \end{array}$$

and

$$C(x_0) = C(x_{2M+1}) = 0 \qquad D(x_0) = x_0 \qquad D(x_{2M+1}) = x_{2M+1}$$

It is true that $0 \le C(x_i) < D(x_i) \le x_i, \forall i = 0, 1, \ldots, 2M+1$, and linear interpolation between each (x_i, x_{i+1}) completes the definition of $C(x)$ and $D(x)$ on $[\frac{l}{N+1}, \frac{l}{N}]$. Obviously $0 \le C(x) < D(x) \le x$ on $[\frac{l}{N+1}, \frac{l}{N}]$. Now define

$$h_x(y) = \begin{cases} \frac{1}{D(x)-C(x)} & y \in (C(x), D(x)), \\ 0 & \text{elsewhere.} \end{cases} \qquad x \in (\frac{l}{N+1}, \frac{l}{N})$$

$$h_x(y) = \begin{cases} \frac{1}{x} & y \in [0, x), \\ 0 & \text{elsewhere.} \end{cases} \qquad x \in (0, \frac{l}{2}) \setminus (\frac{l}{N+1}, \frac{l}{N})$$

Obviously δ satisfies the conditions of Theorem 3.1 and for $k = 1, 2, \ldots, M$

$$p_h(x_{2k-1}) = \int_{[0,l-Nx_{2k-1})} h_{x_{2k-1}}(y)\,\mathrm{d}y = 0$$
$$p_h(x_{2k}) = \int_{[0,l-Nx_{2k})} h_{x_{2k}}(y)\,\mathrm{d}y = 1$$

□

B Specifications

This appendix contains specifications defined by the software implementation and important pieces of codes.

B.1 Format: sdata

The `sdata` extension indicates that the specific file conforms to the `sdata` container rules. The `sdata` file stores triples of `float` number which is defined in Table 3.2 of [IEEE754] as binary32 type. There is no guarantee of validation, for example, the file might be empty (no data) or the file size might be of 13 bytes (not triples). It is commonly used to store points (x_i, y_i, z_i).

B.2 Tool: actualWidths

NAME

`actualWidths` — measures the width of the left and right extrusion in a given `sdata` file and then prints the result.

SYNOPSIS

`actualWidths -h|--help`

`actualWidths [-t num] [-j num] [-T num] [-S num] [--quiet] -H num [-f] INFILE`

DESCRIPTION

The `actualWidths` assumes each profile in the input `sdata` file has 1280 points. It detects the widths of points within each profile that lie within the height range $[H - T, H + T]$. Breakages are described by the jumper constant, that is, only discontinuity of y coordinates larger than j will be considered as a breakage.

The following options are available:

`-f file, --input-file=file`

This option specifies the input file and must be provided.

`-h, --help`

Prints a brief help message

`-H num, --height=num`

Specifies the height in the range $[H-T, H+T]$ to be checked. Points with height within this range are considered as from the top surfaces. It must be specified by the user.

`-j num, --jumper=num`

Specifies the jumper constant. Only points with difference in y larger than the jumper constant are considered as breakages. The default value is 2.

`--quiet`

If toggled, the amount of output is suppressed.

`-S num, --sparse=num`

Formats the output in the following way that when specified as 10 the outputs are set to one digit, 100 two digits, 1000 three digits. The default value is 10.

`-t num, --threshold-height=num`

Specifies the threshold for validity of points. Points with $z < t$ are treated as invalid points. The default value is 10.

`-T num, --tolerance=num`

Specifies the tolerance in the range $[H - T, H + T]$. Points with height within this range are considered as from the top surface. The default value is 0.5.

EXAMPLES

For sampled file `ex.sdata`, it is known that the top surface is within the range 62.2 ± 0.1, measure the extrusions.

```
$ actualWidths ex.sdata -H 62.2 -T 0.1
```

B.3 Tool: binaryPtFilter

NAME

`binaryPtFilter` — filters the input `sdata` file according to z coordinate (and y coordinate)

SYNOPSIS

`binaryPtFilter -h|--help`

`binaryPtFilter [-H num] [-m num] [-t num] [--not-drop-points] -o OUTFILE [-f] INFILE`

`binaryPtFilter [-H num] [-m num] [-t num] [--not-drop-points] -Y num -o OUTFILE [-f] INFILE`

DESCRIPTION

`binaryPtFilter` filters points in the input `sdata` file. It tests the points with conditions and the decides whether it should be dropped or recorded.

In case a point is to be recorded, if `-Y` is not specified, `binaryPtFilter` simply writes the point to the specified output file. If `-Y` is specified, `binaryPtFilter` further checks the y coordinate of the points and stores the result. The output is stored in one of the two `sdata` files with suffixes `.left.sdata`, `.right.sdata` to the output file name for sections with points whose $y \leq Y$ and $y > Y$ respectively.

To determine whether a point should be recorded or dropped, points are tested against the validity threshold m. If $z < m$, then `binaryPtFilter` checks further whether `--not-drop-points` is toggled. If not toggled (the default), the point is dropped; and if toggled, the point is recorded anyways. In case $z \geq m$ the point is then tested for the range $(H - t, H + t)$. If it is within the range it is recorded, otherwise dropped. The logic is presented by the flow chart Fig. B.1.

The following options are available:

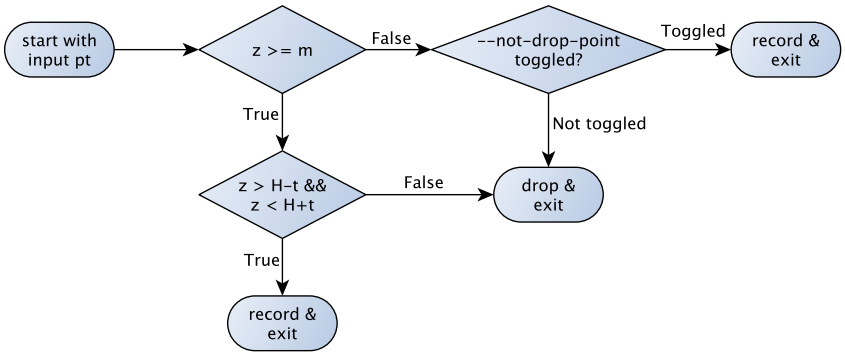

Figure B.1: Work flow of `binaryPtFilter`

`-f file, --input-file=file`

This option specifies the input file and must be provided.

`-h, --help`

Prints a brief help message

`-H num, --height=num`

Specifies the height of the top surface. The $(H-t, H+t)$ height test is after the validity threshold check. The default value is 64.

`-m num, --min-height=num`

Specifies the validity threshold. It is tested firstly for every point. The default value is -100.

`--not-drop-point`

By default this is not toggled. If toggled `binaryPtFilter` will capture all the points that failed the validity threshold check.

`-o file, --output-file=file`

Sets the output to file in `sdata` format, must be specified.

`-t num, --tolerance=num`

Specifies the tolerance range for the top surface. The $(H-t, H+t)$ height test is after the validity threshold check. The default value is 0.5.

`-Y num, --division-y=num`

If specified a test for the y coordinate will be imposed during the recording procedure. Two `sdata` output files with `.left.sdata` and `.right.sdata` suffixes to the specified output file name will be produced containing points whose $y \leq Y$ and $y > Y$ respectively

EXAMPLES

Filter the points in `ex.sdata` for points with $z \in (62.9 - 0.1, 62.9 + 0.1)$ and save the result to `out.sdata`.

```
$ binaryPtFilter ex.sdata -o out.sdata -H 62.9 -t 0.1
```

Filter the points in `ex.sdata` for points with $z \in (62.9 - 0.1, 62.9 + 0.1)$. Furthermore find the parts with $y \leq 25$ and $y > 25$.

```
$ binaryPtFilter ex.sdata -o out.sdata -H 62.9 -t 0.1 -Y 25
```

B.4 Tool: binaryPtFilterSparse

NAME

`binaryPtFilterSparse` — thin out the input `sdata` file and outputs to another `sdata` file

SYNOPSIS

`binaryPtFilterSparse -h|--help`

`binaryPtFilterSparse [-s num] [-e num] -o OUTFILE [-f] INFILE`

DESCRIPTION

`binaryPtFilterSparse` assumes each profile in the input `sdata` file has 1280 points. It outputs only the points from beams

$$\mathfrak{b}_s, \mathfrak{b}_{s+e}, \mathfrak{b}_{s+2e}, \ldots$$

The following options are available:

`-e num, --every-pt=num`

Specifies the sparse constant e_s. The default value is 1.

`-f file, --input-file=file`

Specifies the input file and must be provided by the user.

`-h, --help`

Prints a brief help message

`-o file, --output-file=file`

Specifies the output file file in `sdata` format, must be provided by the user.

`-s num, --str-index=num`

Specifies the starting index per each profile, should be smaller than 1280. The default value is 0.

EXAMPLES

Take points from beam $\mathfrak{b}_4, \mathfrak{b}_{11}, \mathfrak{b}_{18}, \ldots$ from file `ex.sdata` and save it to `out.sdata`

```
$ binaryPtFilterSparse ex.sdata -o out.sdata -s 4 -e 7
```

B.5 Tool: fullScaleStatistics

NAME

`fullScaleStatistics` — counts the number of full scales and reports statistical results for samples

SYNOPSIS

```
fullScaleStatistics -h|--help
fullScaleStatistics [--detailed-output] [-t num] [--sparse num] [-o
OUTFILE] [-f] INFILE
```

DESCRIPTION

`fullScaleStatistics` counts the number of full scales in each sampled profile from the given `sdata` file. By convention it assumes that different profiles are distinguished by the x coordinates. After execution, statistical data will be printed to the `stdout`. The reported output contains result sets defined in chapter 3 of the thesis.

The following options are available:

`--detailed-output`

If toggled, more details on each profile will be printed. By default it is not toggled.

`-f file, --input-file=file`

Specifies the input file and must be provided by the user.

`-h, --help`

Prints a brief help message

`-o file, --output-file=file`

If this option is set, the tool will save the output to file in addition to the standard output.

`--sparse=num`

Prints more information on every sampled profile. It controls the `DArray` density. The output will be formatted in the way that 10 for one digit, 100 for two digits, 1000 for three digits. The default value is 100. If set to default value, the output is suppressed. This option is for debug purposes only.

`-t num, --threshold=num`

Points with $z < t$ are considered as invalid. The default value is 10.

EXAMPLES

Find out the number of full scales and other statistical data from file `ex.sdata`.

```
$ fullScaleStatistics ex.sdata
```

B.6 Tool: histogramAnalyzer

NAME

`histogramAnalyzer` — analyzes the histogram of the height coordinate of points in a given `sdata` file and prints the output.

SYNOPSIS

`histogramAnalyzer -h|--help`

`histogramAnalyzer [-N num] [-d num] [-D] [-m num] [-M num] [-o OUTFILE] [--silent] INFILE`

DESCRIPTION

`histogramAnalyzer` builds a histogram of the height coordinate of points from a given input `sdata` file, automatically detects the peaks and then outputs the result. User specifies the range of height to be analyzed and the fineness of intervals. The automatic height detection algorithm follows [Sez90].

The following options are available:

`-d num, --discretion=num`

Specifies the interval length of the histogram. The statistic data will be counted for intervals $[\underline{\text{num}}\, i, \underline{\text{num}}(i+1)]$. The default value is 0.05.

`-D, --display-histogram`

Toggles detailed outputs of the histogram. The frequencies of each interval will be listed for examination.

`-h, --help`

Prints a brief help message.

`[--input-file] file`

Specifies the input file.

`-m num, --min=num`

Specifies the minimum value for the histogram. Only the points with height coordinate larger than or equal to num will be processed. The default value is 0.

`-M num, --max=num`

Specifies the maximum value for the histogram. Only the points with height coordinate less than or equal to num will be processed. The default value is 100.

`-N num, --SezanN=num`

Specifies the constant for peak detection. The tool follows [Sez90] for automatic peak detection, and this options sets the constant N in the paper. One should set it to be odd and positive, otherwise $\min(2\lfloor N/2 \rfloor + 1, 3)$ will be used. The default value is 5.

`-o file, --output-file=file`

If this option is set, the tool will save the output to `file` in addition to the standard output.

`--silent`

Suppresses the output to the standard output.

EXAMPLES

Find out peaks of histogram ranging $0 \sim 50$ with a step 0.1 using the Sezan constant 23 from file `ex.sdata`:

```
$ histogramAnalyzer -N 23 -m 0 -M 50 -d 0.1 ex.sdata
```

Check the previous result in detail:

```
$ histogramAnalyzer -N 23 -m 0 -M 50 -d 0.1 -D ex.sdata
```

B.7 Tool: sdataSneakViewer

NAME

`sdataSneakViewer` — prints triples of floats from a given `sdata` file

SYNOPSIS

`sdataSneakViewer -h|--help`

`sdataSneakViewer [-s num] [-e num] [-l num] [--silent] [-o OUTFILE] [-f] INFILE`

DESCRIPTION

`sdataSneakViewer` retrieves the binary float numbers in the given `sdata` file and prints every triple to the standard output. Starting from a given index, `sdataSneakViewer` prints triple at a fixed step away from the previous output. The output is delimited by spaces.

The following options are available:

`-e num, --every-pt=num`

Sets the tool to print every num triple. The default value is 1.

`-f file, --input-file=file`

Specifies the input file and must be provided by the user.

`-h, --help`

Prints a brief help message

`-l num, --length=num`

Specifies the total number of outputs of triple to be num. By default, this is set to 10.

`-o file, --output-file=file`

If this option is set, the tool will save the output to file in addition to the standard output.

`-s num, --str-index=num`

Specifies the starting index of output. The default value is 0.

`--silent`

Suppresses the output to the standard output.

EXAMPLES

Print first 15 triples in the file `ex.sdata`:

```
$ sdataSneakViewer -l 15 ex.sdata
```

Print the 2, 12, 22, 32, ..., 102 triples from the file `ex.sdata`:

```
$ sdataSneakViewer -s 2 -e 10 -l 11 ex.sdata
```

B.8 Tool: sensorErrorCorrection

NAME

`sensorErrorCorrection` — corrects obvious failures on top surface and outputs to an `sdata` file

SYNOPSIS

`sensorErrorCorrection -h|--help`

`sensorErrorCorrection [-t num] [-j num] [-T num] [--quiet] -o OUTFILE -H num [-f] INFILE`

DESCRIPTION

`sensorErrorCorrection` assumes each profile contains 1280 points in the input file. It corrects the sensor failures of the pattern that invalid points are between valid top surface points. The top surface points are those whose z coordinate lies within the interval $[H - T, H + T]$. Points with z coordinate smaller than t are treated as invalid. To distinguish the following cases

$$v_1, v_2, i_3, v_4, \cdots \qquad\qquad v_1, v_2, i_3, i_4, \ldots, i_{100}, v_{101}$$

where v stands for valid points and i stands for invalid points, `j` the jumper constant is used. If $|v_4.y - v_2.y| < j$ then i_3 is considered as a failure of sensor,

while if $|v_2.y - v_{101}.y| > j$ then all points from i_3 to i_{100} are considered as a discontinuity of top surface.

The following options are available:

`-f` file, `--input-file=`file

Specifies the input file and must be provided by the user.

`-h`, `--help`

Prints a brief help message

`-H` num, `--height=`num

Specifies the height for top surface and must be provided

`-j` num, `--jumper=`num

Specifies the jumper constant to num. By default, this is set to 2.

`-o` file, `--output-file=`file

Specifies the output file, must be provided by the user.

`--quiet`

Suppresses the amount of output to `stdout`.

`-t` num, `--threshold-height=`num

Specifies the threshold for validity to num. By default, this is set to 10.

`-T` num, `--tolerance=`num

Specifies the tolerance for top surface points. By default, this is set to 0.5.

EXAMPLES

Fix top surface errors in file `ex.sdata`, with known height range of the top surface 63.9 ± 0.4 and save the correct file to `after.sdata`. It is know that there is a 3.5mm-wide groove on the top surface.

```
$ sensorErrorCorrection ex.sdata -o after.sdata -H 63.9 -T
0.4 -j 3
```

C Basics of Probability

This section aims at making the thesis self-explanatory by providing a quick reference to the basics of measure theory and statistics. The review mainly follows [Hal14] [AL06] for measure and probability and [SI11][ISO3534-1] for statistics.

Let Ω be a nonempty set and $\mathcal{P}(\Omega) = \{A|A \subseteq \Omega\}$ denote the power set of Ω. Then a collection of sets $\mathcal{F} \subseteq \mathcal{P}(\Omega)$ is an algebra if for any $E, F \in \mathcal{F}$, $E \cup F \in \mathcal{F}$ and E^c, the complement of E, is also in $\mathcal{F}$. An algebra $\mathcal{F}$ is a σ-algebra if for any $E_i \in \mathcal{F}, i \in \mathbb{N}$, the union $\cup_{i\in\mathbb{N}} E_i \in \mathcal{F}$. Let μ be an extended real-valued function on a σ-algebra $\mathcal{F}$, then μ is a measure if for any $E \in \mathcal{F}, \mu(E) \geq 0$, $\mu(\varnothing) = 0$, and for any disjoint family $E_i, i \in \mathbb{N}$, $\mu(\cup_{i\in\mathbb{N}} E_i) = \sum_{i\in\mathbb{N}} \mu(E_i)$. Although a more general definition of measure is possible on rings instead of σ-algebras, this definition is adequate for discussions within this thesis. μ on a σ-algebra $\mathcal{F}$ of set Ω is a probability measure if for every $E \in \mathcal{F}, \mu(E) < +\infty$ and $\mu(\Omega) = 1$. $E \in \mathcal{F}$ is σ-finite if there are $E_i, i \in \mathbb{N}, E_i \in \mathcal{F}$ such that $E \subseteq \cup_{i\in\mathbb{N}} E_i$ and $\mu(E_i) < \infty, \forall i$. A measure is σ-finite if every E is σ-finite.

Given a topological space X, let $\mathcal{B}(X)$ denote the σ-algebra generated by the open sets of X; and $\mathcal{B}(X)$ is the Borel σ-algebra on X. Typically when X is $\mathbb{R}$ the real numbers, $\mathcal{B}(\mathbb{R})$ the Borel σ-algebra is also known to be generated by all intervals of the form (a, b) where $-\infty \leq a < b \leq +\infty$. A function μ_L^0 mapping an open interval (a, b) to $\mu_L^0((a, b)) = b - a$ can be extended to $\mathcal{B}(\mathbb{R})$ through some tricks. Avoiding the details, the completion of this μ_L^0 on $\mathcal{B}(\mathbb{R})$ can be made, and this is known as the Lebesgue measure. Throughout this thesis μ_L will be used to denote the Lebesgue measure, and $\mu_L((a, b)) = b - a$ is a convenient fact.

A measurable space is a pair $(\Omega, \mathcal{F})$ where $\mathcal{F}$ is a σ-algebra of Ω. A measurable space $(\Omega, \mathcal{F})$ becomes a measure space if further a measure μ on $\mathcal{F}$ is assigned. A probability space is a measure space whose measure is a probability measure. Given measurable spaces $(\Omega_i, \mathcal{F}_i), i = 1, 2$, a function $f : \Omega_1 \to \Omega_2$ is measurable or $\langle \mathcal{F}_1, \mathcal{F}_2 \rangle$-measurable if for every $E \in \mathcal{F}_2$, $f^{-1}(E) \in \mathcal{F}_1$. A random variable is a function f from a probability space $(\Omega, \mathcal{F}, P)$ to $\mathbb{R}$, that is, $\langle \mathcal{F}, \mathcal{B}(\mathbb{R}) \rangle$-measurable. If f is a random variable on $(\Omega, \mathcal{F}, P)$, then the induced measure $P_f = P \circ f^{-1}$ on $(\mathbb{R}, \mathcal{B}(\mathbb{R}))$ is the probability distribution of f.

For a given measure space $(\Omega, \mathcal{F}, \mu)$ and $E \in \mathcal{F}$, the characteristic function of E is defined as $\chi_E(x) = 0$ if $x \notin E$ and $\chi_E(x) = 1$ if $x \in E$. A simple function $f = \sum_{i=1}^{n} \alpha_i \chi_{E_i}$ is a finite linear combination of characteristic function. For a given

simple function $f = \sum_{i=1}^{n} \alpha_i \chi_{E_i}$, it is integrable if $\mu(E_i) < \infty$ and thus the integral of f is defined as

$$\int_\Omega f(x)\,\mathrm{d}\mu(x) = \int f\,\mathrm{d}\mu = \sum_{i=1}^{n} \alpha_i \mu(E_i)$$

Avoiding the details, the definition can be extended to all non-negative measurable functions. For a general measurable function f, it can be written as $f = f_+ - f_-$ where $f_+ = \max(f, 0)$ and $f_- = -\min(f, 0)$ are measurable and non-negative. Then formally $\int f\,\mathrm{d}\mu$ can be defined as $\int f_+\,\mathrm{d}\mu - \int f_-\,\mathrm{d}\mu$ if at least one of f_+, f_- has finite integral. f is integrable or μ-integrable if $\int f\,\mathrm{d}\mu$ is finite. If $E \in \mathcal{F}$ then $\int_E f\,\mathrm{d}\mu$ is defined as $\int \chi_E f\,\mathrm{d}\mu$. Let $L^p(\Omega, \mathcal{F}, \mu)$ or $L^p(\Omega)$ denote the set of measurable functions, where $f \in L^p(\Omega, \mathcal{F}, \mu)$ if and only if $|f|^p$ is integrable. A random variable is a measurable function f on a probability space $(\Omega, \mathcal{F}, P)$, and the expectation or mean is defined to be the integral

$$E(f) = \int_\Omega f\,\mathrm{d}P$$

if it exists. As an example, a random variable with Cauchy distribution $\frac{1}{\pi(1+x^2)}$, does not have an expected value.

Given two measures μ, ν on a measurable space $(\Omega, \mathcal{F})$, ν is absolutely continuous with respect to μ if $\mu(E) = 0$ implies $\nu(E) = 0$ for every $E \in \mathcal{F}$, denoted by $\nu \ll \mu$. Now suppose that μ, ν are σ-finite measures on a measurable space $(\Omega, \mathcal{F})$ such that $\nu \ll \mu$, then there exists a measurable function f such that

$$\nu(E) = \int_E f\,\mathrm{d}\mu$$

for all $E \in \mathcal{F}$. This is known as the Radon-Nikodym theorem, and this f, denoted by $\frac{\mathrm{d}\nu}{\mathrm{d}\mu}$ is the Radon-Nikodym derivative. For example, μ_δ defined as $\mu_\delta(E) = 1$ if $0 \in E \subseteq \mathbb{R}$ and $\mu_\delta(E) = 0$ if $0 \notin E \subseteq \mathbb{R}$, is known as the Dirac measure on $\mathbb{R}$. μ_δ is not absolute continuous with respect to μ_L, the Lebesgue measure.

$A \in \mathcal{F}$ sometimes is also called an event. Given events A, B in a probability space $(\Omega, \mathcal{F}, P)$ with $P(B) > 0$, then the conditional probability of A given B is defined as $P(A|B) = \frac{P(A \cap B)}{P(B)}$. Then immediately the following identity holds true

$$P(A|B) = \frac{P(B|A)P(A)}{P(B)}, \tag{9.1}$$

and this is the Bayes' formula. Hypotheses on probability distributions can be asserted based on experimental outputs. Null hypothesis and alternative hypothesis usually denoted by H_0 and H_1 divide the probability distribution family into two parts which are then examined by statistical tests to decide whether a null hypothesis is to be rejected in favor of an alternative hypothesis [ISO3534-1].

Although there are many different ways to conduct statistical tests, the likelihood ratio test (LR test) proposed by Neyman-Pearson [NP33] is mainly used in this thesis. Deep statistical analysis is avoided because it is less relevant to the measurement method proposed in this thesis. Suppose event A is observed, and then by Bayes' formula it holds

$$\Lambda(A) = \frac{P(H_0|A)}{P(H_1|A)} = \frac{P(A|H_0)P(H_0)/P(A)}{P(A|H_1)P(H_1)/P(A)} = \frac{P(H_0)P(A|H_0)}{P(H_1)P(A|H_1)} \tag{9.2}$$

If assuming no bias on H_0, H_1, that is, $P(H_0) = P(H_1)$, then equation (9.2) is simplified to be

$$\Lambda(A) = \frac{P(A|H_0)}{P(A|H_1)}.$$

Λ is known as the likelihood ratio function. A constant c can be chosen and accept H_0 if $\Lambda \geq c$ otherwise H_1. Type I error refers to the error by rejecting H_0 cases and Type II error refers to the error by accepting H_1 cases.

D Rationale and Thoughts Behind PBM

This appendix is a response to the suggestions received on the dissertation day that some of the thoughts and rationale behind the scenes should be stated. It all begins with the Micro-Fast, where different die-punch sets are manufactured for different products. Although the size of final products can be as large as 5cm, small features, such as, chamfers, teeth on cogs and thin walls can be as small as 50μm. Devices, like laser scanners, provide good measurement results on the vertical direction, however the results on lateral directions are coarse and unstable.

Trials using the gantry to generate small moves along the lateral directions have been conducted. The linear stages used in the lab can reliably provide doubled resolution on the lateral direction, however it is not optimistic to expect for further improvements. Disturbances, especially table vibration, linear stage hysteresis and illumination, increase the inconsistency of readings around the small features. Without another investment to improve the overall lab environment, this approach is practically unfeasible. At the same time, one decision was made in the Micro-Fast project that conveyor belts would be used to transfer the die-punch sets. It means that one should always expect vibrations and errors in placement — the positioning error of the die-punch set should be some tens of micrometers.

Different (possible) solutions were proposed by Micro-Fast partners, for example, to use back-light silhouette systems for small features. For the Micro-Fast project, this approach only works for sintered parts, but not the die-punch sets, because the designed dies have their bottoms sealed and the punches attached to a base. Considerations using other sensor have also been conducted, for example, probes, which is immediately rejected for its slow speed, interferometers, confocal microscopes. During the process, the author begins to feel that the lateral resolution is the bottleneck.

Suppose the lateral resolution is solved, and the pixel resolution is improved to 100nm. Then a 1280×960 image sensor only covers $128\times96\mu$m^2, which covers merely about 0.00049% of the 5×5cm^2 area of the largest component. This degenerates to probe-based approaches, like CMM or AFM. It is reasonable to think that the features are of limited number and the locations are known; therefore with the help of a large-range sensors this problem can be greatly simplified. Yet, there are still features like long-thin walls to be solved, which requires fine resolution for thickness and large scope for uniformity.

The interest is then quickly narrowed down to the image sensors, which are used as components in the laser scanners, interferometers and silhouette imaging systems. The author quickly realizes that it is financially impossible to "make new sensors", and thus begins to consider potential improvements without changing the tools.